UNIVERSITY OF AGDER

Piston Driven Yaw Mechanism

by

Geir Kirkeby
Jørgen Rosendahl Simonsen

Supervisors:
Michael R. Hansen
Johan Johnsen

Status: Final

This master's thesis is carried out as a part of the education at the University of Agder and is therefore approved as a part of this education. However, this does not imply that the University answers for the methods that are used or the conclusions that are drawn.

Grimstad, June 2, 2014
Department of engineering
Faculty of technology and science

Abstract

The current thesis presents a piston driven yaw mechanism for wind turbines. Traditionally the yaw mechanism has been one of the mayor contributors to down time and repair has been costly. The proposed design aims to improve the reliability of the yaw mechanism by reducing the point loads and by using hydraulic cylinders instead electrical motors to generate torque. In addition the design is modular allowing the mechanism to be disassembled and components to be replaced without the requirement of complicated or costly machinery. The current thesis presents an analysis of the state of the art and discusses concepts which may solve some of the challenges with existing yaw mechanisms. Further on a conceptual model of the mechanism is developed. Modelling and simulation is carried out to verify the suitability of the concept. It is found that the proposed yaw mechanism may be suitable for modern wind turbines and that the design may increase the reliability and reduce cost of repair compared to current solutions.

Preface

This paper is written, and all work described within is performed, by Geir Kirkeby and Jørgen R. Simonsen. The paper is our finishing thesis of a master's degree in mechatronics, at the University of Agder. The paper is produced over a period from early January to early June of 2014. All figures and pictures are created by us if nothing is cited. The nomenclature is found at the start of the paper and present all parameters and variables used throughout the paper. The paper is written U.K. English.

We would like to give great thanks to industrial supervisor Johan Johnsen for his advices and always being ready to counsel and give feedback. We are grateful for your time and effort in making our contribution better. Our thanks also go to our supervisor, Professor Michael Rygaard Hansen, for his expertise and counselling. He has been a great resource in the field of simulation and the general academic approach. In addition, we would like to thank: Michael Dahlhoff, from ThyssenKrupp Rothe Erde, for his guidance and assistance in the field of large diameter slew bearings; and Claus Rask, from Svendborg Brakes, for his counselling in the study of hydraulic brake callipers and for supplying a free brake pad specimen for testing.

Grimstad, Norway June 2, 2014

Geir Kirkeby

Jørgen Rosendahl Simonsen

List of Figures

List of Tables

Nomenclature

Symbols and descriptions of parameters and variables used throughout the thesis. General variables, e.g area (A) and velocity (v), are used in a general expression of a repeated operation.

	Symbol:	Name:	Unit:
A	A	Area	[m^2]
	A_{eqv}	Equivalent area	[m^2]
	A_p	Piston-side area	[m^2]
	A_{pb}	Brake pad area	[m^2]
	A_r	Rod-side area	[m^2]
	A_{sa}	Swept rotor area	[m^2]
	A_v	Orifice area	[m^2]
B	b	Distance between the interaction points of the two cylinders on the inner ring	[m]
C	c	Length in Figure 3.19	[m]
	C_d	Damping constant	[$\frac{Ns}{m}$]
	C_s	Spring constant	[$\frac{N}{m}$]
	C_t	Thrust coefficient, for ideal turbines	[-]
	C_v	Flow coefficient	[$\frac{Nm}{s}$]
D	d	Diameter	[m]
	D	Outer perimeter diameter of the mechanism	[-]
	d_{eqv}	Equivalent diameter	[m]
	D_i	Inner diameter of brake disc	[m]
	d_p	Diameter of cylinder piston	[m]
	D_{pid}	Derivative parameter	[-]
	d_r	Hydraulic cylinder rod diameter	[m]
E	e	Length in Figure 3.19	[m]
	E	Young's modulus	[Pa]
	e_d	Diametrical expansion	[m]
F	f	Length in Figure 3.19	[m]
	F_a	Axial force in yaw bearing	[N]
	F'_{a1}	Axial force for load combination 1	[N]
	F'_{a2}	Axial force for load combination 2	[N]
	F_b	Brake force	[N]
	F_c	Clamping force	[N]
	F_c	Coulomb force	[N]
	F_{cyl}	Cylinder force	[N]
	F_e	Excitation force	[N]
	F_{hub}	Force from rotor on hub	[N]
	F_{t1ri}	Tangential force from cylinder 1 on inner disc	[N]
	F_{t1ro}	Tangential force from cylinder 1 on outer disc	[N]
	F_{t2ri}	Tangential force from cylinder 2 on inner disc	[N]
	F_{t2ro}	Tangential force from cylinder 2 on outer disc	[N]
	F_r	Radial force in yaw bearing	[N]
	F_{r1ri}	Radial force from cylinder 1 on inner disc	[N]
	F_{r1ro}	Radial force from cylinder 1 on outer disc	[N]

	Symbol:	Name:	Unit:
	F_{r2ri}	Radial force from cylinder 2 on inner disc	[N]
	F_{r2ro}	Radial force from cylinder 2 on outer disc	[N]
	F_s	Stiction force	[N]
	f_{stat}	Load factor	[-]
	F_v	Viscous friction force	[N]
	F_1	Force from cylinder 1	[N]
	F_2	Force from cylinder 2	[N]
G	g	Gravitational constant	$[\frac{\mathrm{m}}{\mathrm{s}^2}]$
	G	Weight	[N]
	G_n	Weight of nacelle	[N]
H	h	Length in Figure 3.19	[m]
I	I_i	Moment of inertia of inner disc	$[\mathrm{kgm}^2]$
	I_o	Moment of inertia of outer disc	$[\mathrm{kgm}^2]$
	I_{pid}	Integral parameter	[-]
	I_r	Polar moment of inertia of a circle	$[\mathrm{m}^4]$
K	k	Bearing friction parameter	[-]
	K	End-condition factor	[-]
	k_v	Viscous friction coefficient	$[\frac{\mathrm{Ns}}{\mathrm{m}}]$
	K_1	Tangential factor, Figure 5.6	[-]
	K_2	Tangential factor, Figure 5.6	[-]
	K_3	Tangential factor, Figure 5.6	[-]
	K_4	Tangential factor, Figure 5.6	[-]
L	l	Length of lever arm	[m]
	L	Length of hydraulic cylinder barrel	[m]
	l_b	Length from centre in brake pads to centre of system	[m]
	L_e	Length of extended cylinder	[m]
	L_{gx}	Horizontal distance from centre of mass to centre of yaw bearing	[m]
	l_{hy}	Height from yaw bearing to hub	[m]
	L_r	Length of retracted cylinder	[m]
	L_{rod}	Length of rod	[m]
M	m	mass	[kg]
	M	Frictional torque	[Nm]
	M_{Ao}	Frictional torque between callipers on outer disc and nacelle	[Nm]
	M_{Ai}	Frictional torque between callipers on inner disc and tower	[Nm]
	M_b	Brake torque	[Nm]
	M_{Bi}	Frictional torque between callipers on inner disc and nacelle	[Nm]
	M_{Bo}	Frictional torque between callipers on outer disc and tower	[Nm]
	m_i	Mass of inner ring	[kg]
	M_i	Torque of inner disc	[Nm]
	M_k	Tilting moment	[Nm]
	M'_{k1}	Tilting moment for load combination 1	[Nm]
	M'_{k2}	Tilting moment for load combination 2	[Nm]
	m_n	Mass of nacelle	[kg]
	M_{nt}	Frictional torque between nacelle and tower	[Nm]
	m_o	Mass of outer ring	[kg]
	M_o	Torque of outer disc	[Nm]
	M_{oi}	Friction torque between outer and inner disc	[Nm]
	M_{ot}	Frictional torque between outer disc and tower	[Nm]
N	N	Normal force	[N]
	n_{cal}	Number of callipers	[-]
	n_{cyl}	Number of cylinders	[-]
R	r	Radius	[m]
	r_c	Normal distance from rotational centre to hydraulic cylinder	[m]
	r_i	Distance from centre of rotation to the interaction points on the inner disc	[m]

	Symbol:	Name:	Unit:
	r_o	Distance from centre of rotation to the interaction points on the outer disc	[m]
	r_{oi}	Radius to bearing between outer and inner disc	[m]
	r_{ot}	Radius to bearing between outer disc and tower	[m]
	r_{nt}	Radius to bearing between nacelle and tower	[m]
P	p	Period	[s]
	P	Power	[W]
	p_{atm}	Atmospheric pressure	[Pa]
	p_b	Operating pressure for hydraulic brake	[Pa]
	p_c	Operating pressure for hydraulic cylinders	[Pa]
	p_{pid}	Gain parameter	[-]
	p_s	Supply pressure	[Pa]
	p_{theta}	Position gain	[-]
S	s_b	Signal input	[-]
	s_d	Design stress	[Pa]
	SF_{cyl}	Safety factor	[-]
	s_1	Stroke, cylinder 1	[m]
	s_2	Stroke, cylinder 2	[m]
T	t	Time	[s]
	T_b	Required brake torque	[Nm]
	t_{cyl}	Thickness of cylinder wall	[m]
	T_i	Torque on inner disc from cylinders	[Nm]
	T_o	Torque on outer disc from cylinders	[Nm]
	T_{req}	Required torque	[Nm]
	T_{ri}	Inner disc torque from cylinders	[Nm]
	T_{ro}	Outer disc torque from cylinders	[Nm]
U	u	Signal input to valve	[-]
	u_{fb}	Feedback signal	[-]
	u_{ref}	Reference signal	[-]
V	v	Velocity	$[\frac{\mathrm{m}}{\mathrm{s}}]$
	v_d	Damping velocity	$[\frac{\mathrm{m}}{\mathrm{s}}]$
	v_{fb}	Feedback velocity	$[\frac{\mathrm{m}}{\mathrm{s}}]$
	v_s	Stribeck velocity	$[\frac{\mathrm{m}}{\mathrm{s}}]$
	v_{ref}	Reference velocity	$[\frac{\mathrm{m}}{\mathrm{s}}]$
	v_{t1ri}	Tangential velocity in connection between cylinder 1 and inner disc	$[\frac{\mathrm{m}}{\mathrm{s}}]$
	v_{t1ro}	Tangential velocity in connection between cylinder 1 and outer disc	$[\frac{\mathrm{m}}{\mathrm{s}}]$
	v_{t2ri}	Tangential velocity in connection between cylinder 2 and inner disc	$[\frac{\mathrm{m}}{\mathrm{s}}]$
	v_{t2ro}	Tangential velocity in connection between cylinder 2 and outer disc	$[\frac{\mathrm{m}}{\mathrm{s}}]$
	v_{r1ri}	Radial velocity in connection between cylinder 1 and inner disc	$[\frac{\mathrm{m}}{\mathrm{s}}]$
	v_{r1ro}	Radial velocity in connection between cylinder 1 and outer disc	$[\frac{\mathrm{m}}{\mathrm{s}}]$
	v_{r2ri}	Radial velocity in connection between cylinder 2 and inner disc	$[\frac{\mathrm{m}}{\mathrm{s}}]$
	v_{r2ro}	Radial velocity in connection between cylinder 2 and outer disc	$[\frac{\mathrm{m}}{\mathrm{s}}]$
	v_w	Wind speed	$[\frac{m}{s}]$
Q	Q	Hydraulic flow	$[\frac{\mathrm{m}^3}{\mathrm{s}}]$
	Q_{fb}	Feedback hydraulic flow	$[\frac{\mathrm{m}^3}{\mathrm{s}}]$
	Q_{ref}	Reference hydraulic flow	$[\frac{\mathrm{m}^3}{\mathrm{s}}]$
X	x_s	Distance from calliper to brake disc	[m]
Z	z	Average bristle deflection	[m]

	Symbol:	Name:	Unit:
α	α_i	Angular acceleration of inner disc	$[s^{-2}]$
	α_n	Angular acceleration of nacelle	$[s^{-2}]$
	α_o	Angular acceleration of outer disc	$[s^{-2}]$
δ	δ_v	Constant dependant on application geometry	[-]
	Δp	Pressure drop	[Pa]
ϵ	ϵ_d	Diametrical unit strain	[-]
θ	θ	Angular displacement between outer and inner disc	[-]
	θ_{fb}	Feedback angular displacement	[-]
	θ_i	Angular displacement of inner disc	[-]
	θ_m	Required rotation	[-]
	θ_o	Angular displacement of outer disc	[-]
	θ_r	Angular displacement	[-]
	θ_{ref}	Reference angular displacement	[-]
	θ_1	Angle in Figure 3.19	[-]
	θ_2	Angle in Figure 3.19	[-]
	θ_3	Angle in Figure 3.19	[-]
	θ_4	Angle in Figure 3.19	[-]
κ	κ_{cyl}	Cylinder ratio	[-]
μ	μ_b	Friction coefficient between brake pad and disc	[-]
	μ_b	Friction coefficient in bearing	[-]
	μ_c	Coulomb friction coefficient	[-]
	μ_s	Stiction coefficient	[-]
ν	ν	Poisson's ratio	[-]
ρ	ρ	Air density	$[\frac{kg}{m^3}]$
σ	σ_0	Stiffness parameter	$[m^{-1}]$
	σ_1	Damping parameter	$[\frac{s}{m}]$
ϕ	ϕ_1	Angle in Figure 3.19	[-]
ω	ω_{Ai}	Relative angular velocity of inner disc	$[s^1]$
	ω_{Ao}	Relative angular velocity between outer disc and nacelle	$[s^1]$
	ω_{Bi}	Relative angular velocity of nacelle and inner disc	$[s^1]$
	ω_{Bo}	Relative angular velocity of outer disc	$[s^1]$
	ω	Angular velocity	$[s^{-1}]$
	ω_{fb}	Feedback angular velocity	$[s^{-1}]$
	ω_i	Angular velocity of inner disc	$[s^{-1}]$
	ω_n	Angular velocity of nacelle	$[s^{-1}]$
	ω_o	Angular velocity of outer disc	$[s^{-1}]$
	ω_r	Angular velocity	$[\frac{^\circ}{s}]$
	ω_{ref}	Reference angular velocity	$[s^{-1}]$

Abbreviations

Abbreviations and acronyms used in the report is listed in alphabetical order bellow.

EU	European Union
EWEA	European Wind Energy Association
HAWT	Horizontal-axis wind turbine
IPCC	Intergovernmental Panel on Climate Change
REN Alliance	International Renewable Energy Alliance
Stiction	Static friction
UiA	Universitetet i Agder (University of Agder)
VAWT	Vertical-axis wind turbine

Contents

Chapter 1

Introduction

Windmills have been used for three thousand years and have evolved into the massive constructions we know today as wind turbines. Grinding grain or pumping water was the main purpose of windmills until the early 1970's when the first oil price shock rose interests in alternative energy sources. Environmental concerns also gave an additional boost in clean energy research, with wind power as a favourite candidate. In 1996 the production of installed and planed wind plants around the world, were estimated to be 6000[MW] [28]. In June 2013 the worldwide wind capacity was 296[GW], around 3.5% of the world's electricity demand [29]. International Renewable Energy Alliance (REN Alliance) present intermediate targets for future green energy production based on Intergovernmental Panel on Climate Change (IPCC) mitigation scenario [25]. By 2035, the REN Alliance believes that 50% of energy supplies will be covered by renewable energy (100% soon thereafter) [1]. The European commission presented in 2008 key achievements from the 20/20/20% targets, including reduction in green gas emission, share of renewable energy and improvement in energy efficiency. Currently progress shows positive results in all sectors. In the share of newly installed renewable energy, EU reached 13% in 2012 and is expected to reach 21% by 2020 [4].
Present technology in wind energy has achieved a high cost reduction and suggests onshore wind turbines as the cheapest option for new electricity generations. Availability can still be improved as outage from miscellaneous failures is still a problem and requires heavy duty machinery for maintenance. Downtime because of critical errors in wind turbines has resulted in implementation of more surveillance of systems, to add precaution. As wind turbines expand their swept area, an equal growth in engineering challenges from even higher forces is anticipated. One of the worst case scenarios today in wind turbines are critical failures in the yaw mechanism. Damaged bearing or gears may require repairs where the nacelle has to be removed in order to replace defect components, inducing severe downtime. Improving and developing new, modular yaw mechanism that manages these forces are highly desirable to the increasing wind energy market and an alluring task for product developers.

1.1 Problem description

The problem is stated as a proposition for a master's thesis in mechatronics at the University of Agder, spring of 2014. The problem is formed by Johan Johnsen on the behalf of Incepti AS. The problem definition, further defined in collaboration with Michael R. Hansen (UiA), states the following problem:

> '*Develop a concept for a hydraulic piston drive capable of controlling the orientation of a wind turbine rotor around its yaw axis as well as parking the rotor in any orientation around the yaw axis.*'

The original problem description can be seen in Appendix A. The essence of the idea is to make the yaw mechanism modular, for simple assembly, disassembly and repair. The idea has to be developed and tested using mathematical models, to prove functionality of the mechanism. Major fields of work proposed by the client are listed below:

1. Development of piston driven yaw mechanism
   (a) Evaluate ideas

   (b) Identify the best, feasible candidate
   (c) Select components
   (d) Create a 3D-CAD model

2. Mathematical model
   (a) Create a mathematical model
   (b) Implement dynamic friction
   (c) Investigate functionality of the mechanism
   (d) **If time allows:** Create visualization on how the system works

3. **If time allows:** Finite element analysis

Table 1.1: Product specifications for the piston driven yaw mechanism, requested by supervisor Johnsen and Hansen.

Description	Metric	Unit
Outer diameter of tower	3.5	$[m]$
Cylinder diameter	max 350	$[mm]$
Hydraulic pressure	max 350	$[bar]$
Barrel/stroke ratio for hydraulic cylinder	$2:1$	$[-]$
Angular velocity [27, p. 161]	0.37	$[\frac{^\circ}{s}]$
Angular rotation	$3 \cdot 360$	$[^\circ]$
Steady torque load	$7 - 8 \cdot 10^6$	$[Nm]$
Peak torque load	$11 \cdot 10^6$	$[Nm]$
Boundaries (x, y, z)	$[3.5, 3.5, 0.7]$	$[m]$
Mass	20	$[tonn]$
Operating temperature	-30 to 50	$^\circ C$
Cut-in wind speed	4	$[\frac{m}{s}]$
Cut-out wind speed	25	$[\frac{m}{s}]$
Modular	Yes	$[-]$

To develop a good concept, a well defined set of product requirements are needed. Supervisors supplied relevant information needed to set the restrictions of the system. Generally, the piston driven yaw mechanism is to be designed for use in 3.5[MW] wind turbines, giving approximate demands to size and shape. Detailed product requirements can be found in Table 1.1.
Through discussion and exchange of ideas with supervisor Johnsen, three ideas were developed and investigated. The ideas where investigated in the order stated below, with the intention of finding an optimal solution. Ideas investigated can be seen in Figure 1.1 and are described more in detail below.

Radial engine: Consisting of a number of cylinders with one end mounted to the nacelle/tower, with equal angular spacing, and the other to a crank. The crank is connected to the centre of rotation for the tower/nacelle. Through extending and retracting the cylinders in sequence, the crank and nacelle will be rotated. A sketch of the idea can be seen in Figure 1.1a.

Cogwheel: Consisting of a number of cylinder pairs mounted to the tower/nacelle, using symmetry about the centre-point of the tower. The two cylinders in each pair will be connected to each other, and respectively push and pull on a rotating notched cogwheel connected to the nacelle/tower with a periodic motion. Half of the periodic motion involves moving the nacelle/tower, and the other half involves relocating the joint cylinder point in a new cogwheel-notch to again move the nacelle/tower. A sketch of the concept can be seen in Figure 1.1b.

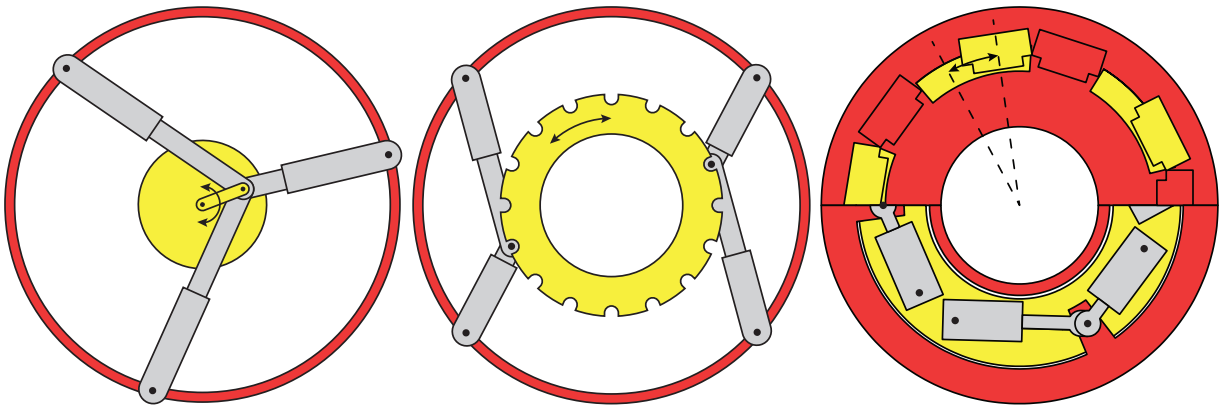

(a) Radial engine (b) Cogwheel (c) Grip and rotate

Figure 1.1: Simplified sketches of the three ideas described in the problem description, Section 1.1. Red and yellow indicate the difference between the two members rotating in relation to each other. Hydraulic cylinders are coloured grey.

Grip and rotate Consisting of a number of hydraulic cylinders mounted between two freely rotating discs. One disc will connect to the tower and the other to the nacelle. Extending/retracting the hydraulic cylinders will then rotate the nacelle relative to the tower. When full stroke of cylinders is reached, the discs will switch connections and the cylinders-motion will reverse, resulting in the nacelle continuing its rotation in the same direction as before. Connections between the discs and nacelle/tower will be made using large brake callipers and brake discs. This sequence will have to be generalized and controlled to ensure user-definable rotation speed, steady rotation of nacelle, and safe operation. The major advantage of this concept is that it could be made modular and has no problem delivering the required torque.

1.2 Motivation

A new alternative solution for the yaw mechanism in wind turbines is highly attractive. Based on previous experience by supervisor Johnsen and Hansen, slew mechanisms with geared rings and pinions are troubled with high point-loads in gear teeth. Several institutions are developing alternatives utilizing other solutions, avoiding problems with point-loads in gears. Uneven distribution of forces may cause motor failure. These solutions are described in detail in Section 2.3.3. The existing yaw mechanisms, and the ones under development, have the disadvantage of being large and causing long downtimes when a failure occurs. It is very desirable to have a yaw mechanism which can be easily dismantled. Defect parts can be brought out and new parts in, without dismantling the entire mechanism.

1.3 Report outline

A rough outline of the report can be found in this section. This includes a brief description of the content of each chapter.

Chapter 1: Introduction This chapter sets the baseline for the problem by giving a short overview of the topic background. It contains the revised problem description, in addition to motivation and limitations of the project.

Chapter 2: Wind turbines This chapter is a literary study of past and present wind energy technology, including specific information and terminology of horizontal-axis wind turbines.

Chapter 3: Design and development This chapter describe the steps behind designing and developing the idea to a stage where it can be made into a mathematical model. The chapter contains calculations and choices throughout the process, for dimensioning essential parts of the mechanism.

Chapter 4: Friction This chapter give a brief literary study in the topic of tribology, before the LuGre friction model is presented. LuGre is investigated and expanded to fit for the purpose in this project.

Chapter 5: Modelling and simulation This chapter describe the mathematical model, as created in SimulationX, with its features and limitations.

Chapter 6: Results This chapter present results retrieved from simulations and discuss its significance. It discusses the effect of changes in the friction model as well as different velocity profiles for nacelle motion.

Chapter 7: Conclusion This chapter sums up the project in short, and states the conclusion to the problem stated in the introduction.

Chapter 2

Wind turbines

Modern wind turbines harvests kinetic energy from the wind and converts it into mechanical energy. Mechanical energy is produced by rotation of the blades on a wind turbine, converting rotational energy into electricity with a generator. This chapter introduces the wind turbines and gives a brief introduction in wind power, main components and characteristics of different wind turbines. The wind turbines presented will be the conventional horizontal axis type, where flow of wind is parallel to the rotational axis of the rotor.

2.1 Power in the wind

Design of wind turbines has evolved through time and is one of the main categories of renewable energy. With an increase in energy demand, the size of wind turbines are also influenced as the current largest windmill, E-126, reaches up to 7.5[MW] [6]. E-126, by Enercon, has a swept area of 12.668[m^2] and consists of three massive blades with a diameter of 127 [m] [9]. Large swept area is one of the main reasons why this wind turbine achieves such a high rated power. The power in wind is represented by Equation 2.1. The theoretical maximum efficiency any wind turbine equals 0.593, and is called the Betz limit. When designing a wind turbine, requirements of strength and durability can further lower the efficiency.

$$P = \frac{1}{2}\rho A_{sa} {v_w}^3 \tag{2.1}$$

High end wind turbine designs and good site evaluation are reaching its maximum potential. The evolution of wind turbines show us that swept area is one parameter that increases steadily over time. Wind turbine height increases with swept area, leading to larger loads. In order to achieve high reliability, this challenge must be overcome.

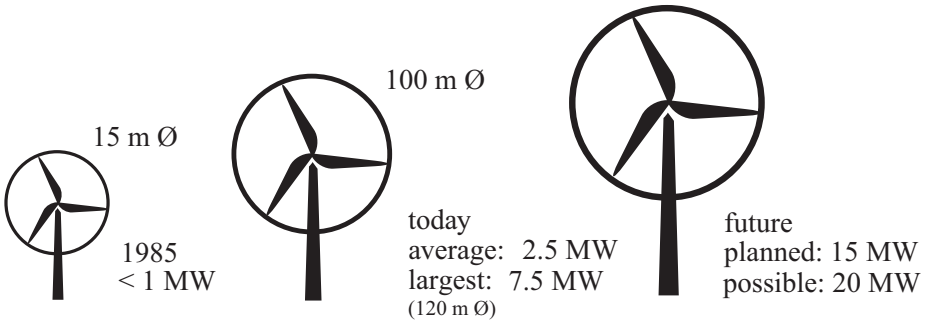

Figure 2.1: Past, present and future wind turbine sizes and power (EWEA).

2.2 Horizontal-axis wind turbine (HAWT)

Wind turbines are divided into two major groups: Horizontal-axis wind turbines (HAWT) and vertical-axis wind turbines (VAWT). The distinction is the orientation of the rotor relative to the ground, and thereby

(a) Horizontal-axis wind turbine. (© Bob Collowan, CC-BY-SA-3.0, Wikimedia Commons)

(b) Vertical-axis wind turbine. (W.Wacker, Public domain, Wikimedia Commons)

Figure 2.2: The two major types of wind turbines.

wind direction. This thesis only considers the horizontal-axis wind turbine as this is the only one utilizing an active yaw system. The horizontal-axis wind turbine is the conventional wind turbine evolved from wind mills. These wind turbines have the rotor axis parallel with the wind direction. The energy is extracted from the wind by the rotor, which turns a shaft. The mechanical energy in the shaft is transferred to electrical energy using a generator. [28, p. 35-36] The main components of a horizontal-axis wind turbine are the rotor, drive train, yaw system, nacelle and tower structure. The rotor consists of the blades, hub and aerodynamic controls. The drive train includes the gearbox (if any), generator, mechanical brake, main shaft and couplings connecting them. The housing for the drive train is called the nacelle. The components of a yaw system vary if the yaw system is active or passive, but all yaw systems have a yaw bearing. In addition, an active yaw system will have a yaw drive installed. Conventionally the yaw drive consists of a gear rim, gear motor, yaw brake and yaw damper. The nacelle includes the main frame and nacelle cover, holding and protecting the drive train and the rotor. The tower structure includes the tower, foundation and (if any) the means of self-erection. The components of the wind turbine can be seen in Figure 2.3 and are more diligently described in the remainder of this chapter. [17]

2.2.1 Rotor

The rotors purpose is to extract energy from the wind and transform it into rotational energy. Wind turbines have to operate under conditions that include steady as well as periodical and stochastically variable loads. These loads occur over a large number of cycles, which make fatigue a large concern in the design of the rotor. [17, p. 276] The following three paragraphs will discuss the major parts of the rotor: the blades, aerodynamic controls and hub.

Blades The blades are the most important part of the rotor, as they convert wind energy into mechanical energy. The major design considerations for blades are the aerodynamic performance and structural strength. Underlying all design decisions made for these two areas, is the need to minimize the life time cycle cost of energy. The rotors ability to convert wind energy to mechanical energy efficiently relies heavily on blade design.

Aerodynamic controls To ensure efficient, constant and safe energy production with wind turbines, it is desirable to have control over the aerodynamic performance of the rotor. This is achieved by altering pitch of the blades, move aerodynamic control surfaces, or with passive control. The pitching of the blades is done with a mechanism in the hub. Control surfaces come in several forms, because they have to be designed

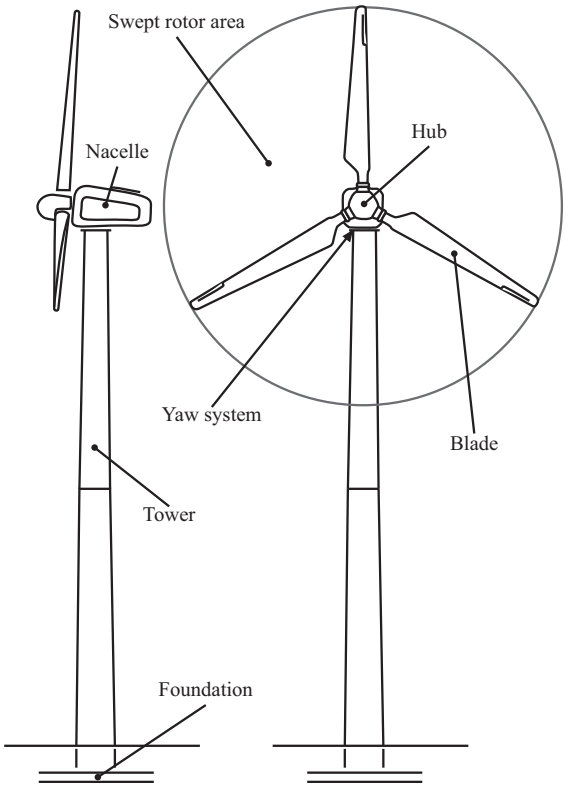

Figure 2.3: Main components of horizontal-axis wind turbines. This particular wind turbine has three blades. [28]

with respect to the shape of the blades. An example of passive control is the use of blades, which are curved upwind when unloaded. When loaded they will bend back and change the aerodynamic performance.

Hub The hub is the connection between the blades and the drive train. It is normally made in steel and has to transfer all the loads created in blades to main shaft and main frame.

2.2.2 Drive train

Components of the drive train convert rotational, mechanical energy into electrical energy. Major components of the drive train are main shaft, couplings, gearbox, generator and brakes. These components are described in the following paragraphs.

Main shaft The main shaft, also known as low-speed shaft or rotor shaft, connects the hub to the generator or gearbox, if the drive train has a gearbox. It is normally made out of steel and dimensioned to withstand the large torque and bending moment from the rotor. The main shaft is supported by bearings allowing it to rotate freely. Specific design may vary with turbine type and manufacturer.

Couplings The purpose of couplings is to connect shafts. Couplings may also be designed to dampen torque fluctuations. Couplings are mostly used in the connections between the main shaft and gear box, and between the gearbox output shaft and the generator.

Gearbox Between the generator and rotor lays the gearbox. The gearbox has a low-speed/high-torque input shaft, connected to rotor, and a high-speed/low-torque output shaft, connected to generator. The gearbox is one of the heaviest and most expensive components of a wind turbine [17, p. 294]. By use of direct drive generators, the gearbox may be eliminated.

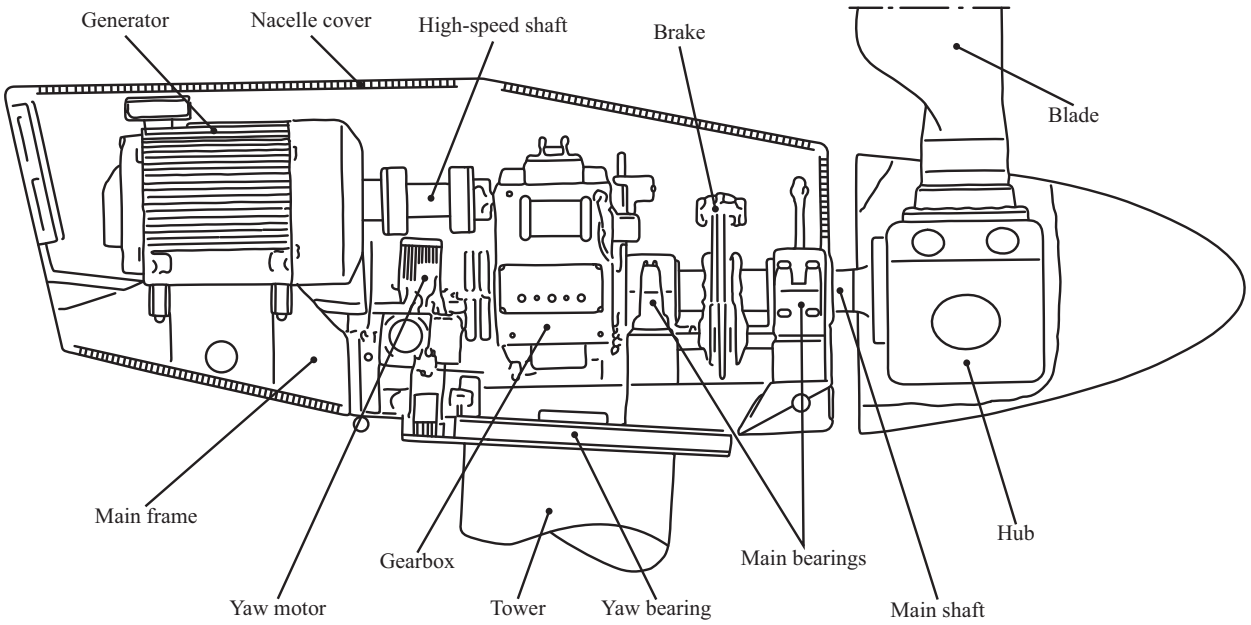

Figure 2.4: Components within a nacelle. This particular nacelle have a gearbox and use gear motors and a pinion-gear rim connection to control the yaw of the wind turbine. [28]

Generator The generator converts the rotational mechanical energy of the rotor into electrical power. Conventionally, until a few years ago, wind turbines only produced power at a constant speed. But as better solutions have been developed, most large scale wind turbines can produce power with variable rotor and generator speed.

Brakes All larger wind turbines have a mechanical brake in the drive train. Most wind turbines have an additional aerodynamic brake. The brakes are used to stop the rotor and hold the rotor still when parked. Disc brakes and clutch brakes are most common in wind turbines. The location of the brakes may be on both the low-speed and high-speed shaft. If the brakes are on the low-speed shaft, they have to exert more torque on the shaft, and thereby be larger. If the brakes are on the high-speed shaft, a lower torque is required to brake, but the gearbox will take load instead, increasing wear of the gearbox.

2.2.3 Nacelle

The nacelle house principal components of the wind turbine and connected to the tower via a yaw system. Components included are the main frame and nacelle cover, which are discussed in the following paragraphs.

Main frame Generator, gearbox and brakes are all mounted on the main frame. The purpose of the main frame is to be a rigid structure, maintaining proper alignment between these components. The yaw system is attached to the bottom of the main frame. Normally, the main frame is a steel casting or weldment.

Nacelle cover The purpose of the nacelle covers is to shield the internal components of the nacelle from environmental factors. Shape of the nacelle is designed to reduce the turbulence behind the wind turbine. The nacelle cover is not a load bearing component and only need enough strength to withstand inflictions from the environment and its own weight. Usually made out of fibreglass, the nacelle cover is light and relatively strong.

2.2.4 Tower structure

The tower structure supports and raises the nacelle and rotor above the ground. Tower, foundation and, if any, means of self-erection are components in the tower structure. These components are discussed in the following paragraphs.

Tower The structural component which lifts the nacelle and rotor above ground is called tower. Normally the tower is at least as high as the rotor diameter. The tower needs to withstand both steady and dynamic loads. Steady loads are aerodynamically generated forces and torques, and the weight of the wind turbine itself. Dynamic loads are generated from the rotor, while rotating. The dynamic load can be critical if the natural frequency of the tower is similar to rotor frequency or the blade-passing frequency [17, p. 304]. Wind turbine towers are usually made of steel, but can also be made in reinforced concrete.

Foundation The foundation is usually a reinforced concrete block to which the tower is mounted. Foundations have to be heavy enough, and buried sufficiently, to keep the wind turbine up-right.

Means of self-erection Some smaller wind turbines have their own means of self-erection. The purpose is to lay the wind turbine horizontally for safety or easier accessibility.

2.2.5 Yaw system

Yaw systems transfers loads from nacelle to tower. The yaw system also enables the nacelle to rotate in relation to the tower, to ensure that the rotor always stays perpendicular to the wind direction or to rotate away from the wind to minimize loads during extreme wind conditions. The major components of the yaw system are explained in the following paragraphs, and more detailed information about yaw systems can be found in Section 2.3.

Yaw bearing The purpose of the yaw bearings is to transfer steady and dynamic loads from the nacelle to the tower.

Yaw drive The purpose of the yaw drive is to control the nacelles orientation around the yaw axis at all times. The yaw drive is made in many different variations. Although they look and work differently, they all have the same features: generate rotational torque, brake and dampen. Conventionally gear motors and a geared rim are components of the mechanism generating torque. For more information about different solutions for yaw drive, see Section 2.3.3. Brakes holds the nacelle when parked and decelerates the nacelle if necessary. Brakes, in combination with dampers, helps take sudden and dynamic high loads away from the yaw drive.

2.3 Yaw systems in horizontal-axis wind turbines

Rotation or yaw of a wind turbine rotates the nacelle and rotor about the vertical axis of the tower. Implementation of a yaw system is used to face the rotor perpendicular to the wind direction. Inspections, maintenance and other similar scenarios require the possibility of locking the yaw system. Yaw systems in general differ between active and passive yaw systems. Active systems rotate the nacelle with help from actuators and are used on larger wind turbines that require large torque. Passive yaw systems utilize force created by the wind, correcting the orientation of the rotor.

2.3.1 Traditional yaw systems

Traditionally, yaw systems for a wind turbine with active yaw, consists of a gear rim and a number of gear motors. Motors are mounted to the nacelle, and the gear rim to the tower, through the yaw bearing. The yaw motion is generated by the torque between nacelle and tower, transferred through several pinion-gear connections. Electrical motors are most commonly used, although some suppliers deliver wind turbines with hydraulic active yaw control. Continuous small yaw adjustments are required to adjust for the change in wind direction, resulting in rapid wear in local areas along the gear rim. [17, p. 301] Because the tower and nacelle are flexible structures, the individual meshes between the gear rim and pinion will be different. Therefore the yaw motors do not share the torque equally. This will increase both wear on specific teeth on the gear rim, and risk of motor failure. [26] Active yaw systems using a pinion-gear connection to transfer torque between the nacelle and tower allow for some movement, due to backlash. This connection is often supported by breaks and/or dampers which take up the forces from strong gusts of wind, so that they do not overload the pinion-gear connections. In some yaw systems, brakes are engaged while the nacelle is being

rotated by the yaw drive. This is done to avoid damage to gears and/or motors, as the brakes will take some of the load if a sudden gust of wind should strike the rotor.

2.3.2 Types of yaw systems

This section gives a short description on existing categories of yaw systems. The most commonly adopted strategy for yaw systems is the friction damped yaw.

Fixed yaw The system consists of brakes that prevent unwanted movement in the nacelle acting on a brake disc. Numbers of brakes installed varies, e.g. six brakes on a wind turbine with rotor diameter of 60 [m]. Motors are working against softly clamping brakes, securing a smooth yaw motion.

Friction damped yaw Three different strategies for damping with use of friction are possible with friction damped yaw systems. First option mounts the nacelle on to friction pads were actuators are working against the friction. This option allows slip during extreme loads. Second option, the nacelle is mounted on a bearing with rolling elements. Applied friction works the same way as the fixed yaw system. The last one uses a three-row, roller type, slew bearing with pads of elastomer instead of rolling-elements.

Soft yaw The system uses no yaw brakes during operation, but is heavily hydraulically damped. Lines from each side of hydraulic motors run through a choke valve and into accumulators that dampens sudden yaw movements.

Damped free yaw Almost the same as soft yaw, but with hydraulic pipes connected together in a loop via a check valve. The set-up gives good stability in sudden yaw movements derived from gusts.

Controlled free yaw Same as damped free yaw, but with a higher demand in yaw corrections when necessary.

2.3.3 State of the art

Although most wind turbines still utilize a gear connection to transfer torque in a wind turbines yaw system, the advantages of utilizing a hydraulic solution are many.
High torque, low velocity hydraulic motors is used to simplify a yaw control using gear connections. Avoiding a gearbox with very large reduction rate for each motor is advantageous, but do not solve problems with high point loads in gear connections
Research has lately gone in to developing large hydraulic motors in the shape of a ring. This would replace the entire yaw system with one hydraulic motor. The stator of the motor is bolted directly to the tower and the rotor to the nacelle, or opposite, avoiding all gear connections. The motor can be build to deliver necessary extreme torques, by increasing the maximum pressure in the motor. The motor could also work as brake and damper. [26] In spite of generating large torques, the system is not modular. Problems with downtime remain unsolved.
Mervento has developed a wind turbine, 3.6-118, for cold and harsh environments. Hydraulic cylinders are used to control the active yaw of this wind turbine as illustrated in Figure 2.5c. This method use brake callipers in combination with hydraulic cylinders thereby combining the yaw drive and brakes. [16]

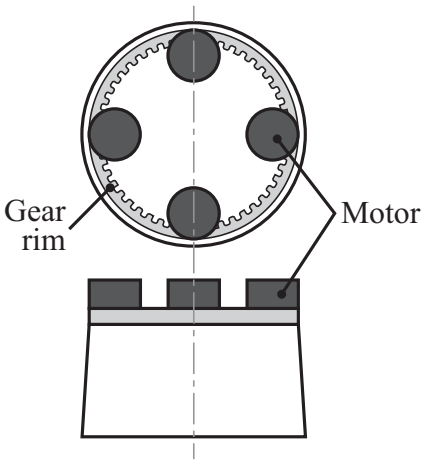

(a) A pinion-gear rim yaw system, with four hydraulic motors connected to the nacelle. The gear rim is connected to the tower. [26]

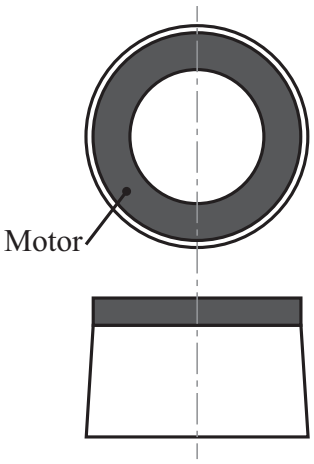

(b) Single large hydraulic motor. The stator is connected to the tower, and the rotor to the nacelle. [26]

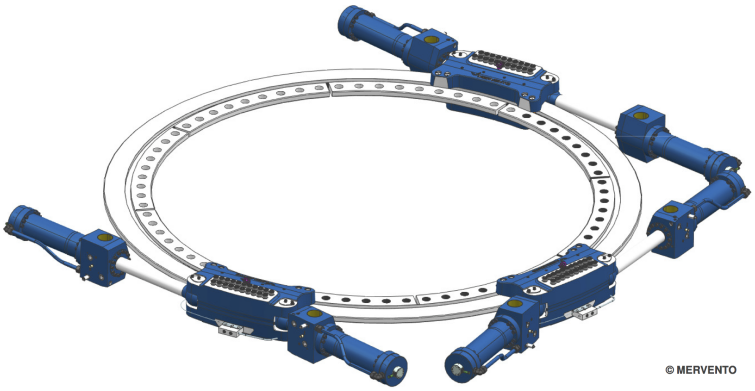

(c) Hydraulic yaw system, used in the wind turbine Mervento 3.6-118. [16]

Figure 2.5: State of the art solutions for hydraulic yaw drive of horizontal-axis wind turbines.

Chapter 3

Design and development

Three ideas stated in the problem description (Section 1.1), are investigated. If an idea meets the set requirements (Table 1.1), it will be further developed. Going from a simple sketch, or just a thought, into a 3D-model and technical drawings of a mechanism with approved functionalities, and as few uncertainties as possible. This chapter does not include the development of a full-worthy concept, because the ideas are only developed in such extent that they are possible to model and simulate. This chapter cover a more general development, with a focus on implementation in a mathematical model.
Product development, as conducted in this project, is shown in Figure 3.1. Starting with a problem description and product requirements, a number of ideas for solving the problem are developed. If an idea fulfils the requirements, it is developed into a general design. This is then modelled as a 3D-CAD model to better see the basic structural and functional properties of the idea and sort out the errors. If the general design fulfils the requirements, the idea is more thoroughly investigated with mathematical modelling determining the details of the idea. If this final investigation determines the idea as feasible, the idea becomes a concept. As Figure 3.1 illustrate, our product is on the on border between a concept and developed idea.

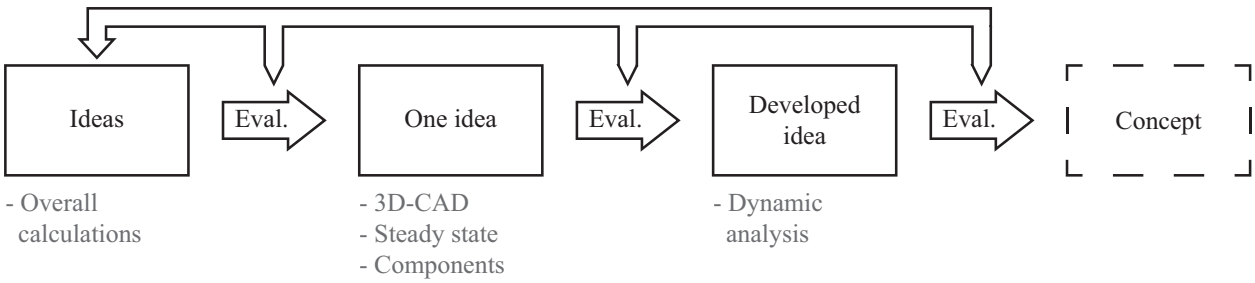

Figure 3.1: Description of milestones in the process of developing a product.

3.1 Piston driven yaw mechanism

In collaboration with supervisor Johnsen, three ideas for piston driven yaw mechanism are developed from the problem description. Ideas have to be tested, and one is further developed as it is the only one meeting the requirements with a simple and safe construction. The ideas were investigated on request of supervisor Johnsen, which has the last word in discarding or further developing the ideas. This section describes the analysis performed to assist and consult Johnsen in his decision. The best viable concept is further investigated and developed in the remainder of this chapter.

3.1.1 Radial engine

This idea is based on radial engines, frequently used in aircraft before turbine engines became predominant. It consists of n number of hydraulic cylinders mounted with one end to a circular frame with equal angular spacing. The other end of all the cylinders is mounted to a crank shaft. This configuration can be seen for three and five cylinders in Figure 3.2a and 3.2b, respectively.

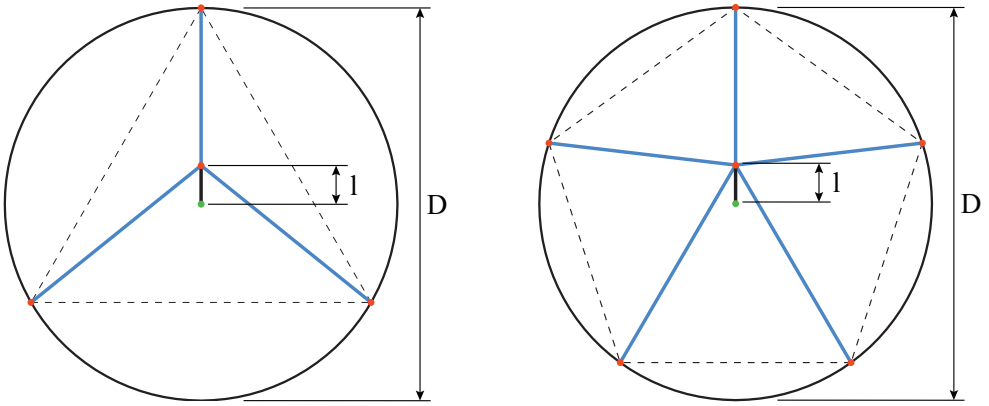

(a) Radial engine with three cylinders. (b) Radial engine with five cylinders.

Figure 3.2: Hydraulic cylinders (blue lines) mounted with equal angular distance on the outer perimeter (black circle) at one end, and to a crank shaft (black line) at the other end. Red and green dots represent hinged joints, where the green is the centre of rotation.

The first and most critical uncertainty of this idea is its ability to generate the required torque of 8[MNm]. This can be investigated by finding the largest lever arm possible. The hydraulic cylinders limit how large the lever arm can be, due to their ratio between length when extracted and retracted. This ratio often lies in the area from 60% to 70% and is defined in Equation 3.1. In the following calculations the ratio is set to $\kappa_{cyl} = \frac{2}{3}$. Equation 3.3, derived from Equation 3.2, gives the maximum leverage arm, from the cylinder ratio,κ_{cyl}, and outer perimeter diameter, D. This equation can be expressed as an equation giving the maximal leverage arm length. For the given cylinder ratio, κ_{cyl}, the leverage arm can be no longer than $l_{max} = \frac{D}{10}$.

$$\kappa_{cyl} = \frac{L_r}{L_e} \tag{3.1}$$

$$\frac{D}{2} - l > \kappa_{cyl}(\frac{D}{2} + l) \tag{3.2}$$

$$l < \frac{D - D\kappa_{cyl}}{2\kappa_{cyl} + 2} \tag{3.3}$$

As the outer perimeters of the system are limited by the problem description (Table 1.1), the maximum length of the leverage arm equals 350[mm]. This solution loses a lot of efficiency because all cylinders cannot work optimally at all times. Each hydraulic cylinder has two points throughout one cycle of rotation where they are positioned co-linear with the crank shaft, and must be passive. With a piston diameter of 300[mm] and a pressure of 350[bar], the solution with three cylinders generates 1.35[MNm] and the one with five cylinders generates 2.58[MNm].
Even though this concept has many advantages in simplicity, ease of assembly/disassembly and accessibility, it is not feasible for this purpose as the torque generated is far below the requirement. The project group and industrial supervisor Johnsen, on behalf of Incepti AS, made the final decision of discarding this idea.

3.1.2 Cogwheel

This idea consists of an even number of hydraulic cylinders mounted in pairs with one end mounted to the tower. The other end of the two paired cylinders is connected to each other. This point is free to move and holds a connector which allows it to connect to the nacelle at a selection of interaction points, equally spaced around a perimeter. This allows the hydraulic cylinders to have a cyclic motion, where they push the nacelle an angular distance, reposition and push the nacelle again.
This idea is very customizable, which makes it able to supply the required torque of 8[MNm] in several variations. The concept will not be further developed, because of the complications with the interaction between hydraulic cylinders and nacelle. This connection will be subject to heavy wear as well as the initiation of contact would require control of high accuracy. The system would need an assisting cylinder to guide the hydraulic cylinders into the notches on nacelle. And without proper control of these cylinders,

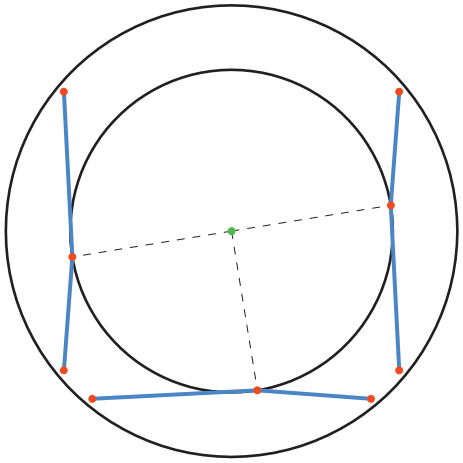

(a) Cogwheel idea with six hydraulic cylinders (blue lines) mounted in pairs. One end hinged to the outer perimeter (black ring) and the other to each other, in interaction with the inner perimeter (black ring). The red and green dots are hinged joints, where the green indicates the centre of rotation.

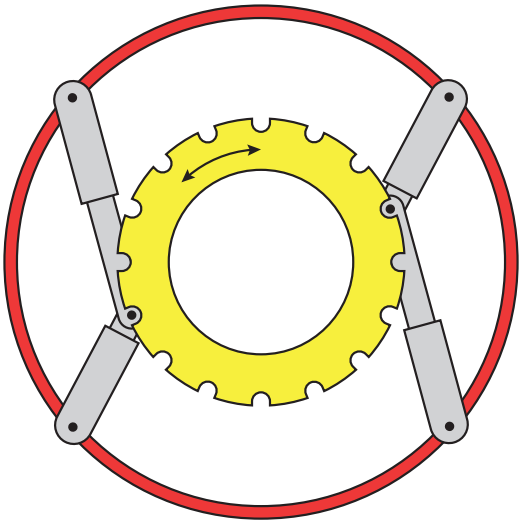

(b) Illustration of an example cogwheel mechanism. Red and yellow indicate the difference between the two members rotating in relation to each other. Hydraulic cylinders are coloured grey.

Figure 3.3: The cogwheel idea illustrated to show both geometry and function.

the system will have a high risk of singularity, and the hydraulic cylinders jamming. The cogwheel would be under high pressure and the design would have to take extra care to wear in the interaction points. The project group and industrial supervisor Johnsen, on behalf of Incepti AS, made the final decision of discarding this idea.

3.1.3 Grip and rotate

The idea of gripping something and then rotate it is an action which falls naturally to humans. In this context the two tasks are carried out using brakes to grip and hydraulic cylinders to rotate. This idea exists today, developed by Mervento and present in the wind turbine: 3.6-118. Mervento's solution is described in Section 2.3.3. This mechanism is inspiration to the alternative idea presented by Incepti AS. The new idea consists of a number of hydraulic cylinders mounted between two freely rotating discs, which then may rotate relative to each other. The discs can grip on to either the nacelle or tower, using hydraulic brake callipers. As one disc clamp onto the tower and the other to the nacelle, a controlled relative motion between the tower and nacelle is possible. The hydraulic cylinders are controlled so that the two discs move relative to each other, which in turn rotate the nacelle relative to the tower.
The yellow and red brakes shown in Figure 3.5b are connected to either the inner or outer disc. The underside of the yaw mechanism is similar to the top as shown in Figure 3.7. The yaw mechanism is able to rotate the nacelle with help from cylinders and brakes, explained in four simplified stages below, and illustrated in Figure 3.6. Description represents counter-clockwise direction, clockwise rotation requires opposite grips and push/pull from cylinders.

Stage 1 Brakes are released. Top brakes connected to inner disc are clamping. Bottom brakes connected to outer disc are clamping.

Stage 2 Cylinder pair's pulls/pushes nacelle and inner disc in counter-clockwise direction.

Stage 3 Brakes are released. Top brakes connected to outer disc are clamping. Bottom brakes connected to inner disc are clamping.

Stage 4 Cylinder pair's pushes/pulls nacelle and outer disc in counter-clockwise direction.

After the fourth stage, the yaw mechanism is back to its starting point and ready to repeat the sequence. The required angular rotation of $3 \cdot 360[^\circ]$ is achievable and will only be limited by eventual hoses or wires between rotating and stationary members. This is though a solvable problem, with several existing solutions. Cylinder

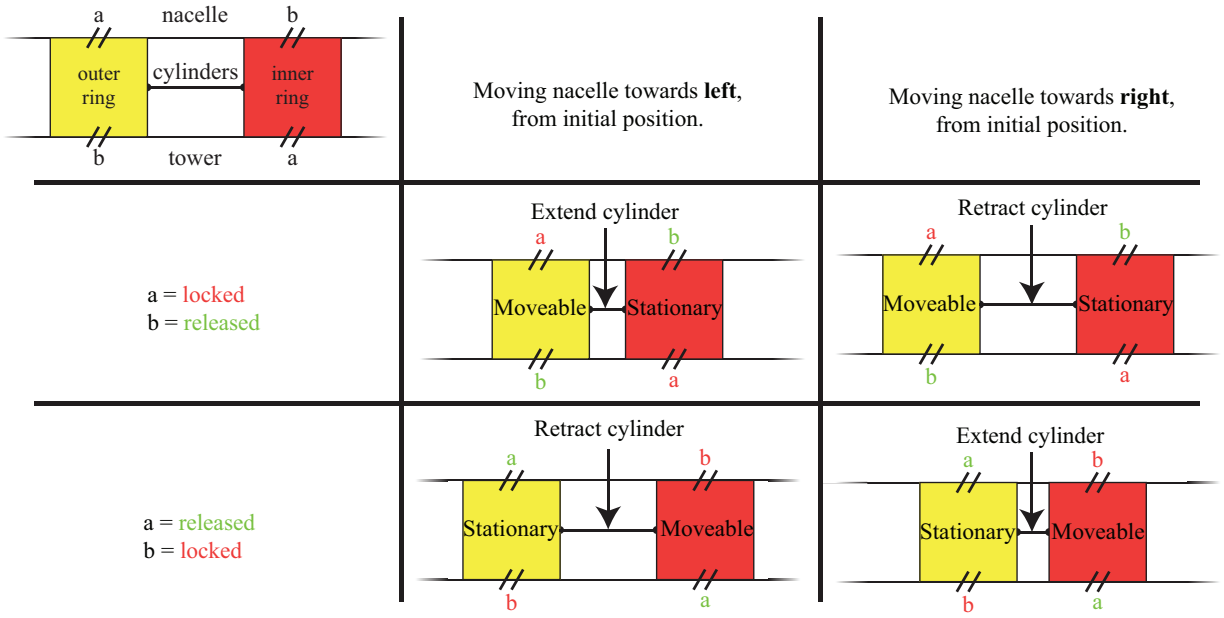

Figure 3.4: Grip and rotate mechanism illustrated in as a simplified, translational version.

placement and their connection to inner and outer disc are shown in Figure 3.5a. More on configurations regarding cylinder placement is described in Section 3.3.
Hydraulic brakes on both top and bottom discs are coupled with a frictional connection to either inner or outer disc. When performing yaw motion, only half of the brakes on either side will be used. One sequence, as described in four steps above, will result in an angular rotation of the nacelle, relative to the tower, of approximately 18[°]. The angular rotation is restricted by space between brakes, stroke of cylinders, space requirements in disc assembly and levers connected to cylinders and outer disc. A cross-sectional isometric view of the yaw mechanism, visualizing connection between brakes and discs, is shown in Figure 3.7.
Among the presented three piston driven yaw mechanisms, grip and rotate represents itself as the best solution in performing yaw motion to a wind turbine. The project group and industrial supervisor Johnsen, on behalf of Incepti AS, concludes grip and rotate is viable and suitable for further development.

3.2 Disc profile

The two discs are the two freely rotating parts of the mechanism. They are connected to each other with hydraulic cylinders and, if necessary, a bearing connection. Brake callipers are used to connect and disconnect the discs to both the nacelle and tower. The discs must have interfaces to hold all required components and still be compact. Only the outline for a profile for these two discs is discussed in this thesis. The idea developed is meant as a proof of concept. Therefore, no evaluation of the structural strength and stiffness of the discs is conducted, but is taken into consideration when discussing advantages and disadvantages with different variations.

3.2.1 Specification

Both of the discs are loaded similarly. Hydraulic cylinders connect the two discs are used to generate a torque between them. The brake callipers, when activated, induce a frictional torque which acts in the opposite direction of the torque generated by the hydraulic cylinders. The two discs will therefore be subjected to torsion, radial stress and some minor axial stresses.

3.2.2 Disc profile variations

Disc profile is referred to as the cross-section cut in the rz-plane (polar coordinates with origin in disc centre). Example of disc profiles can be seen in Figure 3.8 and 3.9. The profile has to be designed in a way which

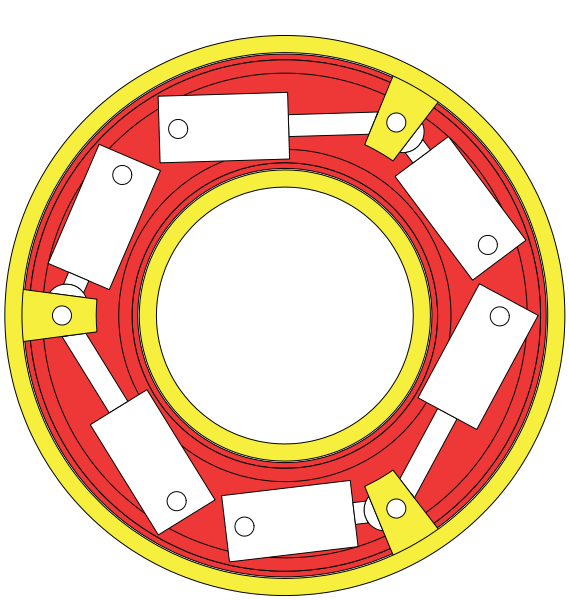

(a) Principal drawing representing hydraulic cylinder placement and their connections to inner (red) and outer disc (yellow).

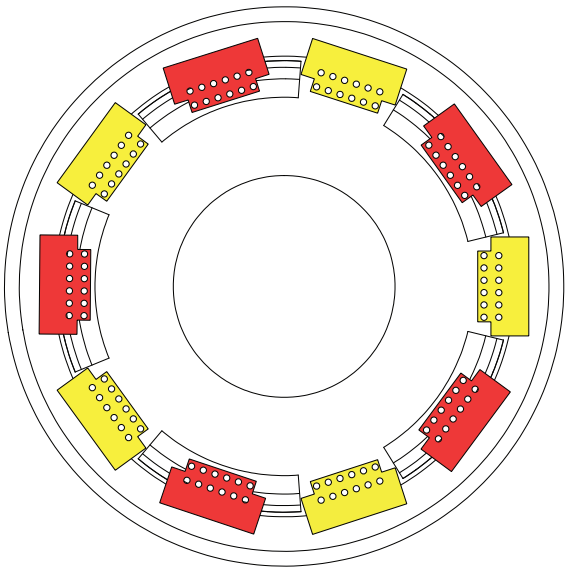

(b) Principal drawing of the yaw mechanism from a top-view. Red colour represents hydraulic brakes connected to inner disc. Yellow ones are connected to outer disc.

Figure 3.5: Illustrated geometry and function of the grip and rotate idea.

uniformly distributes the radial and axial stresses in the discs. It is not only required that each disc may do this individually, but a stable and secure connection between the two discs are also required.

Draft

The disc profile shown in Figure 3.8 is made mainly to investigate space required for components and size of the discs. The model gave insight in future improvements and how maintenance can be performed. The concept also gave valuable information on how important access to cylinders can be.

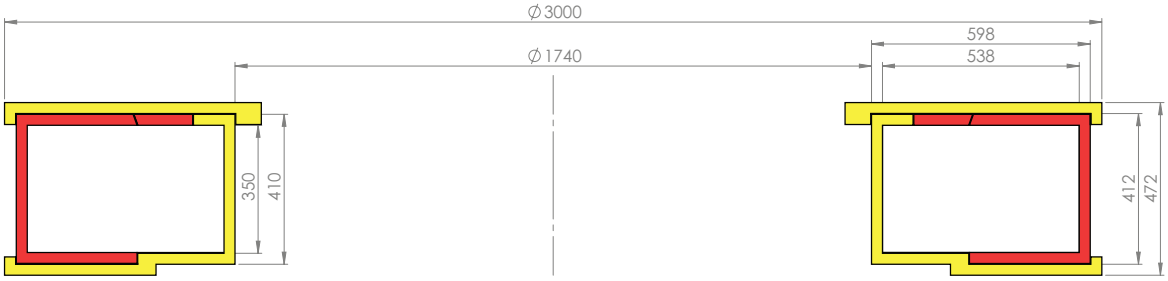

Figure 3.8: Draft of the disc profile. Red and yellow represent the inner and outer disc, respectively.

Pros:

- Spacious.

Cons:

- Limited access to cylinders.
- Weak structure.

Box girder

The disc profile is based on box girders. These have the feature of handling stresses uniformly and reacting well to torsion and bending. They are a more efficient version of the very common H-beam, but will require

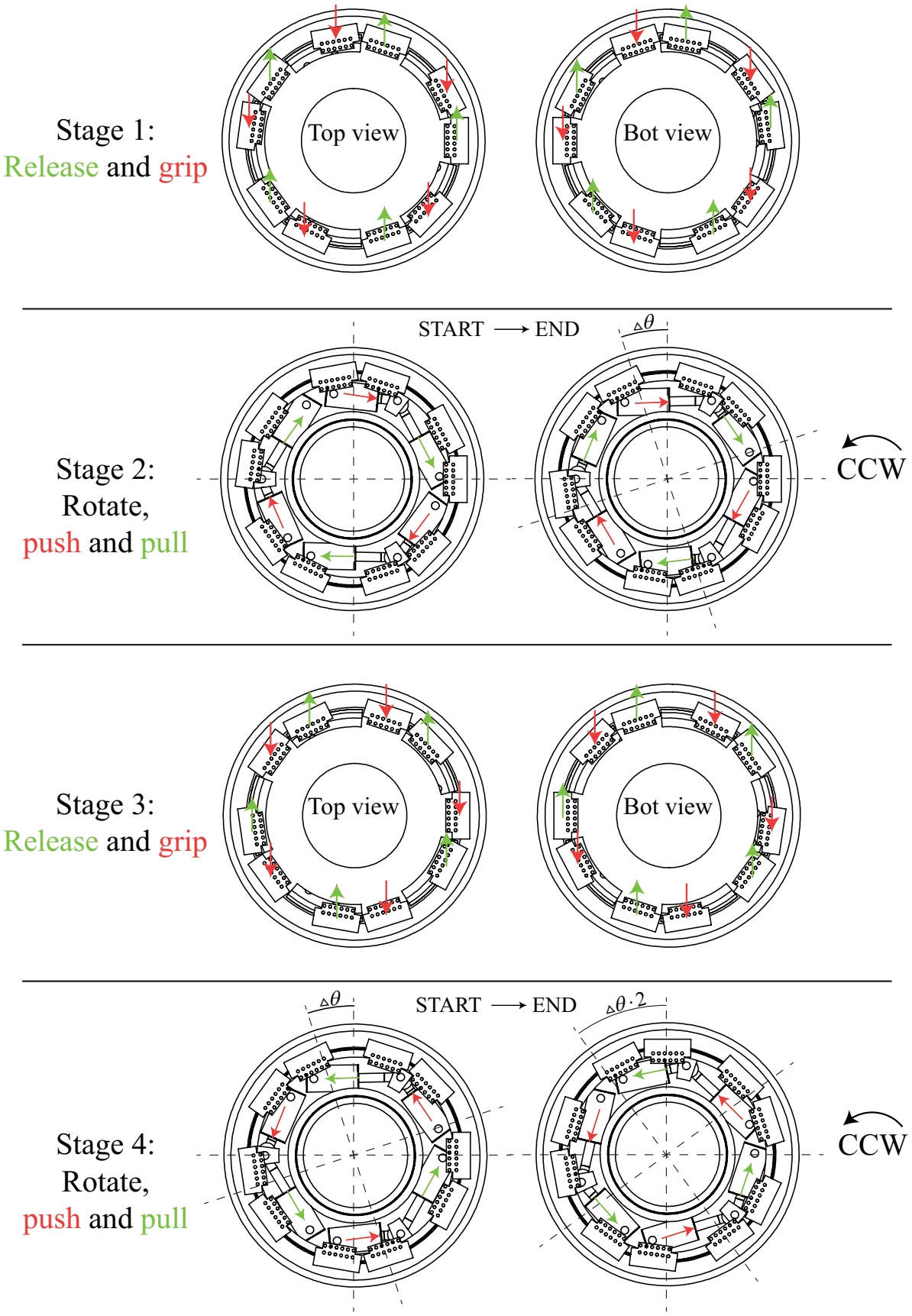

Figure 3.6: Grip and rotate sequence explained, divided into four stages, rotating in counter-clockwise direction. Bottom view in stage one and three is top view flipped horizontally. Description represents counter-clockwise direction, clockwise rotation requires opposite grips and push/pull from cylinders.

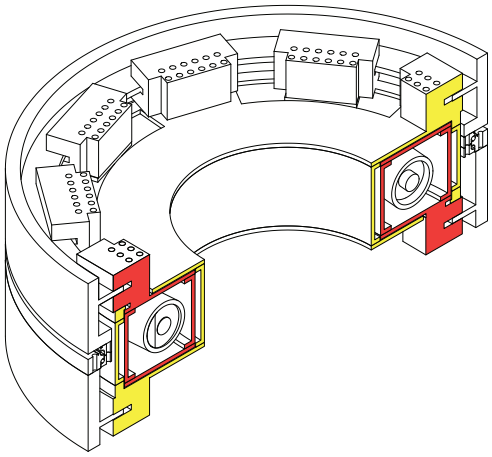

Figure 3.7: Principal cross-section drawing of the yaw mechanism from an isometric view. Red colour represents inner disc and shows one of the hydraulic brakes connected to it. Yellow colour shows outer disc and a hydraulic brake connected to it.

more material. The features of the box-profile will be weakened, as it is divided into several parts. Figure 3.9 show both rings consisting of a bottom-, top- and two side-elements. These are bolted together, making a weaker structure, but enables the ability to disassemble the system for service after installation. This is a highly attractive feature. The discs support each other through slide bearings or plates, which will help strengthen the overall structure. Benefits of using a cylindrical shape will help with the very dominant torsion. Cylindrical shapes are excellent at uniformly distributing stress due to torsion.

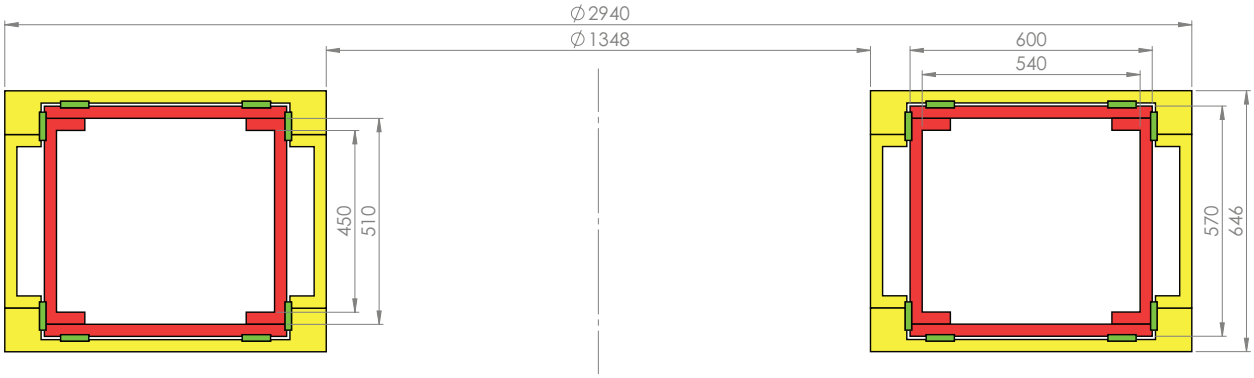

Figure 3.9: Disc profile based on box girder concept. Red colour represents inner disc, yellow is outer disc and green are bearings.

Pros:

- Uniform stress distribution
- Easy assembly and maintenance.

Cons:

- More material required.
- Difficult mounting of brake callipers.

3.3 Hydraulic cylinders

The purpose of the hydraulic cylinders is to rotate the nacelle about the centre of the tower. This section discuss how the cylinders should be mounted within the system to best complete this task. The placement of the hydraulic cylinders is crucial to ensure maximal efficiency throughout the entire stroke of the cylinder. The two main factors in achieving this are: (1) minimizing the dimensions of the cylinders without sacrificing power and (2) the orientation of the cylinders should aim to obtain the largest lever arm possible.

3.3.1 Specifications

The placing of cylinders must be done within the boundaries of the discs.

Table 3.1: Specifications related to the placement of the hydraulic cylinders.

Symbol	Name	Value	Comment
T_{req}	Torque	$8 \cdot 10^6$ [Nm]	Torque between the two discs, generated by the hydraulic cylinders.
θ_r	Angular displacement	20[°]	Angle of rotation between stator and rotor.
ω_r	Angular velocity	$0.37[\frac{^\circ}{s}]$	Required angular velocity.

3.3.2 Hydraulic cylinders variations

Four different concepts for the layout of the hydraulic cylinders were developed. The hydraulic cylinders were implemented in a 3D-model to ensure they would fit within the discs and utilize its stroke. This gave a great basis to investigate different layouts, their advantages and disadvantages.

Tangent and equally spaced

The most obvious solution is to mount one end of the cylinders to the stator, and the other end to the rotor, as illustrated in Figure 3.10. This is done in such a way that each cylinder is tangent to the circle of rotation midway through its stroke. The system will be most efficient when the cylinders are mounted like this. The cylinders are equally spaced around the centre of rotation. The stress in rotor and stator will be uniform due to symmetry, as long as the number of cylinders is an even number.

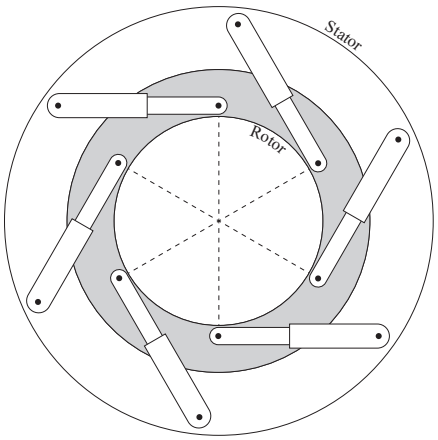

Figure 3.10: Six hydraulic cylinder placed with a 60[°] shift in angle.

Pros:

- Uniform stress distribution in the rings.
- If the stroke is short, one can stack many cylinders.

Cons:

- The torque generated by the cylinders is not the same for each direction of rotation, given the same hydraulic pressure.

Inverted

This layout is a variation of the previously described layout, Tangent and equally spaced. By mounting every other hydraulic cylinder opposite of the others, as illustrated in Figure 3.11, the torque produced for each direction of rotation will be the same, as long as the number of cylinder is an even number. Because the cylinders do not produce the same amount of force at a given time, the stress distributions will not be uniform in this case. Non-uniform deformations are not desirable in a rotary system, as the system may jam. When the barrels of all the cylinders are mounted to the same unit (stator/rotor) as the hydraulic power

unit (HPU), one can use metal pipes for the hydraulic fluid. For this layout, one has to use tubes and some sort of flexible support for the tubes, for those cylinders which are mounted in reversed orientation.

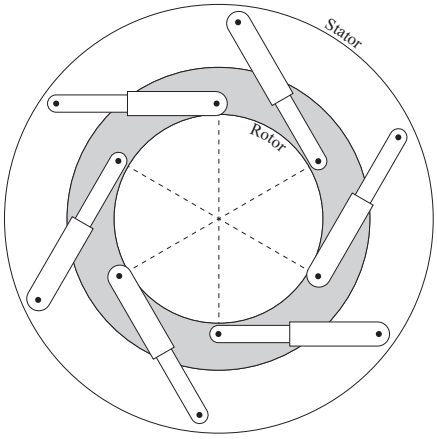

Figure 3.11: Six hydraulic cylinder placed with a 60[°] shift in angle. Every other cylinder is mounted backwards.

Pros:

- If the stroke is short, one can stack many cylinders.
- The torque generated by the cylinders is the same for each direction of rotation, given the same hydraulic pressure and an even number of hydraulic cylinders.

Cons:

- Non-uniform stress distribution in the rings.
- It is advantageous to have the barrel of all hydraulic cylinders mounted to the unit which holds the HPU.

Lever arms

By equipping the rotor with extra long lever arms, as illustrated in Figure 3.12, one can obtain more torque from a layout very similar to the layout in Tangent and equally spaced. Complications with adding these extra lever arms, is reduced space. This limits the size of the cylinders further and will make the assembling and disassembling of the system more difficult.

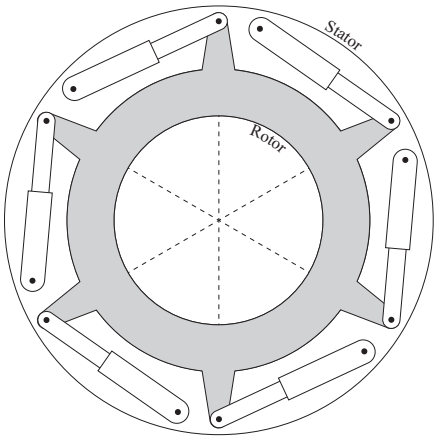

Figure 3.12: Six hydraulic cylinders placed with a 60[°] shift in angle. Lever arms give extra torque.

Pros:

- Uniform stress distribution in the rings.
- The cylinders will give more torque to the system, due to longer lever arm.

Cons:

- The torque generated by the cylinders is not the same for each direction of rotation, given the same hydraulic pressure.
- The lever arms will be subjected to large bending moments.

Pairs

As long as one use an even number of cylinders, one can mount them in pairs, as illustrated in Figure 3.13. This will pay off in more even force distribution and the same torque independent on direction of rotation. When the cylinders are mounted in pairs and work together, the undesired radial forces will somewhat cancel each other out. This layout would limit the number of cylinders one can use, as it is a very space-inefficient layout.

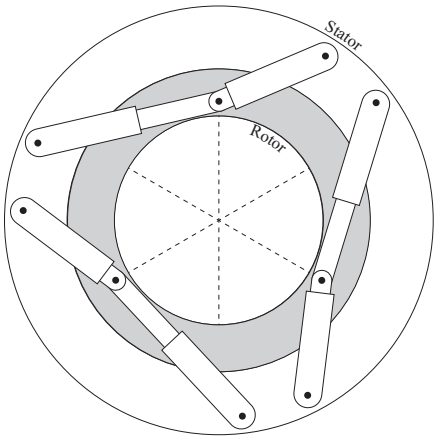

Figure 3.13: Six hydraulic cylinders placed in opposing pairs, with a 120[°] shift in angle.

Pros:

- Partially cancellation of radial forces.
- The torque generated by the cylinders is the same for each direction of rotation, given the same hydraulic pressure.

Cons:

- High tangential forces in the lever arms.
- Not uniform stress distribution in the rings.

3.4 Yaw bearings

Yaw bearings used for this project are all slew bearings. These are bearings which allow a load to rotate on top of another object. They are great at handling large axial loads, minor radial loads and tilting moments. This concept uses several slew bearings: a main yaw bearing between tower and nacelle, slewing bearing between the outer ring and tower, and slewing bearings between the outer and inner ring. These have different requirements, i.e. axial load, size and friction. The main yaw bearings purpose is to transfer loads from the nacelle to the tower. This must be done while maintaining controlled and safe rotation. The bearing must handle the weight of the nacelle, as well as changing loads from wind, without heavy wear or slack. The weight of the nacelle is assumed to be approximately 230[tonne], this is an estimation based on data from several existing wind turbines. The bearings between the rings and tower do not have to handle loads as large as the main yaw bearing. The bearing between the outer ring and tower mainly have to support the axial load from the mass of the two rings (approximately 8.8[tonne]) and some minor radial loads. The bearings between the two rings have to transfer loads between the rings. These loads include the mass of the inner ring (approximately 3.5[tonne]) and the radial loads generated by the hydraulic cylinders.

3.4.1 Specification

Several different types of bearings have been discussed. It is advantageous to consider using a number of different types of bearings for the different bearing connections, as the specifications are quite dissimilar. The specifications for the bearings are given in Table 3.2.

Table 3.2: Specifications relevant to the main yaw bearing.

Symbol	Name	Value	Comment
m_n	Mass of nacelle	230000[kg]	Mass of nacelle, included rotor.
m_i	Mass of inner ring	3500[kg]	Mass of inner ring.
m_o	Mass of outer ring	5300[kg]	Mass of outer ring.
θ_m	Required rotation	$3 \cdot 360[^\circ]$	Required rotation of the mechanism.

3.4.2 Yaw bearing variations

Several ideas were proposed as good yaw bearings for the different bearing connections. Two conventional, ball/roller bearing and slide bearing, and one somewhat more unconventional, hydrostatic bearing. The advantages and disadvantages of these solutions are listed in this section along with a short description of the workings of the bearings.

Ball/roller bearing

A traditional ball or roller bearing requires good attention to detail when designing and producing. Manufacturers of these types of bearings have many years of experience underlining their expertise. This would be an expensive option, due to the time required to produce a bearing of the size needed for this mechanism. On the other hand it is a safe option, as the manufacturers of these bearing have the credibility to guarantee the stable operation of the bearing under the conditions required.

(a) Example of the standard series KD320; a double-row ball bearing slewing ring.

(b) Example of the standard series RD900; a three-row roller bearing slewing ring.

Figure 3.14: Example bearing profiles from TyssenKrupp Rothe Erde India's catalogue. [14]

Pros:

- Compact.
- Low friction.
- Conventional, safe option.
- Will have pre-made and reliable lubrication systems.

Cons:

- Expensive.
- Not modular. Must remove nacelle to replace bearing.

Slide bearing

A slide bearing generally consists of two layered compounds which slide on top of each other. These compounds are often a combination of two or more materials which together give a beneficial effect on friction

and wear rate. By using a slide bearing, one have greater freedom when it comes to size, diameter and general customization of the design, without increasing the cost significantly. Figure 3.15 show a slide bearing from igus Inc. This solution would be better used for the connections with lower axial loads, as the friction could become critical if the load where to large.

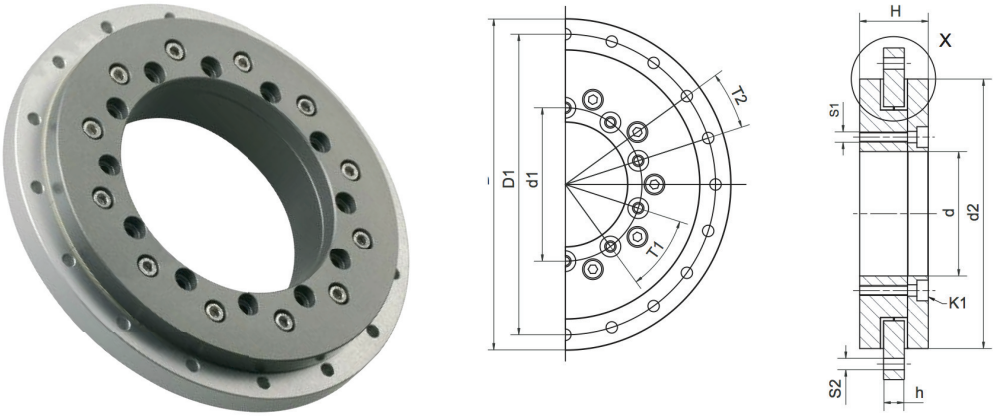

Figure 3.15: Slide bearing, iglide PRT slewing ring bearing. [13]

Pros:

- Compact.
- Inexpensive.
- Could be made somewhat modular.

Cons:

- Larger friction compared to other alternatives.
- Many wearing parts which could shorten the lifetime of the bearing.

Hydrostatic bearing

The idea behind a hydrostatic bearing is to use the hydraulic pressure to lift the two rotating surfaces from each other and create a connection, only limited by fluid friction. This idea will result in a powerful and low-friction bearing. The major disadvantage with a hydrostatic bearing is that it requires a continuous pressure supply to function. In spite of several existing patents and operational versions of hydrostatic bearings, a large amount of testing will have to go into developing a hydrostatic bearing for the purpose of this thesis.

Figure 3.16b is an example of a hydrostatic bearing which takes up both radial and axial forces. This can be transfused into a slew bearing of the type shown in Figure 3.16a. This is conceptual illustration of a hydrostatic bearing, showing only its profile. The yellow and red parts are mounted to the tower and nacelle respectively. The grey area is filled with fluid and is under a variable pressure. The green parts are slide bearings. The blue parts are casing, which together with black gaskets hold the system and fluid in place.

Pros:

- Low friction.
- Is modular. Most parts can be replaced easily.

Cons:

- Require constant hydraulic pressure.
- Leakage of hydraulic fluid.
- Large in size.
- Unusual for this purpose. Testing and approval required.

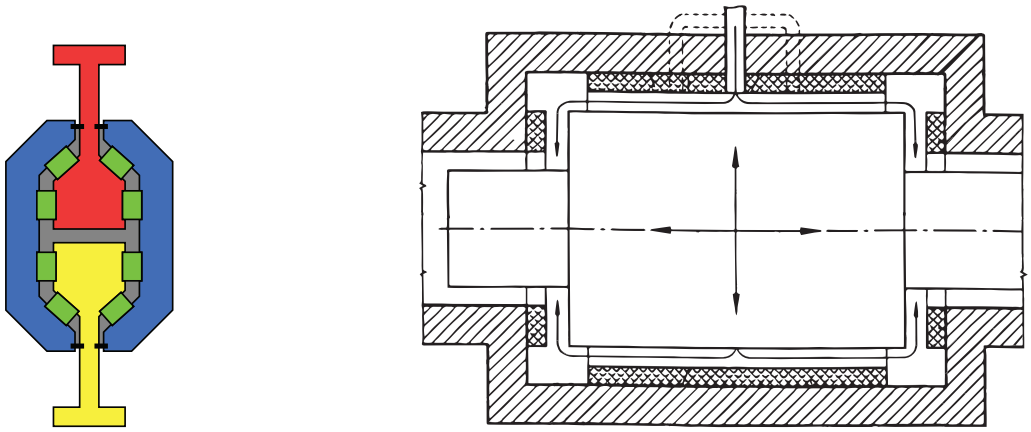

(a) Conceptual drawing of a hydrostatic slew bearing profile.

(b) Rotary axial and radial hydrostatic bearing. Described by M.W.E. Michiels in United States Patent 6761483. [18]

Figure 3.16: Hydrostatic bearings.

3.5 Brake Calliper

The hydraulic brake callipers purpose is to hold the nacelle and tower to the correct disc, to enable the rotation of the nacelle relative to the tower. The callipers have to be made large enough to hold the nacelle when parked, and withstand expected peak torques given in the problem description (Section 1.1). The callipers also have to be designed in a way that allow for good stress distribution, simple and sturdy mounting and a small envelope.

3.5.1 Specification

Brake callipers should be able to deliver a brake torque of $11 \cdot 10^6$[Nm] with parameters given in Table 3.3. The peak torque is used when the wind turbine remains parked in a high wind speed scenario.

Table 3.3: Specifications for brake callipers.

Symbol	Name	Value	Comment
T_b	Required brake torque	$11 \cdot 10^6$ [Nm]	Torque created from cylinders and high wind speeds
μ_b	Friction	0.4 [-]	Expected friction coefficient from brake discs
p_b	Operating pressure	$205 \cdot 10^5$ [Pa]	Hydraulic pressure used in callipers
l_b	Length of arm	1.4 [m]	Length from centre in brake pads to centre of system

3.5.2 Brake calliper variations

The calliper can be made with either one or two pistons. These two variations have the same clamping force, given the same hydraulic pressure, p_b, and brake area, A_b. Discs in the yaw system discussed in this thesis are very large and the loads applied are both high and stochastic.

Single Piston

With one piston, the calliper will use the piston to push the disc against a stationary part of the calliper, as illustrated in Figure 3.17.

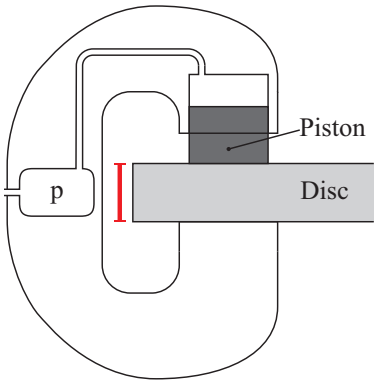

Figure 3.17: External pressure source acting on a single piston, resulting in a brake moment on the brake disc.

Pros:

- Cheaper alternative.
- Produces the same brake force as double pistons.

Cons:

- No vertical movement.
- Risk of deformation due to bending in the disc.

Double Piston

Choosing two pistons, the calliper will use both pistons to clamp against the over- and under-side of the disc with equal force. This will hold the disc, but also allow for small vertical movements, only restricted by friction in the hydraulic fluid, as both pistons are connected to the same pressure source. This can be seen in Figure 3.18.

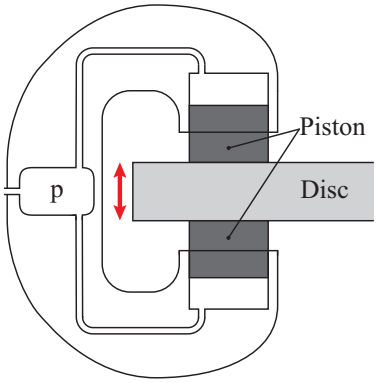

Figure 3.18: External pressure source divided into two chambers acting on two pistons, resulting in a brake moment on brake disc.

Pros:

- Allows vertical movement.
- Avoids deformation and bending in the disc.

Cons:

- Expensive alternative.

3.6 Component calculations

This section includes calculations regarding component sizes and parameters on final concepts. Computed values are mainly parameters needed to run the mathematical model. Essential product requirements can be viewed in Table 1.1.

3.6.1 Hydraulic cylinder

The purpose of the hydraulic cylinders is to rotate the entire nacelle relative to the tower. This section discuss the process of designing a hydraulic cylinder which provide the required force within the requirements to weight, size and other factors. The number of cylinders used, the stroke length and piston diameter are critical factors in the design. The challenge is balancing these, and still obtaining the required angular rotation of the nacelle. By designing the hydraulic cylinders, instead of buying from a supplier, one can get a cylinder tailored to the situation. This is a critical factor as the space internally in the system is limited. The client, *Incepti AS*, have the means to produce the cylinders locally. Calculations of piston size, rod diameter and wall thickness are discussed in this section to get an insight in the envelope of the cylinders. Some general data used throughout the calculations related to the hydraulic cylinders can be found in Table 3.4.

Table 3.4: Frequently used parameters in the design-calculations for the hydraulic cylinders.

Symbol	Description	Unit	Value
T_{req}	Required combined torque from all hydraulic cylinders	$[Nm]$	$8 \cdot 10^6$
p_c	Operating pressure for hydraulic cylinders	$[Pa]$	$350 \cdot 10^5$
r_c	Normal distance from rotational centre to hydraulic cylinder	$[m]$	1.0

Number of cylinders

The number of cylinders is found from an initial calculated guess. The preferred solution for the cylinder layout is a combination of *Pairs* and *Lever arms*, from Section 3.3. An initial guess for how many cylinders that is required can be made from the desire to have a cylinder diameter of less than 350[mm] and a leverage arm for the cylinders equal to approximately $r = 1$[m].

$$\begin{aligned} n_{cyl} &= \frac{T_{req}}{r_c p_c A_c} = \frac{4T_{req}}{\pi r_c p_c {d_p}^2} \\ &= \frac{4 \cdot 8 \cdot 10^6[\text{Nm}]}{\pi \cdot 1[\text{m}] \cdot 350 \cdot 10^5[\text{Pa}] \cdot (0.250[\text{m}])^2} \\ &= 4.65 \end{aligned} \tag{3.4}$$

A rough approximation, as shown in Equation 3.4, is performed to identify a guiding value for the number of cylinders. Because of the properties of the preferred cylinder layout, an even number of cylinders are required. That is why a number of cylinders equal to $n_{cyl} = 6$ is a good initial guess.

Piston size

The study of alternative piston driven yaw mechanisms has shown the importance of a large lever arm to acquire the torque in demand. From this concept, the lever arm will vary throughout the cycle of rotation. This have to be investigated, to ensure that the torque will not drop below the required 8[MNm] throughout the stroke. Figure 3.19a show the basic lengths and angles of the mechanism. Notice that the system consists of three pairs of cylinders, as pictured in Figure 3.19a. Lengths and angles are known, except for θ_1, θ_2, s_1 and s_2, which are considered as unknown. This is because of the desire to express them as an equation of the relative rotation between the outer and inner disc, θ.

Table 3.5: Known or estimated parameters required to calculate the tangential forces.

Symbol	Value	Description
r_i	1.13[m]	Distance from centre of rotation to the interaction points on the inner disc.
r_o	1.17[m]	Distance from centre of rotation to the interaction points on the outer disc.
b	1.74[m]	Distance between the interaction points of the two cylinders on the inner ring.
L	0.8[m]	Length of hydraulic cylinder barrel.
n_{cyl}	6	Number of hydraulic cylinders in total.
d_p	0.28[m]	Hydraulic cylinder piston diameter.
d_r	0.11[m]	Hydraulic cylinder rod diameter.

The parameters described in Table 3.5 are known or estimated parameters, required to calculate the tangential forces which generate the rotational torque. Lengths are found from the 3D-CAD model and rounded, but for the diameters d_p and d_r which are estimated and found through iterative calculations. The rod diameter, d_r, is estimated to be approximately 40% of the piston diameter, d_p. The goal of this calculation is to dimension the cylinders to ensure their capacity to deliver required torque throughout their entire cycle.

$$h = {r_o}^2 \sin(\theta) \tag{3.5}$$
$$f = \sqrt{2{r_o}^2 - 2{r_o}^2 \cos(\theta)} \tag{3.6}$$
$$e = \sqrt{f^2 - h^2} \tag{3.7}$$
$$\phi_1 = \operatorname{asin}\Big(\frac{b}{2r_i}\Big) \tag{3.8}$$
$$s_1 = \sqrt{{r_i}^2 + {r_o}^2 - 2r_i r_o \cos(\phi_1 + \theta)} - L \tag{3.9}$$
$$s_2 = \sqrt{{r_i}^2 + {r_o}^2 - 2r_i r_o \cos(\phi_1 - \theta)} - L \tag{3.10}$$
$$c = r_o - e - r_i \cos(\phi_1) \tag{3.11}$$
$$\theta_1 = \operatorname{acos}\Big(\frac{c}{s_1 + L}\Big) + \theta \tag{3.12}$$
$$\theta_2 = \operatorname{acos}\Big(\frac{c}{s_2 + L}\Big) - \theta \tag{3.13}$$
$$\theta_3 = \frac{\pi}{2} - \phi_1 - \theta_1 \tag{3.14}$$
$$\theta_4 = \frac{\pi}{2} - \phi_1 - \theta_2 \tag{3.15}$$

Figure 3.19b show the detailed definition of angles and lengths and geometry used to calculate the angles, θ_1, θ_2, θ_3 and θ_4. The four angles are used to calculate the resulting rotational torque for two separate cases, because this concept involve the inner disc rotating in relation to the stationary outer disc and vice versa. Angles θ_1 and θ_2 are used when the outer disc is rotating, and θ_3 and θ_4 are used when the inner disc is rotating. These four angles are described in Equations 3.12 through 3.15.

Equation 3.16 through 3.19 show the definition of tangential forces as functions of the angles θ_1 through θ_4 expressed in Equation 3.12 through 3.15 and seen in Figure 3.19b. From the calculated tangential forces the resulting total torque can found as described in Equation 3.20 and 3.21. By calculating the torque for number of steps throughout the stroke of the mechanism, the torque curve in Figure 3.20 is graphed. This displays the calculated torque for both cases when the outer (yellow line) and inner disc (red line) rotate. It shows how the torque does not drop below the required 8[MNm] within its entire stroke. This proves the diameters, $d_r = 0.28$[m] and $d_p = 0.11$[m], as acceptable.

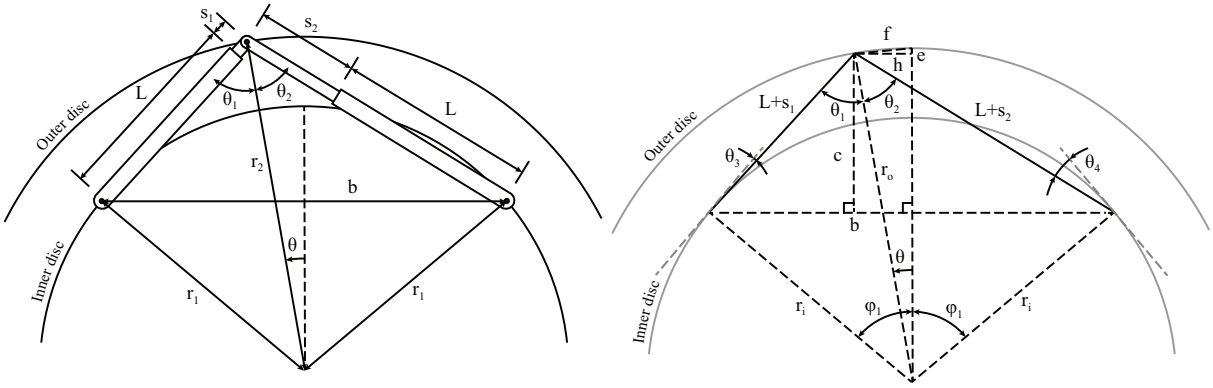

(a) Basic layout and elementary lengths of the mechanism.

(b) Definition of angles and lengths used to calculate the tangential cylinder forces.

Figure 3.19: Illustrations showing the basic layout of one of the three pairs of hydraulic cylinders. All variables are known, except θ_1, θ_2, s_1 and s_2.

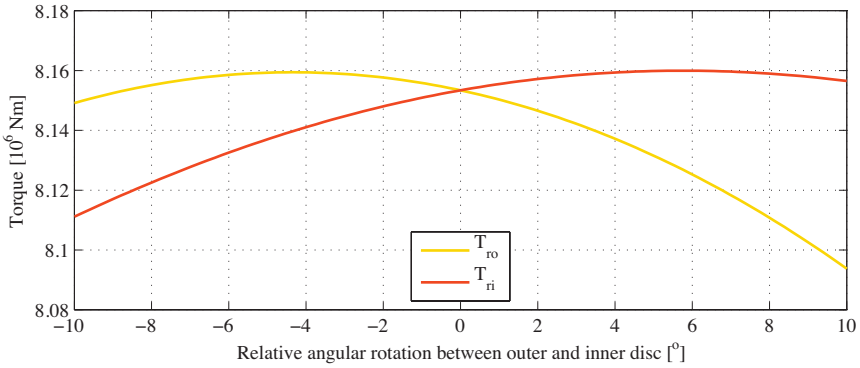

Figure 3.20: Torque generated by the hydraulic cylinders throughout the stroke of the mechanism. Note the operational area of the mechanism is defined as $-9[^\circ] \leq \theta \leq 9[^\circ]$. T_{ro} and T_{ri} is defined in Equation 3.20 and 3.21, respectively.

$$F_{t1ro} = F_1 \cos(\frac{pi}{2} - \theta_1) \tag{3.16}$$

$$F_{t2ro} = F_2 \cos(\frac{pi}{2} - \theta_2) \tag{3.17}$$

$$F_{t1ri} = F_1 \cos(\theta_3) \tag{3.18}$$

$$F_{t2ri} = F_2 \cos(\theta_4) \tag{3.19}$$

$$T_{ro} = \frac{1}{2} n_{cyl} r_o (F_{t1ro} + F_{t2ro}) \tag{3.20}$$

$$T_{ri} = \frac{1}{2} n_{cyl} r_i (F_{t1ri} + F_{t2ri}) \tag{3.21}$$

Stroke

The cylinder stroke is chosen to achieve a maximum angular displacement between outer and inner disc. Chosen stroke will have great impact on buckling of the cylinder. The stroke is found from geometrical properties of the structure, such as the maximum angular rotation between the two rings, θ_r. But as the cylinders will be enclosed by the rings, the available space will limit the stroke.
The stroke (s), cylinder diameter (d) and lever arm (l) have great infliction on each other, as illustrated in Figure 3.21. If the lever arm is halved, the stroke is halved, and the cylinder has to be four times thicker.

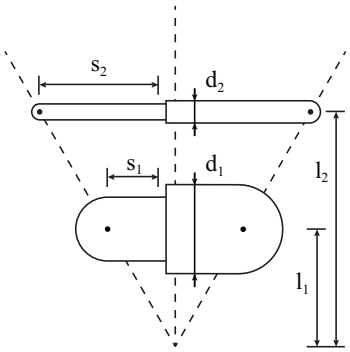

Figure 3.21: Illustration of two scenarios of cylinder placement with equal stroke angle. The figure shows the effect of lever arm (l) on stroke (s) and cylinder diameter (d).

The stroke is determined by trial and error, and by fitting the given number of cylinders within the boundaries of the ring, with enough spare room for them to move. The stroke is set to be 340$[mm]$, which allows for 18$[°]$ of rotation. It would be highly desirable to have the cylinders alone achieve an angular stroke of the mechanism of about 20$[°]$. This would enable the brake callipers to be more inactive. But due to the geometric properties of the discs and the required size of the hydraulic cylinders, this is the maximum stroke achievable.
An investigation of wind phenomena, over a lower time scale, is recommended. This would yield information about the minor fluctuations of the wind and how often wind changes over the stroke covered by the hydraulic cylinders. These kinds of investigations are not covered in this thesis. For more information about this topic, the book *European Wind Atlas* by *Troen* and *Petersen* is recommended.

Material

The selection of material for the hydraulic cylinder is not decisive. It is done to get a perspective on the wall thickness required and check the rod diameter. This is done by looking for diametrical expansion of the barrel and buckling in the cylinder. To ensure that that none of these cases occur, a safety factor, $SF_{cyl} = 2$, is included in the calculations. Data given for the material used can be found in Table 3.6.

Table 3.6: Material properties used in design of hydraulic cylinders. See Appendix B for data sheets.

Description	Unit	AISI 1030
Density	$[\frac{kg}{m^3}]$	7850
Yield Strength	$[Pa]$	$345 \cdot 10^6$
Ultimate tensile strength	$[Pa]$	$550 \cdot 10^6$
Young's Modulus, E	$[Pa]$	$205 \cdot 10^9$
Poisson's ratio, ν	$[-]$	0.29
Design stress, $s_d = \frac{\text{Yield stength}}{SF_{cyl}}$	$[Pa]$	$172.5 \cdot 10^6$

Cylinder wall thickness

The cylinder wall thickness is an important factor when designing a hydraulic cylinder. This is because the barrel wall thickness has to be large enough to withstand bulging and thereby internal leakage. When discussing the wall thickness of a cylinder, the points bellow have to be taken into consideration. [22, p. 290] [7, p. 79]

1. *Is the material used brittle or ductile?*
   A material is considered brittle if it breaks without significant deformation. This is often seen as the yield strength lie close to the ultimate tensile strength. A ductile material will deform plastically before breaking.

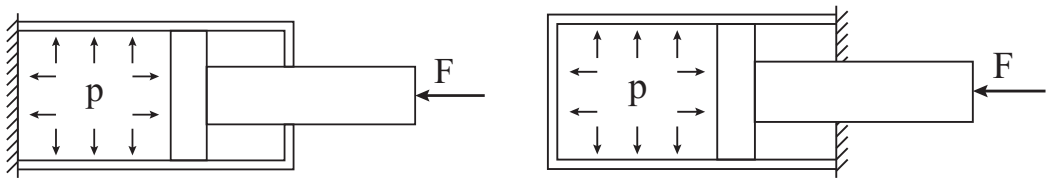

(a) Open-end type. (b) Closed-end type.

Figure 3.22: Illustrations of typical cylinder mounting, which will result in open- and closed-end cylinder design. [7]

- The material used is AISI 1030 (see Appendix B), which experience a large elongation (32%) and reduction of area (57%) before breaking. This typical for a ductile material.

2. *Is the cylinder classed as a thin- or a thick-walled cylinder?*
   In a thin-walled cylinder the stress is uniformly distributed, resulting in a lower maximum stress in the cylinder. A thick-walled cylinder will have areas with higher stresses than other, and thereby no uniformity. A cylinder is considered thin-walled when the ratio between the inner diameter and the wall thickness equals 0.1 or less. If the ratio is larger than 0.1, the cylinder is considered thick-walled. [22, p. 290]

   - The hydraulic cylinder is assumed to be thick-walled due to the large hydraulic pressure. This means that a thickness larger than one tenth of the piston diameter is expected: $t_{cyl} > \frac{d_p}{10} = 27[\text{mm}]$.

3. *Is the cylinder end constructed as open or closed?*
   An open-ended hydraulic cylinder is a cylinder where the hydraulic pressure induces an axial stress in the barrel. Typical ways of mounting, resulting in open- or closed-end cylinder design, can be seen in Figure 3.22.

   - The hydraulic cylinder will not be entirely closed-ended at all times, due to the type of attachment. Therefore it is reasonable to consider it open-ended, as this requires a larger thickness.

Birnie's equation (see Equation 3.22) recommended for open-end, thick-walled cylinders made in ductile materials [7]. The maximum allowable stress in the cylinder barrel is set to half of the yield strength of the material: $s_d = \frac{s_y}{SF}$, where SF is a safety factor. Material properties required to calculate the cylinder wall thickness can be found in Table 3.6. Other general parameters can be found in Table 3.4. The thickness is found to be $32.7[mm] \approx 30[mm]$, from Equation 3.22.

$$t_{cyl} = \frac{d_p}{2}\left(\sqrt{\frac{s_d + p_c(1-\nu)}{s_d - p_c(1+\nu)}} - 1\right) \tag{3.22}$$

Diametrical expansion The cylinder wall thickness has to be checked by investigating the diametrical expansion in the cylinder barrel walls. This is done by obtaining the diametrical unit strain, ϵ_d, as described in Equation 3.23. The allowable diametrical unit strain depends on the allowable leakage in the cylinder. For many applications, an allowable diametrical unit strain of $0.1778[mm]$ has been found appropriate. [7, p. 80] The diametrical expansion is thereby found as in Equation 3.24, to be $0.0252[mm]$ which is less than $0.1778[mm]$. A cylinder wall thickness of 30 [mm] is thereby applicable.

$$\epsilon_d = \frac{s_d}{E} = \frac{0.1725[GPa]}{205[GPa]} = 8.4146 \cdot 10^{-4} \tag{3.23}$$

$$e_d = \epsilon_d t_{cyl} = 8.4146 \cdot 10^{-4} \cdot 30[mm] = 0.0252[mm] \tag{3.24}$$

Rod diameter

The rod diameter has been set to 110[mm] previously in this Chapter. To verify this diameter, one must check for buckling in the hydraulic cylinder. Shafts like the cylinder rod often have a small diameter in relation to length. Failure due to buckling will occur if this relation is out of bounds. This can be controlled by utilizing Euler's formula for buckling in columns, given in Equation 3.25. By combining Euler's formula and the formula for polar moment of inertia of a circle (Equation 3.26), Equation 3.27 gives the minimal allowable rod diameter, with respect to buckling. Cylinders designed in this thesis, have their rod fixed to the piston in one end, unable to rotate, hinged and free to rotate in the other end. This gives the end-condition factor $K = 2$, according to Fitch and Hong [7].

$$F_{cyl} = \frac{K\pi^2 I_r E}{{L_{rod}}^2} \tag{3.25}$$

$$I_r = \frac{\pi {d_p}^4}{32} \tag{3.26}$$

$$d_r = \sqrt[4]{\frac{32 F_{cyl} {L_{rod}}^2}{K\pi^3 E_r}} \tag{3.27}$$

Solving Equation 3.27 gives a rod diameter of $d_r = 42.2[mm]$. Far less than the one used. Buckling in the rod will not be a problem.

3.6.2 Yaw bearing

The main yaw bearing of the system joins the nacelle to the tower. The main task of the yaw bearing is to transfer axial load from the mass of the nacelle. The bearing will also experience bending moment from the misaligned centre of mass and wind forces on the rotor. The bearing must perform safely and without heavy wear or slack. It must handle the continuously varying bending moment.

Table 3.7: Assumed parameters for a 3.5[MW] wind turbine. Based on existing wind turbines of similar size and production rate.

Symbol	Value	Description
m_n	230000[kg]	Mass of nacelle with rotor.
d_r	115[m]	Rotor diameter.
l_{hy}	1.2[m]	Height from yaw bearing to hub.
l_{gx}	0[m]	Horizontal distance from centre of mass to centre of yaw bearing.
ρ	1.225[$\frac{kg}{m^3}$]	Density of air at 15 [$^\circ C$].
C_t	$\frac{8}{9}$[$-$]	Thrust coefficient, for ideal turbines.

Calculation of bearing forces

There are few sources to consult for excising calculations or recordings of forces in a wind turbine yaw bearing. None of the contacted manufacturers of either bearings or wind turbines are willing to give any specific information on the topic. The calculation of forces is therefore done on the basis of several rough assumptions. The simplified nacelle can be seen in Figure 3.23. It is assumed that the bearing is mounted normally to the direction of gravity.
The axial force, F_a, is calculated from the sum of forces in the vertical direction. Equation 3.28 gives the axial force, as the nacelle is assumed to only be affected by the gravitational force in the vertical direction. The radial force, F_r, is somewhat more complex, as it is heavily affected by loads from the rotor. The most predominant contribution to this hub-load is the forces generated from flapping of the blades. [17] This flapping is variable and dependant on wind speed, blade shape, rotor diameter and environmental factors. Because these calculations require a level of detail which is not acquired in this project, an assumption suggested by the representative from ThyssenKrupp Rothe Erde is used. Radial load is expected to be one third of the axial load. This corresponds with Equation 3.29. The tilting moment, M_k, is defined by the loads on the nacelle and their respective leverage arm. For this simplified case, Equation 3.30 gives the tilting moment.

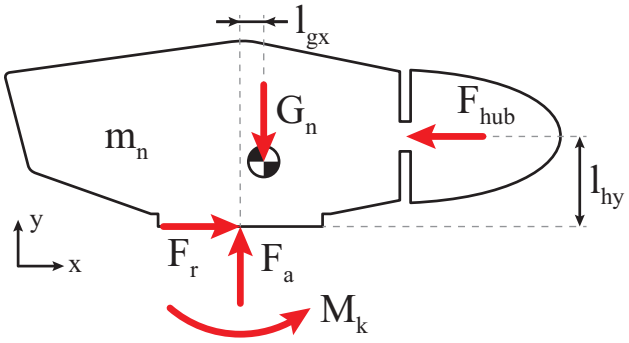

Figure 3.23: Free body diagram of the nacelle. Forces and torques are marked as red arrows, the torque-arrow is curved around the point it affects.

$$F_a = G_n = m_n g = 2256[\text{kN}] \tag{3.28}$$
$$F_r = F_{hub} = \frac{1}{3}F_a = 752[\text{kN}] \tag{3.29}$$
$$M_k = F_{hub} l_{hy} - G_n l_{gx} = 902[\text{kNm}] \tag{3.30}$$

These calculations are assumptions and will hold uncertainty, as the calculated loads do not depend on wind conditions, as they are in reality.

Bearing from ThyssenKrupp Rothe Erde

Large diameter slew bearings are great at handling large loads. These bearings are designed individually for each wind turbine model. This is to ensure a perfect fit and some flexibility in the design of the wind turbine. ThyssenKrupp Rothe Erde supplies a catalogue of standard large diameter bearings. [14] This catalogue has instructions on how to identify a suitable bearing and how to find the bearing loads. This selection of a bearing is meant to be a preliminary estimation, because in order to get a final bearing would require some more knowledge about the loading conditions in wind turbine yaw systems. Nevertheless, knowing approximate dimensions of the bearing will aid designing rest of the product.
By recommendation from the manufacturer, single- and double row ball bearings are under investigation. Double row ball bearings are complicated to investigate independently given the load case for this project, as the catalogue states [14]:

> '*Radial loads $F_r \leq 10\%$ of the axial load can be neglected in selecting bearings [...]. If the radial load is $F_r \geq 10\%$ of the axial load, the supporting angle must be taken into account. The respective calculation will be done by us.*'

Based on this statement, no calculations are performed on double row ball bearings since the manufacturer does not supply the approach to do so.
Single row ball bearings are found by investigating two load cases and ensuring none of them exceed the belonging static limiting load curves and service life curves. The reference loads for load combination one is given in Equation 3.31 and 3.32, and the reference loads for load combination two are given in Equation 3.33 and 3.34. The parameter f_{stat} is a load factor which varies from 1 to 1.75, depending on the use of the bearing. The manufacturer supply a table with a number of suggested values, but none for wind turbine yaw mechanisms. The load factor is set to $f_{stat} = 1.25$ because this value is used for machines with the approximate same size.

$$F_{a1}' = (F_a + 5.046 \cdot F_r) f_{stat} = 756[\text{kN}] \tag{3.31}$$
$$M_{k1}' = M_k f_{stat} = 113[\text{kNm}] \tag{3.32}$$
$$F_{a2}' = (1.225 \cdot F_a + 2.676 \cdot F_r) f_{stat} = 597[\text{kN}] \tag{3.33}$$
$$M_{k2}' = 1.225 \cdot M_k f_{stat} = 138[\text{kNm}] \tag{3.34}$$

But even tough single row ball bearings where suggested, the catalogue does not contain bearings of this type with diameter larger than 1.5[m]. Because the desired diameter is 3.5[m], the manufacturer must design one especially for this case. An example single row ball bearing was proposed by representative from ThyssenKrupp Rothe Erde, given the loads (Equation 3.28 and 3.29) and the bending moment (Equation 3.30). This bearing is found using a rotational velocity of 0.1[rpm] = 0.6[$\frac{^\circ}{s}$], which is double of what the product requirements demand. The profile can be seen in Figure 3.24. The drawing is a clipping from the technical drawing supplied, Appendix D, indicating the general size of the bearing, raceway and sealing details.

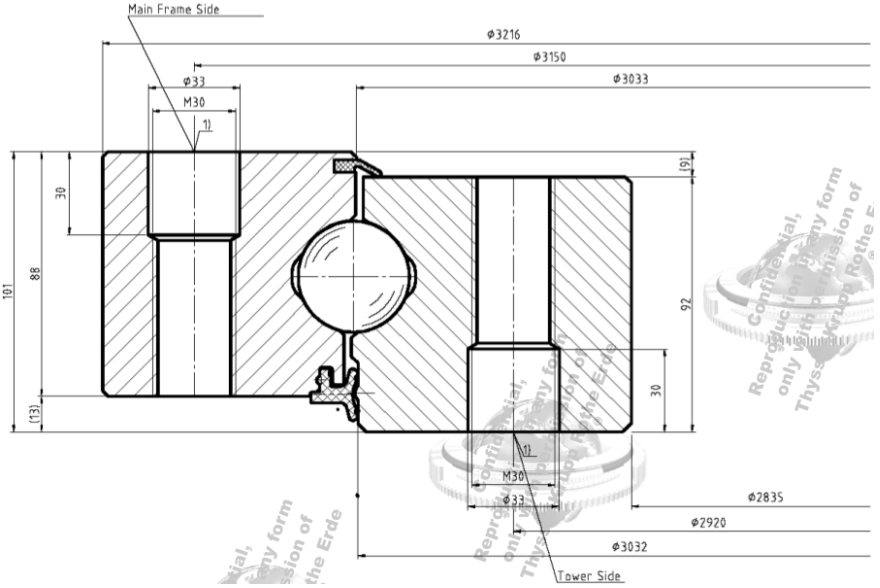

Figure 3.24: Single row slew bearing designed by ThyssenKrupp Rothe Erde for this purpose. Image used with permission from ThyssenKrupp Rothe Erde. See Appendix D.

This bearing, seen in Figure 3.24, was suggested close to the deadline for the report. That is why it is not implemented into the 3D-CAD model. Its low inner diameter of 2838[mm] require changing the entire model as it was designed with respect to a slew bearing with inner diameter 3000[mm]. ThyssenKrupp Rothe Erde states that their production line accept all bearings with diameter between 0.3[m] and 18[m]. Therefore increasing the diameter of the bearing would be no problem and could be done through continuing the consulting with ThyssenKrupp Rothe Erde.

3.6.3 Brake calliper

As the hydraulic brake callipers are important to the functionality of the mechanism, one has to be sure the callipers chosen will deliver the required braking torque of 11[MNm]. The sensitive areas when it comes to brake callipers are how many callipers are needed to get enough braking torque, and if there is enough space for these callipers.

Svendborg Brakes

There are several suppliers of hydraulic brake callipers. One of those, and the supplier used in this project, is Svendborg Brakes. The calliper model DEB-0120-004-DA-MAR, seen in Figure 3.25 and Appendix C, fits the requirements of the mechanism. The torque generated by the callipers is defined as in Equation 3.35, where D_i is the brake disc inner diameter and n_{cal} is the number of callipers. The maximum hydraulic pressure for the calliper is $p = 205$[bar]. With a pad area of $A_{pb} = 339.3$[cm^2], the brake calliper generates 695.6[kN] of clamping force according to Equation 3.37.
Svendborg Brakes have been so kind to supply a sample brake pad. A test of the frictional properties of the brake pad is intended. The brake pad arrived too close to deadline, making it not possible to include in the thesis. The most common frictional coefficient for brake pads is used as an estimate, $\mu_b = 0.4$. This yields a braking force of $556,5$[kN], as described in Equation 3.36.

$$M_b = F_b n_{cal} \frac{D_i + 0.136[\text{m}]}{2} \tag{3.35}$$

$$F_b = 2 \cdot F_c \mu_b \tag{3.36}$$

$$F_c = A_{pb} p_b \tag{3.37}$$

The major features with these brakes is that they are relatively compact, as they measure 572×318×278[mm], but supply high clamping forces. The callipers may be ordered with retraction springs, lifting the pads of the brake disc when they are inactive.

Figure 3.25: The brake calliper, DEB-0120-004-DA-MAR, from Svendborg Brakes. [3] See Appendix C.

Breaking torque

Given the brake callipers from Svendborg, the number of brake callipers needed to deliver the required braking torque can be calculated. The inner radius of the brake disc, D_i, is 2.8[m]. Assuming maximum braking force, $556,5$[kN], Equation 3.38 gives the required number of callipers to hold the required torque of 11[MNm]. Calculation shows that 14 callipers of this type are required.

$$n_{cal} = \frac{11 \cdot 10^6[\text{N}]}{556500[\text{N}] \cdot (2.8[\text{m}] + 0.136[\text{m}])} = 13.47[-] \tag{3.38}$$

Spacing of callipers

Given the number of brake callipers required found above, the spacing must be checked. The functionality of the mechanism states that counteracting peak loads, affecting the yaw mechanism while in movement, a total of $4 \cdot n_{cal}$ is required. Half of these callipers are mounted on top, and half on the bottom. This sets very high demands to the spacing of the callipers.
Figure 3.26 shows the layout of Svendborg Brakes callipers around the brake disc, assuming an inner diameter of $D_i = 2.8$[m]. This reveals that the design cannot hold 28 brake callipers around its circumference. The system also requires a stroke as large as possible, to utilize the full potential of the hydraulic cylinders. Figure 3.26 show how the only ten brake callipers fit around the circumference, giving the system an angular stroke of approximately 18[°]. This is acceptable, although a larger stroke is desirable. As the hydraulic cylinders limit the stroke to this value, there is no use adjusting the callipers further.
If $n_{cyl} = \frac{10}{2} = 5$, the total braking torque generated by the callipers equals 4.1[MNm]. This is too low, but as the system is configured, it is the maximum available torque with these brake callipers. Using another set of callipers would be possible, but no callipers have been found generating more than 500[kN] braking force. The brakes from Svendborg Brakes will be used for modelling purposes and adjusted if needed, even though they do not hold up to the requirements.
This is not a major problem as some thought of the customizations can be made for the brakes to increase its braking force. The recommended solution is increasing the braking force by layering brake discs and friction material. This type of brakes is commonly used in aircraft. This solution would drastically increase the braking force. Assuming each brake disc have a brake pad in contact with them, the braking force will

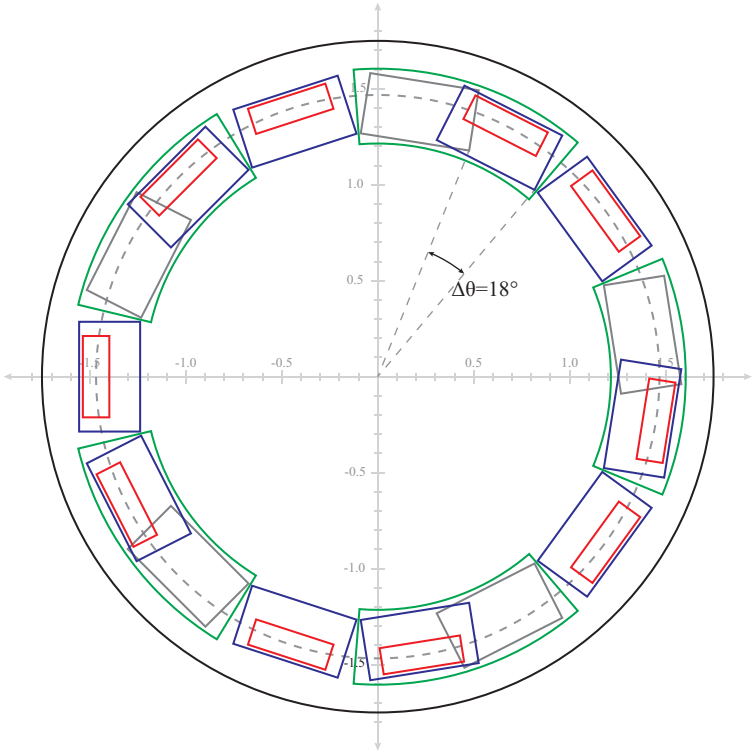

Figure 3.26: The brake calliper layout for Svendborg brakes' DEB-0120-004-DA-MAR. The red square marks the brake pads. The blue square marks the envelope of the brake callipers. The green ring sections represent the field occupied by the callipers throughout the stroke. The black circle marks the maximum size of the mechanism, as stated in product requirements.

double by doubling the number of brake discs. This increase in clamping force does not require any change in calliper size or hydraulic pressure, but will require changing the calliper design.

3.7 Final design

The purpose of product development and design for this project was to get a functional product with such a level of detail that it was possible to model and simulate it with somewhat realistic properties. Properties in terms of: mass, size, geometry and general functionality. The design is visualized in the 3D-CAD software SolidWorks, where the entirety of the mechanism is implemented. This section sums up the choices made and the variation selected for each component, and why.
The model can be roughly divided into five parts: discs, hydraulic cylinders, yaw bearing, hydraulic brake callipers, and parts of nacelle and tower structure. The last is modelled only to get a good view of the size of the system, and have something to attach brake discs and bearings to. Figure 3.27 shows a cut view of the entire mechanism, illustrating how the design is layered. Six hydraulic cylinders are mounted within the inner ring. The outer ring envelopes the inner ring. Hydraulic brake callipers are mounted to the inner and outer ring as described in Section 3.7.4, and clamp on the brake discs, which are placed on both nacelle and tower structure. Brake callipers will act as a surge protection during operative and parked state. Higher wind force surges against the rotor will result in a slip between brakes and brake discs. The tower and nacelle structure are coupled with a large diameter slew bearing. In reality the outer disc must rest on the tower structure as well, connected with a smaller slew bearing of some type. This is not implemented in the model.

3.7.1 Discs

The model consists of two discs, one inner and one outer disc. The naming is a reference to the one nesting within the other. The profile used to build the discs, is the profile Box girder from Section 3.2. This profile

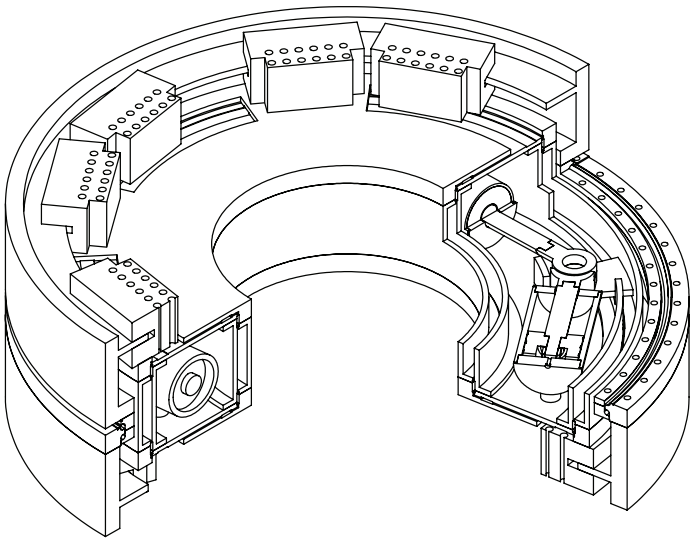

Figure 3.27: A multiple cut, isotropic view of the entire mechanism as modelled in 3D-CAD, using SolidWorks.

can be seen in Figure 3.9. Each disc consists of four parts; an inner ring, outer ring, upper disc and lower disc. Together they make a sturdy, circular box girder. To have a modular system, discs are designed in sections. Five sections are recommended for this particular design. The advantage with this variation is the ability to partially disassemble the mechanism on site for repairs or service. The rectangular profile is symmetric about its mid-plane, which is the cut plane in Figure 3.28b. The openings in the outer disc where the inner disc is seen, is for the hydraulic callipers. These have to correspond to the stroke of the mechanism, so that the callipers may move. The underside of the mechanism will have a similar pattern, but is shifted by 36[°] as the 10 brake callipers are equally spaced. Figure 3.28b show the inside of the discs. This is where the hydraulic cylinders will be mounted. Six cylinders will be mounted with one end to the yellow lever arm, connected to the outer disc, and the other to the holes in the inner disc. Two and two cylinders will have their rod connected to the same lever arm. Note that lever arms are mounted on the outer disc and protrudes the inner disc in order to reach the hydraulic cylinders. A hole, the size of the mechanism stroke, is required in the inner disc. This might weaken the structural strength of the disc and would have to be investigated.

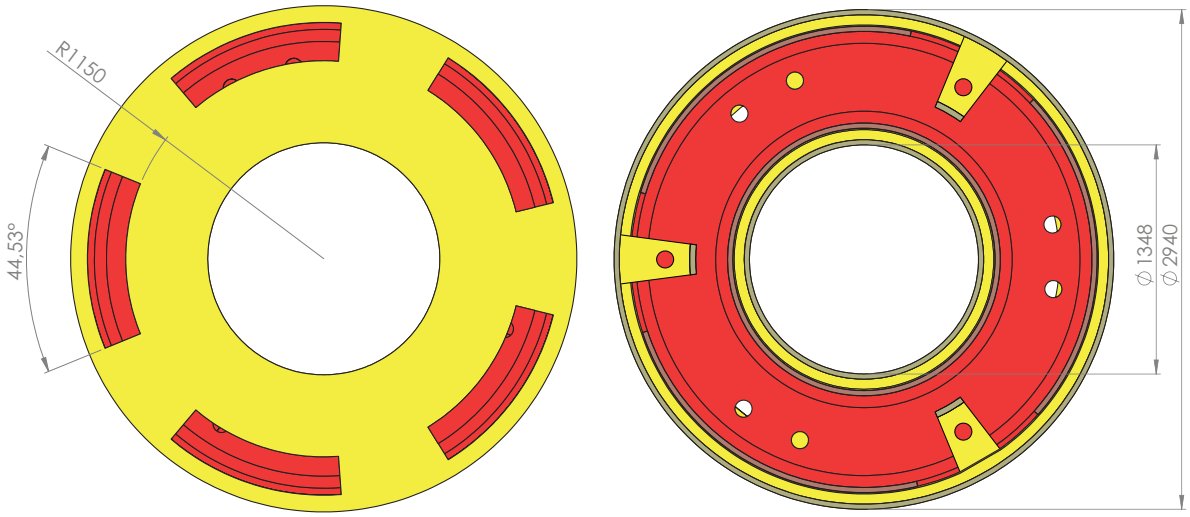

(a) Seen from above.

(b) Cut in its mid-plane and seen from above. Dark areas are the cut planes.

Figure 3.28: Inner and outer disc are identified by respectively red and yellow.

3.7.2 Hydraulic cylinders

Hydraulic cylinders are designed after calculations done in Section 3.6.1. Figure 3.29 show two similar hydraulic cylinders, where the only difference is the rod-end. The rod-ends are made different, because both cylinders are to be connected to each other and the outer disc with a hinged joint. The hydraulic cylinders are designed to roughly indicate its size and stroke. This is why flanges for seals are roughly implemented, but in-/out-flow valves are not included. The cylinders have a stroke of 340[mm], a piston diameter of 280[mm] and a rod diameter of 110[mm].

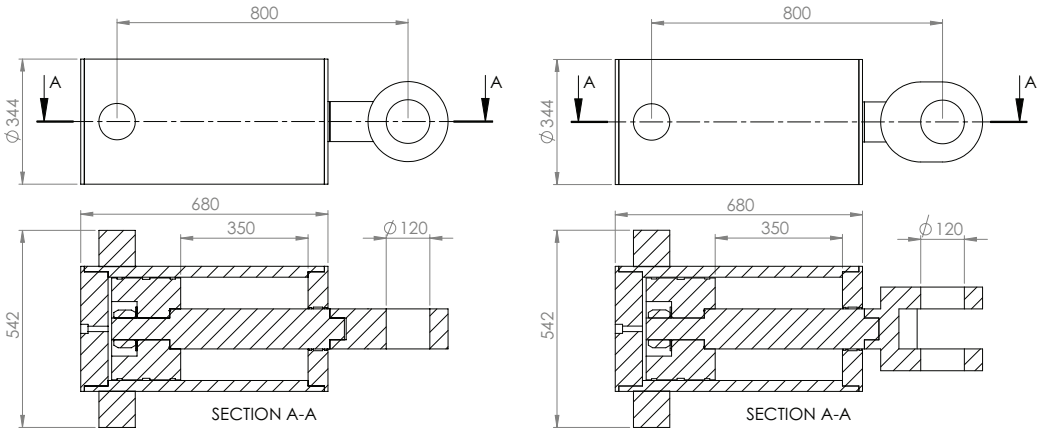

(a) Hydraulic piston with standard hinged rod-end.

(b) Hydraulic cylinder with overlaying hinged rod-end.

Figure 3.29: The two opposing hydraulic cylinders as modelled in 3D-CAD according to the design found in Section 3.6.1.

3.7.3 Yaw bearing

Initially, note that the bearing used in the model is not the one found in Section 3.6.2. It is this way because the bearing found through direct counselling with ThyssenKrupp Rothe Erde arrived to close to the deadline. The implementation of the correct bearing would require major changes to all components of the mechanism, because the bearing found have a smaller diameter than the bearing modelled. As stated in Section 3.6.2, it is no problem for the manufacturer to make a bearing of larger diameter, closer to the limiting envelope of the mechanism. Therefore, the model remains unchanged.

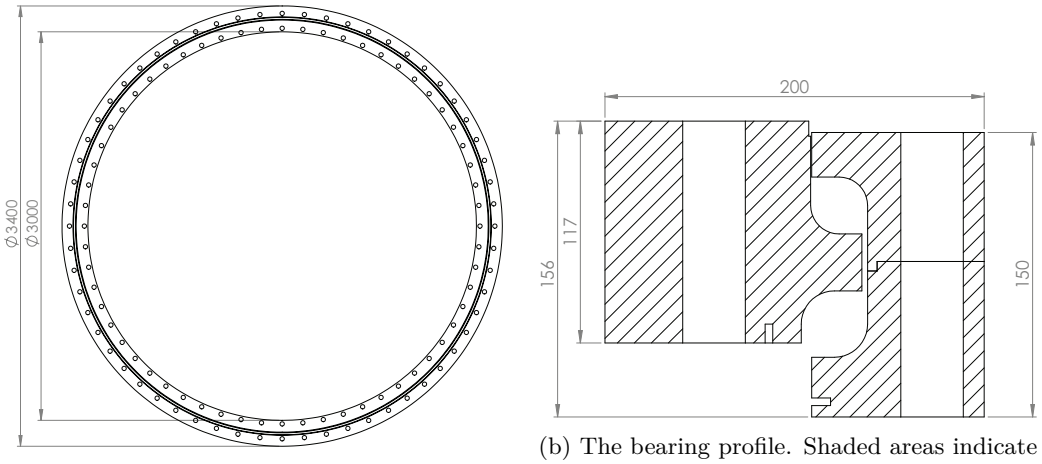

(a) Top-view of the bearing.

(b) The bearing profile. Shaded areas indicate cut plane.

Figure 3.30: Double row ball bearing modelled is the Standard series KD320, from ThyssenKrupp Rothe Erde, with drawing number 011.40.3150.000.11.1502, from the catalogue [14]. Note that this is not the same bearing as found in Section 3.6.2.

The bearing modelled is a bearing found from rough early-stage calculations from ThyssenKrupp Rothe Erdes catalogue [14]. It is from their standard series KD320, and is referred to with the drawing number 011.40.3150.000.11.1502. The dimensions in addition to a figure of the bearing can be seen in Figure 3.31. The main yaw bearing determine the size of the system, as it encircle the entire mechanism.

3.7.4 Brake callipers

Twenty hydraulic brake callipers are implemented in the model of the yaw mechanism, where half of these are mounted on top, see Figure 3.31a, and the other half to the bottom, see Figure 3.31b. On both top and bottom, five and five brake callipers are mounted to the inner and outer disc in an interlacing order. They are placed to clamp on brake discs, one on the tower and one on the nacelle, with an inner diameter of 2800[mm] and a thickness of 40[mm].

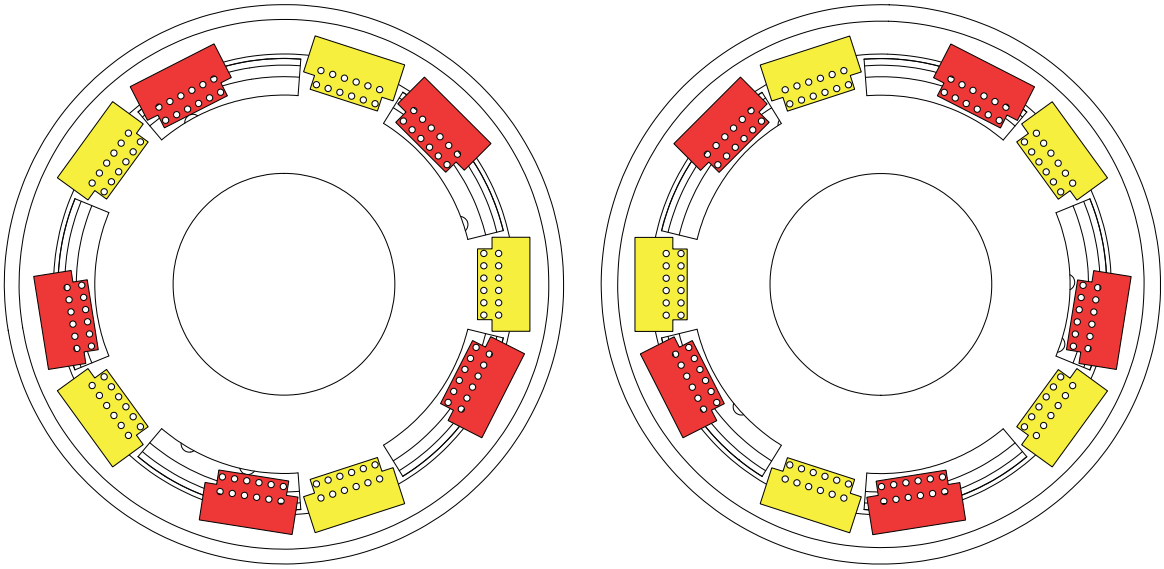

(a) Mechanism seen from above, with brake callipers. (b) Mechanism seen from below, with brake callipers.

Figure 3.31: The hydraulic brake callipers as mounted on the mechanism. Half of them are mounted to the outer disc (yellow), and half to inner disc (red).

The five brakes mounted to the outer disc, on top and bottom are equally spaced around the centre of the disc. The brakes mounted to the inner disc must be mounted on a fixture which protrudes the openings in the outer disc. These brakes will go back and forth in these openings, which correspond to the stroke of the mechanism, $\approx 18[^\circ]$.
The information given by Svendborg Brakes is limited. The only dimensions given by on the brake found in Section 3.6.3, DEB-0120-004-DA-MAR, is the envelope, which equals $572 \times 318 \times 278$[mm]. The callipers are modelled from these measurements, and the rest is estimated for visual purposes only. Further counselling with Svendborg Brakes could yield detailed information about both size and functionality about the brake callipers, which would be useful when improving both the 3D-CAD model and the mathematical model.

Chapter 4

Friction

Tribology is the study of contact between interacting surfaces in relative motion. To know how materials react and respond when they rub against each other are valuable in engineering design, simulation and control. Mechanical design must be conducted with friction in mind, due to the resulting heat and/or wear. In cases of simulation, friction will change the response in a system and an inaccurate friction model could falsify the results. Friction is a very well known problem and thoroughly studied and most mechanisms in friction are known. Present models represent some of these behaviours, but fail to simulate all mechanisms of friction. This chapter contains a discussion of the importance of friction and how it is modelled. This thesis mainly considers the LuGre friction model, described in Section 4.3. Simpler aspects of friction are also covered lightly in this chapter.

4.1 Mechanisms of friction

Friction occurs between all surfaces in contact. Every seemingly planar surface has a microscopic roughness. Dimples and other imperfections on this surface are what defines friction, and is the reason for the characteristic behaviour which is observed. Mechanisms of friction are covered in this section.

4.1.1 Steady velocity friction

The Stribeck curve is a graph of friction force versus relative velocity between friction surfaces, and can be seen in Figure 4.1. The dip in force from stiction, as velocity increases, is known as the Stribeck effect. No universal function can be found for friction, because the friction-viscosity is application dependent and varies with material properties, temperature and wear. [21]

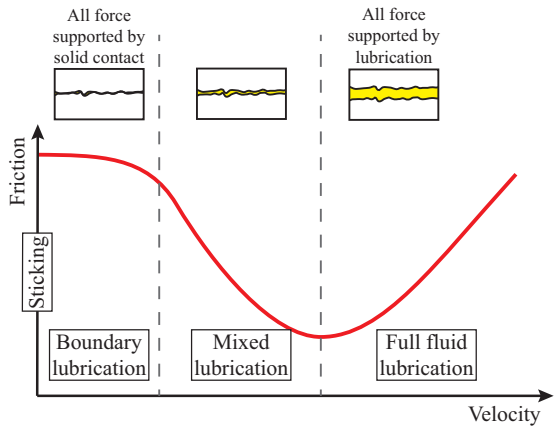

Figure 4.1: Typical Stribeck curve with a description of contact for each lubrication regime. [21]

4.1.2 Static friction and break-away force

As two surfaces in contact start moving in relation to each other, the small imperfections in contact between the surfaces deform elastically and plastically. This deformation is the reason for what is known as stiction (static friction). Break-away force is the force required to overcome stiction and initiate relative motion between the surfaces.

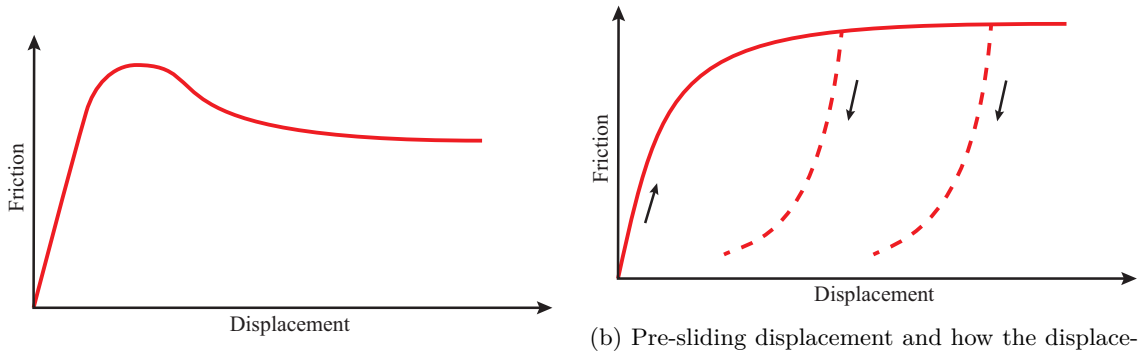

(a) The transition from stiction to dynamic friction.

(b) Pre-sliding displacement and how the displacement is affected by loading and unloading.

Figure 4.2: Friction-displacement curves. [21]

Many studies have been performed to investigate the transition from sticking to sliding. The conclusion is that the transition can be seen in a friction-displacement curve as a drop in friction force, as seen in Figure 4.2a. Stiction was found to persist for distances of the order of 10^{-6}[m] [23]. This was called the pre-sliding displacement and was shown to result in a permanent displacement if the load was removed before sliding started. This effect can be seen sketched in Figure 4.2b

4.1.3 Friction lag

Dynamics are important for the transition between sticking and sliding, but when sliding, experiments have found that dynamics play a great role. Experiments with periodic time-varying velocity show hysteresis for the friction force. The friction force was larger for increasing velocities than for decreasing velocities. The size of the loop increased with normal load, viscosity and frequency of the variation in velocity. [20]

4.2 Friction models

A friction model is considered a mathematical representation of one or more of the mechanisms of friction. Friction models have been divided into three groups: static, dynamic, and special purpose models. Static models are basic, as they do not consider the dynamic behaviour of friction. Dynamic models describe the behaviour of friction more accurately by including dynamics. Special purpose models also consider the physical mechanisms of friction. [21] The LuGre friction model, discussed in Section 4.3, used in this thesis is an example of a dynamic friction model. Figure 4.3 shows a block on a surface, applied an external force, F_e. The motion of this block is what defines the friction force. How this is done is dependant on what friction model is used. This section is a rough introduction to the field of friction models. As these models are quite complex, only an introduction containing the most relevant topics will be presented.

4.2.1 Static friction models

Static models are models which were developed in past centuries, also known as classical models, but also include newer models which improve the emulation of friction behaviour. The classical models are built up by different parts, each describing their own part of the frictional behaviour. Static friction models were developed to give a rough understanding of friction, corresponding with experiments. Leonardo da Vinci (1452–1519) was the first to document the properties of friction. He found that the friction force was the same for two objects of identical weight, but different size. He also found that the friction force doubled as the weight doubled. This gave rise to the conventional, simplistic model of friction, described in Equation

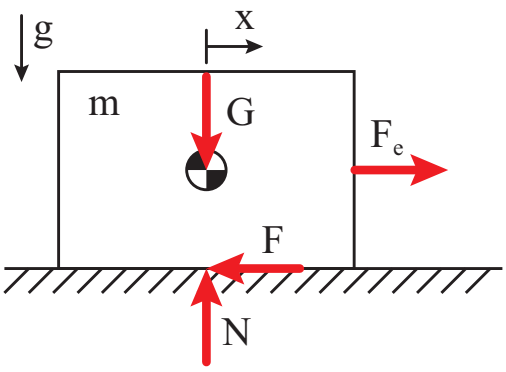

Figure 4.3: Notation used when discussing linear friction. The normal force is defined as $N = G = mg$. The position and velocity is denoted as x and v, respectively.

4.1. The use of a frictional coefficient is common, but this definition alone does not model the dependency on normal force accurately enough to be used in detailed friction modelling.

$$F = \mu N \tag{4.1}$$

The work on friction performed by da Vinci, rediscovered by Guillaume Amonton (1699), and further developed by Coulomb (1785), gave rise to what is known as Coulomb friction. Other names are kinetic friction, dynamic friction or relay-type friction. The definition for Coulomb friction can be seen in Equation 4.2. This is based on the understanding that friction is independent of velocity and restricts motion. The friction force will switch between positive and negative coulomb force, F_c. The greatest disadvantage of this model is its invalidity at zero velocity.

$$F = F_c \text{sign}(v) \tag{4.2}$$

The theory of hydromechanics was developed in the 19^{th} century, leading to the investigation of frictions dependency on lubricant viscosity. [24] Viscous friction is known as the force component which expresses this relation, and is normally described as in Equation 4.3. The viscous friction is not always linear. Equation 4.4 show a more general expression, where δ_v is a constant dependant on application geometry.

$$F = F_v v \tag{4.3}$$
$$F = F_v |v|^{\delta_v} \text{sign}(v) \tag{4.4}$$

Stiction is short for static friction and is used to describe friction at rest, opposed to dynamic friction. In 1833, Arthur Morin [19] published the idea of a friction force at rest which is larger than the Coulomb friction force. Stiction counteracts external forces under a certain limit and thereby hinder the instigation of motion. If the external force reaches beyond the stiction limit, F_s, motion will occur and the friction force will drop to, and follow Coulomb friction as velocity increase. This shows how friction force cannot be described only by velocity. The external force have to be introduced as in Equation 4.5, making the friction force at zero velocity a function which can have any value between $-F_s$ and F_s.

$$F = \begin{cases} F_e, & v = 0 \text{ and } |F_e| < F_s \\ F_s \text{sign}(F_e), & v = 0 \text{ and } |F_e| \geq F_s \end{cases} \tag{4.5}$$

Any combinations of these models are considered classical friction models. These classic models define the viscous friction as linear or constant. Accurate measurements of friction experiments, with steady velocity motion, may yield other dependencies. In his studies from early 20^{th} century, Richard Stribeck observed that low velocity friction force decrease continuously at positive acceleration. This phenomenon is termed Stribeck effect. Stribeck friction is the extra, low velocity friction, larger than the Coulomb limit. Equation

4.6 show the friction force, where $F(v)$ is a function which have several variations, but is most commonly defined as in Equation 4.7. The Stribeck velocity, v_s, determines the decrease in friction force.

$$F = \begin{cases} F(v), & \dot{x} \neq 0 \\ F_e, & v = 0 \text{ and } |F_e| < F_s \\ F_s \text{sign}(F_e), & \text{otherwise} \end{cases} \tag{4.6}$$

$$F(v) = F_c + (F_s - F_c)e^{-|\frac{v}{v_s}|^{\delta_s}} + F_v v \tag{4.7}$$

These models have been used frequently throughout the past, and are still used for simple calculations today. They cover some of the behaviour seen in friction, but none cover enough aspects to be used for detailed modelling. The major disadvantage with the classical models is their inability to detect and determine when the velocity is zero.
Dean Karnopp proposed, in 1985, a model for simulation purposes handling the problems with detection of zero velocity [15], termed the Karnopp model. It has the external force as an input and integrator. This cause problems, as this force is not always explicitly given. The equations therefore have to be defined individually for each specific case. Variations of the Karnopp model are widely used, because they make for efficient simulations. Response in the zero velocity interval, in spite of being detected, does not agree with real friction.

4.2.2 Dynamic friction models

Dynamic friction models, opposed to static models, include variation of velocity. The need for dynamic models came as the demand for precision increased. New hardware has better measuring equipment and better controllers, allowing more detailed real-time analysis of friction. The dynamic models have been developed from the 1960s and onwards with increased interest in the 1990s.
Most dynamic models are developed by slightly modifying static models, such as Armstrong's seven parameter model [2], which has temporal dependencies for stiction and stribeck effect. Armstrong's seven parameter model introduces dynamics to a set of static models, though it does not handle pre-sliding displacement. The model includes separate equations for sticking and sliding, and a mechanism for handling transitions between these.
The Dahl model is a frequently used dynamic friction model, which have been developed and improved throughout the previous five decades, resulting in several variations of the model. A solution proposed in a report by P.R. Dahl in 1968 [5] is based on the assumption that friction force can be described as in Equation 4.8, where F is friction force, x is displacement and t is time. This states that friction is only position dependant. Dahl compared results from simulations with experimental results from ball bearings and found good correspondence between simulated and true friction. The Dahl model is versatile and used for several purposes in several forms, but will not be discussed in detail in this thesis. Dahl has some noteworthy points about friction [5]. Firstly:

> '*The origin of friction is in quasi static bonds that are continuously formed and subsequently broken.*'

and secondly:

> '*The resulting functions behave as a brush whose bristles must bend as the brush moves in one direction and then flop or bend in the opposite direction if the motion is reversed.*'

With this notion, Dahl brought notice to the topic of bristle models. These models consider friction as a contact and deformation between the friction surfaces on a microscopic level. An example of this is the Bristle Model proposed by David A. Haessig and Bernard Friedland [10]. in 1991. The Bristle model considers friction as the deformation of several bristles, which bends until they let go. This emulates the transition from static to coulomb friction and allow for pre-sliding displacement.

$$\frac{dF}{dt} = \frac{dF}{dx}\frac{dx}{dt} \tag{4.8}$$

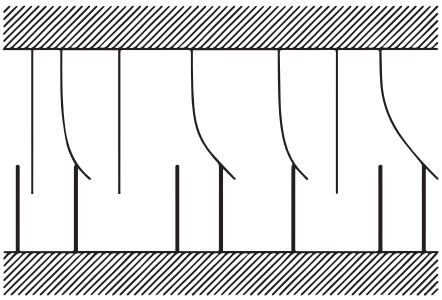

Figure 4.4: Irregular deformation of the imagined bristles between the two surfaces in contact. [21]

Dynamic models are many, varied, with complex functionalities. These models cover the closest relatives to the LuGre friction model, discussed in this thesis, with similar basis. The LuGre friction model is the last dynamic model discussed, and is described in Section 4.3.

4.2.3 Special purpose models

Special purpose models are very different in terms of area of utilization and what principle they are based on. Special purpose models are therefore developed and used for, as the name suggests, special purposes. Examples of these are listed bellow with reference to the original material, where details are found.
J.T. Oden and J. Martins suggested in 1985 the frictional interaction between two materials using continuum mechanics. This method uses a simple function for friction, but a more complex model for contact. Consideration of motion in normal direction of the friction surfaces is extraordinary with this model.
Many dynamic friction models include viscous friction, as this is an important factor in many engineering applications. Several publications have been made on the topic of viscosity in friction between lubricated surfaces. D.P. Hess and A. Soom suggested, in 1990, a way of calculating the frictional coefficient for steady sliding [12]. This model covers all lubrication regimes except sticking, as described in Figure 4.1. A. Harnoy and B. Friedland derived in 1994 a model based on the hydrodynamics of lubricated journal bearings [11]. This model covers both boundary and mixed lubrication regimes.

4.3 The LuGre friction model

The LuGre friction model was proposed as an improvement on the existing dynamic friction models, as they cannot emulate all friction phenomena. LuGre does not cover all friction phenomena, but it covers the problem with definition for low velocity motion. Based on a need for accurate friction models for control and simulation purposes, LuGre was developed [21]. The LuGre friction model, given in Equation 4.9 to 4.12, is based on the principle of considering the two contact surfaces as covered with tiny bristles, as seen in Figure 4.4. As the surfaces move relative to each other, the bristles will deform until they reach a limit, slip and eventually engage with a new bristle of the opposing surface. The friction model only considers the average deflection, z, as the placement of the bristles over the area is random, making their deformation different. Together with the relative velocity between the two surfaces, v, average bristle deflection, z, is the variables of the model. The remaining parameters determine the dependencies between z and v, and their effect on the frictional force, F. Equations 4.9 to 4.12 given and investigated by H. Olsson in his PhD-thesis: Control Systems with Friction [21].

$$\frac{dz}{dt} = v - \frac{|v|}{g(v)}z \tag{4.9}$$

$$g(v) = \frac{1}{\sigma_0}\left(F_c + (F_s - F_c)e^{-(\frac{v}{v_s})^2}\right) \tag{4.10}$$

$$F = \sigma_0 z + \sigma_1(v)\frac{dz}{dt} + K_v v \tag{4.11}$$

$$\sigma_1(v) = \sigma_1 e^{-(\frac{v}{v_d})^2} \tag{4.12}$$

Function $g(v)$

Function $g(v)$, described in Equation 4.10, affects how average bristle deflection depend on relative velocity between the moving surfaces. Function $g(v)$ has similarities with Equation 4.7, which implements the stribeck effect in a static friction model. This Equation is used when the velocity do not equal zero. $g(v) = F_s$ when the velocity is zero, which correspond with observations of frictional behaviour. Function $g(v)$ contains the stribeck velocity v_s, which defines the rate of velocity change when transitioning from static to coulomb friction.

Damping coefficient $\sigma_1(v)$

Damping is used to make the model respond smoothly in the transition between sticking and sliding. The purpose is to model decrease in damping as velocity increases. The LuGre friction model is preferred in cases where the behaviour around zero velocity is investigated. If the $\sigma_1(v)$ is incorrect, the system could oscillate at zero velocity, as demonstrated in Section 4.5.7. Damping velocity, v_d, define the rate of change in damping as the velocity changes. Damping will be at its highest at $v = 0$, where $\sigma_1(v) = \sigma_1$.

Viscous friction $f(v) = K_v v$

Viscous friction is usually combined with Coulomb friction in most traditional friction models. The viscous friction is the last part of Equation 4.11. The LuGre model is open for other definitions of viscous friction. As there are several different viscous friction models, it could be relevant to not have linear friction, as implemented in Equation 4.11. This thesis only consider linear viscous friction, $f(v) = K_v v$, as the velocities are low and the system have a large inertia and low accelerations are expected.

4.4 LuGre friction with variable normal force

Friction created by hydraulic brakes in the yaw mechanism plays critical role. Brakes provide the clamping force, controlling the magnitude of the friction force. The generated friction force is what regulates the motion of the system. Simulations performed in H. Olssons PhD-thesis [21] and previous investigations uses a constant normal force and translational system. The LuGre model has to be modified in order to take the variable normal force into account. This section contains the adaptations done to the LuGre friction model, as discussed in Section 4.3.

$$F_C = \mu_c N \tag{4.13}$$
$$F_S = \mu_s N \tag{4.14}$$

Stiction and coulomb friction force are defined by normal force as expressed in Equation 4.13 and 4.14 respectively. Altering the normal force at current positions make the model invalid for $N = 0$, because Equation 4.10 is the denominator in Equation 4.9. The generalized modified version of the LuGre friction model is therefore defined as in Equation 4.15 to 4.19.

$$\frac{dz}{dt} = v - \frac{|v|}{g(v)} z \tag{4.15}$$
$$g(v) = \frac{1}{\sigma_0}\left(\mu_c + (\mu_s - \mu_c) e^{-\left(\frac{v}{v_s}\right)^2}\right) \tag{4.16}$$
$$F = N(\sigma_0 z + \sigma_1(v)\frac{dz}{dt}) + f(v) \tag{4.17}$$
$$\sigma_1(v) = \sigma_1 e^{-\left(\frac{v}{v_d}\right)^2} \tag{4.18}$$
$$f(v) = \begin{cases} K_v v, & -\infty < N < 0 \\ 0, & N = 0 \\ K_v v, & 0 < N < \infty \end{cases} \tag{4.19}$$

Figure 4.5 shows the layout of the LuGre friction model as described by Equation 4.15 to 4.19. The grey blocks, normal force (N) and relative velocity (v), are input variables. The output friction force is retrieved at the open arrow, at the far right of layout chart.

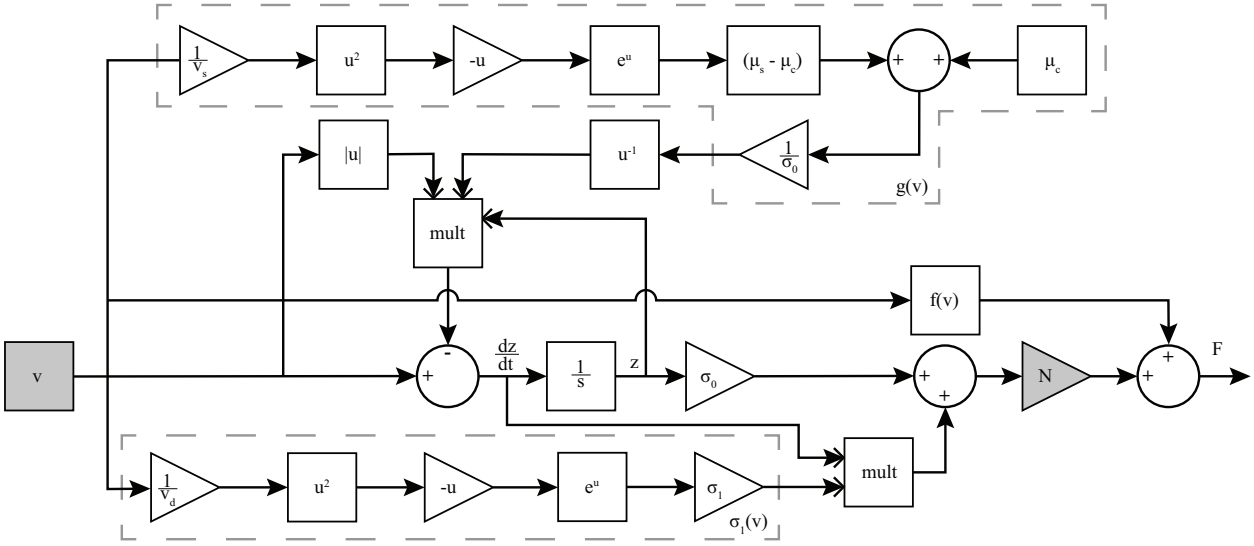

Figure 4.5: Layout chart of Equations 4.15 through 4.19. Equation 4.19 states the definition of the piecewise function $f(v)$.

Table 4.1: Default values used when investigating properties of the individual parameters.

Parameter	σ_0	σ_1	v_s	v_d	K_v	μ_c	μ_s	N
Valve	$2\sqrt{10^5}$	10^5	0.1	0.01	0.4	0.4	0.8	3

The new set of equations have implemented the normal force in a way which does not make them invalid for $N = 0$. Viscous friction, $f(v)$, is the only part of the friction model which is not directly dependant on the normal force. Implementation of the normal force can be seen in Equation 4.17. When the normal force equals zero, the callipers have no contact, i.e. the callipers are inactive and should have no frictional effect on the system. This is modelled with a discontinuous piecewise function as seen in Equation 4.19.

4.5 Investigation of parameters

The parameters in the LuGre friction model have different properties and effects on the resulting friction force. Identification of these will help in understanding the friction model and in using it to emulate friction in the mathematical model of the piston driven yaw mechanism. As a basis for the investigation, a default set of parameters are defined as shown in Table 4.1.

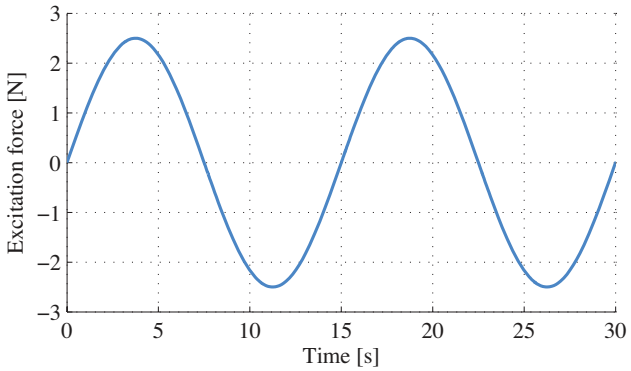

Figure 4.6: The function for the excitation force, $F_e(t)$, graphed against time, t.

A system as illustrated in Figure 4.3 was used in the investigation of parameters. It consists of a unit-mass with an excitation force applied. The excitation force is applied as a sine-function with a frequency of $\frac{1}{15}[\mathrm{s}^{-1}]$

and an amplitude of 2.5[N], as graphed in Figure 4.6. The model was simulated for 30[s] producing a plot of velocity versus resulting friction force. Several plots were made for each parameter, using different values, to see how change would affect the friction force. The following section contains graphs, descriptions and analysis of properties of the individual parameters.

4.5.1 Stiction coefficient, μ_s

The stiction coefficient, μ_s, determines the magnitude of the force required to overcome static friction between the two surfaces. Stiction force is determined as the product of the stiction coefficient and the normal force, N, between the surfaces. When the stiction force is overcome, the friction force drops as the relative velocity increases and follows a linear path determined by coulomb and viscous friction.

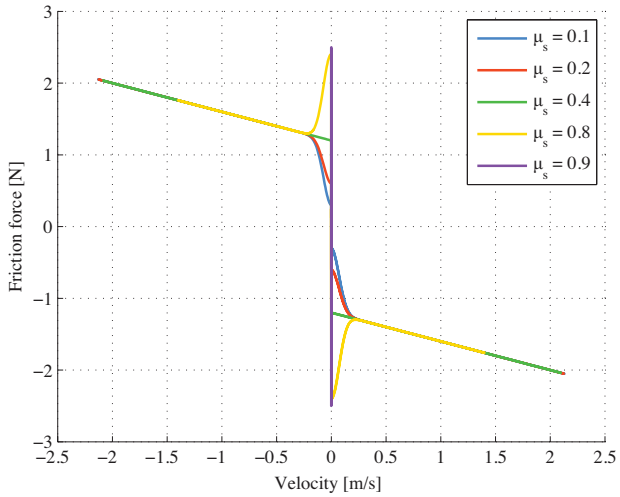

Figure 4.7: System modelled with LuGre friction, using a selection of values for the stiction coefficient, μ_s.

The graph in Figure 4.7 shows results from simulations, using five different values for μ_s. It is apparent that as stiction force increases, the system does not acquire the same absolute maximum velocity. Affirmed by comparing the green ($\mu_s = 0.4$) and yellow ($\mu_s = 0.8$) lines. When the stiction force increases above the force applied, with an amplitude of 2.5[N], the system does not escape the grasp of static friction. This is the case for the purple line ($\mu_s = 0.9$), where stiction force equals $\mu_s N = 0.9 \cdot 3[\text{N}] = 2.7[\text{N}]$. One can see from the graph that the default coulomb friction coefficient, μ_c, equals 0.4, because the green graph ($\mu_s = 0.4$) goes directly from stiction to coulomb friction. Investigations show how the stiction coefficient can be found empirically. A simple experiment where a mass is pulled until stiction is overcome can be used to determine an approximate stiction coefficient.

4.5.2 Coulomb friction coefficient, μ_c

The coulomb friction coefficient, μ_c, determine the magnitude of the force required to have continuous movement between two surfaces, after stiction force has been overcome. Coulomb friction force is determined as the product of the coulomb friction coefficient and the normal force, N, between the surfaces. With no viscous friction, the frictional force would go to a steady-state value equal to the coulomb friction force. This is best seen in the study of the viscous friction coefficient, K_v, in Section 4.5.3.

Figure 4.8 shows how change in μ_c alters the friction force proportionally. The graph shows how the mass acquire a lower absolute maximum as coulomb friction force increases. The purple line ($\mu_c = 0.8$) show how the coulomb friction coefficient equals the stiction coefficient as there is no drop or increase in force when stiction is overcome at $\mu_s N = 0.8 \cdot 3[N] = 2.4[N]$. This investigation show how the coulomb friction coefficient can be found empirically. A simple experiment where a mass is pulled until stiction is overcome, and the force drops to a state where coulomb friction is active. An empirical approach would yield an inaccurate coulomb friction coefficient without a machine able to perform a repeatable experiment and measure accurately.

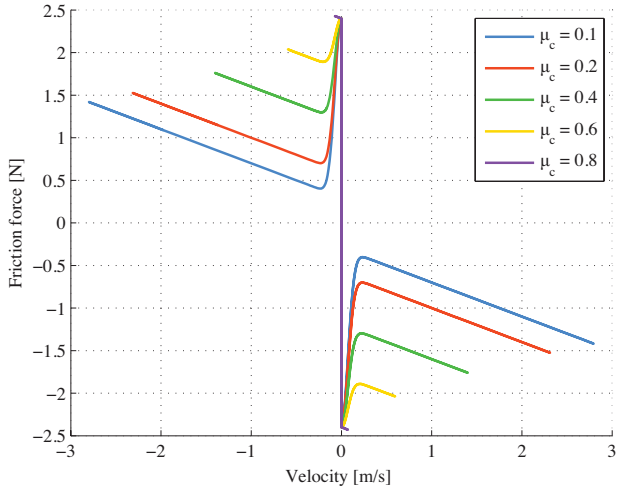

Figure 4.8: System modelled with LuGre friction, using a selection of values for the coulomb friction coefficient, μ_c.

4.5.3 Viscous friction coefficient K_v

The viscous friction coefficient, K_v, determine the behaviour of viscous friction. There are several ways to model viscous friction. A reasonable and simple way is using a linear model, $F_v = K_v v$, where v is the relative velocity between the two surfaces. Increasing slope of frictional force, when stiction is overcome and coulomb friction is reached, can be seen in Figure 4.9 for higher values of K_v.

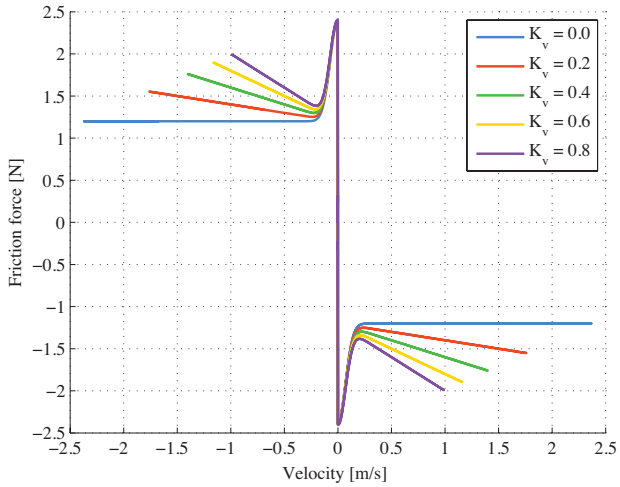

Figure 4.9: System modelled with LuGre friction, using a selection of values for the viscous friction coefficient, K_v.

The blue line, where $K_v = 0$, show that only coulomb friction occur after stiction is overcome. The frictional force is constant as the relative velocity further increase, because viscous friction is absent. Investigations show that identification of viscous friction coefficient empirically, would require a way to accurately measure friction force and relative velocity between the two surfaces.

4.5.4 Stribeck velocity, v_s

The stribeck velocity, v_s, determines the slope of the stribeck effect. Stribeck friction occurs at low velocities in the transition from stiction to coulomb and viscous friction. An increase in stribeck velocity will increase the relative velocity between the surfaces required to have pure coulomb and viscous friction. This effect can be seen in Figure 4.10. The tendency shows that when v_s goes towards zero, the stribeck friction looks more and more like a step from stiction force to coulomb friction force, which the blue line ($v_s = 0.025$) shows.

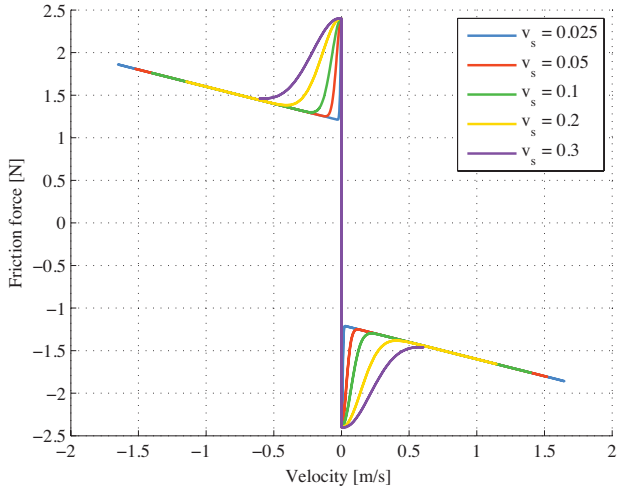

Figure 4.10: System modelled with LuGre friction, using a selection of values for the stribeck velocity, v_s.

4.5.5 Damping velocity, v_d

Damping velocity, v_d, is a part of the function $\sigma_1(v)$ which correspond to damping in the friction force (Equation 4.11). Damping is expressed with an exponential term, reducing damping at higher velocities. The damping velocity determine the velocity at which damping is decreased. Damping is essential at low velocities, as the system has a tendency to oscillate. The oscillations of the undamped system can be seen in Figure 4.11b as the red ($v_d = 10^{-4}$) and, especially, the blue ($v_d = 10^{-3}$) line. This investigation shows how differences due to change in damping velocity happen on a microscopic scale. This makes it difficult to observe in an experiment.

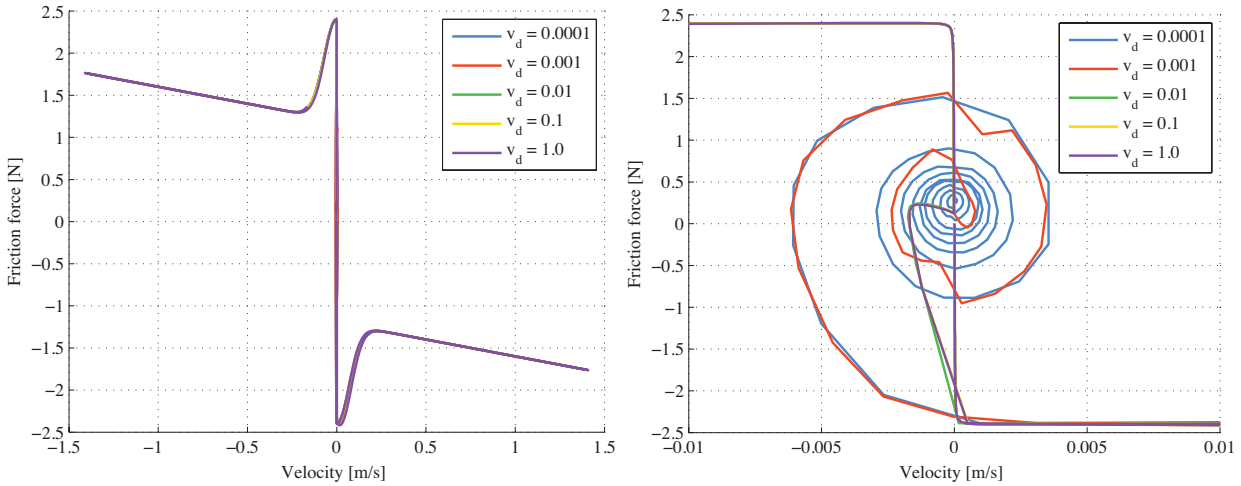

(a) Full view of graphs.

(b) Zoomed in view of graphs

Figure 4.11: System modelled with LuGre friction, using a selection of values for the damping velocity, v_d.

4.5.6 Stiffness parameter, σ_0

The stiffness parameter, σ_0, is part of Equation 4.11. If the contact between the two surfaces is considered as a spring-damper connection, until stiction is overcome, σ_0 can be related to the spring stiffness. Figure 4.12 show the tendencies of the friction force as the parameter σ_0 increases. Figure 4.12a show the general view of the friction force graphed against relative velocity between the two friction surfaces.
Figure 4.12b show a close-up of the area around zero where the largest abnormalities occur. The plots show that the system stiffen as σ_0 increase. The system becomes over-damped as the stiffness decreases, because

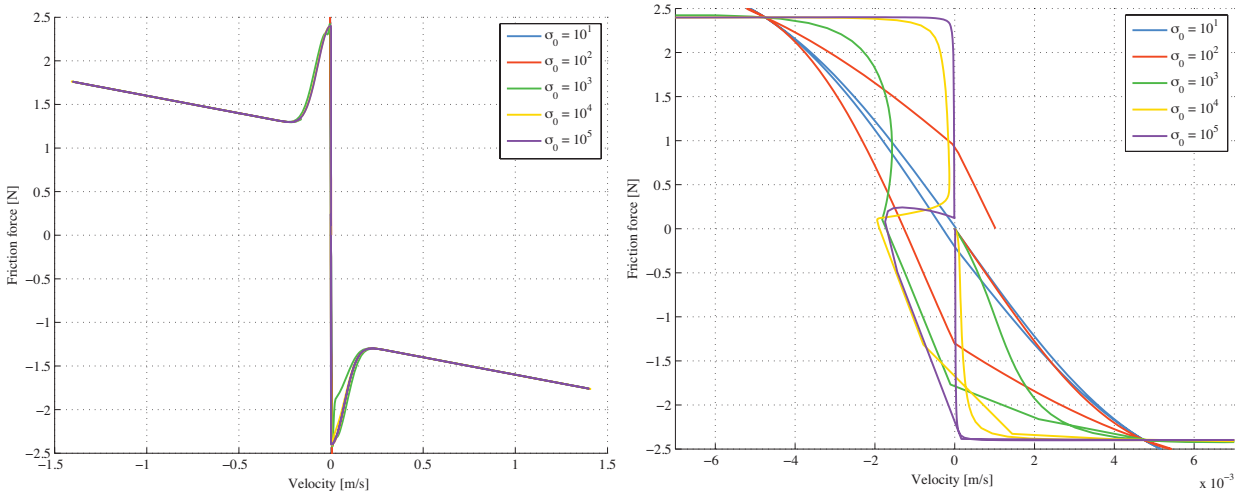

(a) Full view of graphs. (b) Zoomed in view of graphs

Figure 4.12: System modelled with LuGre friction, using a selection of values for the stiffness parameter, σ_0.

damping remains constant. Ultimately, the stiffness, σ_0, can be used to define the shape of the curve in the proximity of origin. If the value is incorrect or, most critically, to low, the LuGre friction model will behave incorrectly. The default value for σ_0 is based on recommendations from previous works [21].

4.5.7 Damping parameter, σ_1

The damping parameter, σ_1, is part of Equation 4.11. If the contact between the two surfaces is considered as a spring-damper connection, until stiction is overcome, σ_1 can be related to the damping coefficient. The purpose of damping in the system is to reduce the LuGre friction models tendencies to oscillate at low velocities. Figure 4.14 shows how the model oscillates at low velocities. Figure 4.14b show a close-up of the graphs seen in Figure 4.14a. Oscillations are very small, but as σ_1 decreases, the system goes into increasingly severe undamped oscillation. Large values of σ_1 are recommended to dampen the oscillations. The purple line ($\sigma_1 = 2\sqrt{10^5}$) show the response for the default value. This value is based on recommended values form previous works. [21]

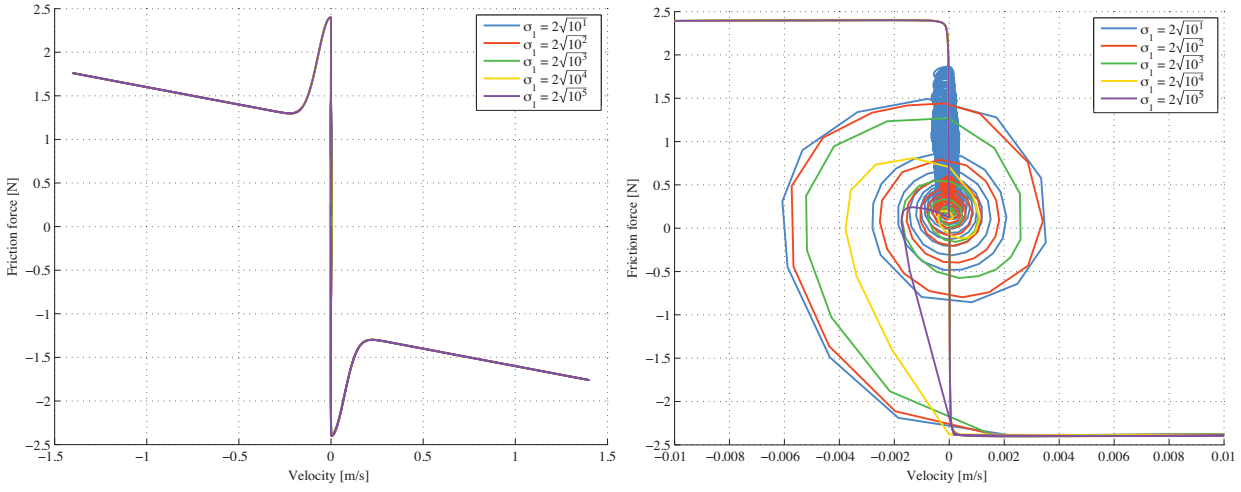

(a) Full view of graphs. (b) Zoomed in view of graphs

Figure 4.13: System modelled with LuGre friction, using a selection of values for the damping parameter, σ_1.

4.6 LuGre friction for rotary systems

Simulations performed in H. Olssons PhD-thesis [21] use the LuGre friction model in a translational system. For simplified modelling of the piston driven yaw mechanism, the LuGre model will be used with relative angular velocity, ω, as input. This can be done using Equation 4.15 to 4.19, from Section 4.4 as basis. The following corrections are required for the models to be correct, where r is the distance from centre of rotation to the middle of the friction interface.

- The relative velocity, v, is substituted with ωr, where ω is the relative angular velocity.
- The frictional torque, M, is calculated from the frictional force, F, as expressed in Equation 4.20.

$$M = Fr \quad , \quad \text{see Eqn. 4.17} \tag{4.20}$$

The LuGre friction model is tested in a rotary system, using the modified equations. Validating the model is critical to ensure proper functionality of the hydraulic brake callipers.

4.6.1 Verification of model

The edited version of the LuGre friction model has to be verified to ensure its functionality. This is done by investigation of two cases which are specially sensitive for brake callipers; clamping and releasing. The modelled system under investigation resembles a brake. It contains a rotary unit-inertia which is affected by an adjustable external torque and the adjustable friction torque, controlled by a normal force. The friction force generates the braking torque. The system is otherwise without friction. The radius to the point on the clutch where the friction force acts is set to 1[m].

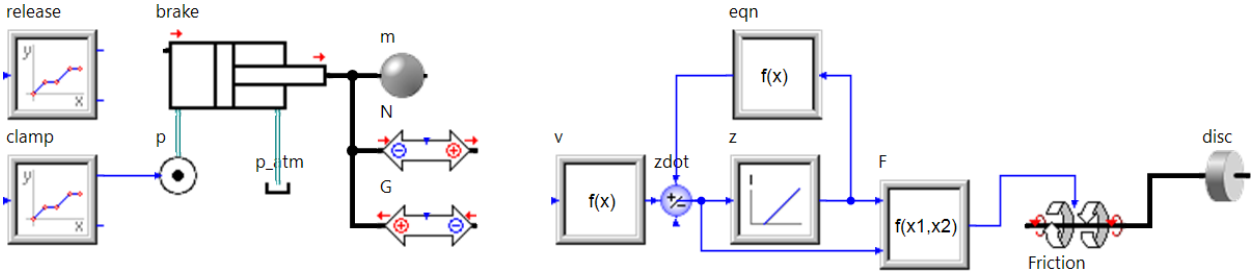

(a) Case 1, where the disc has an initial velocity and is decelerated by the brakes.

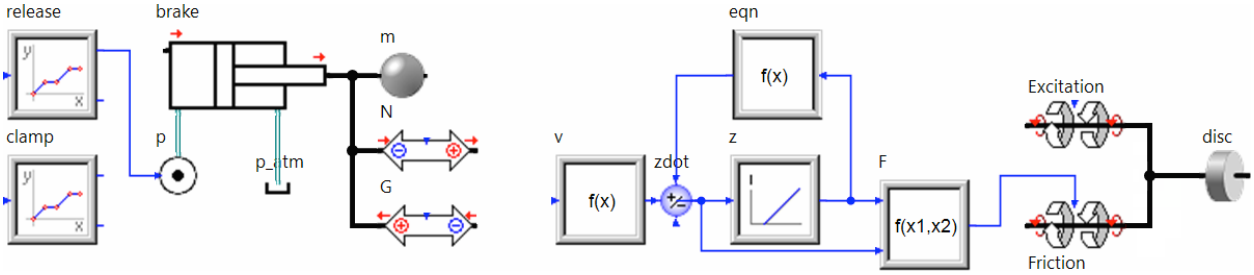

(b) Case 2, where the disc is initially held stationary by the brakes, before accelerated by a excitation-torque.

Figure 4.14: Figures showing the two models as modelled in SimulationX.

Case 1: clamping This case simulate callipers decelerating the system from a initial velocity until it is stationary. The brakes will initially be inactive and the unit-inertia will have an initial angular velocity of $2[s^{-1}]$. Normal force is gradually applied after 1[s], slowing the unit-inertia down. The results of case 1 can be seen as the red lines in Figure 4.15.

Case 2: releasing This case simulate callipers letting go of the system and allowing an external torque to accelerate the system. The unit-inertia is held in place by the callipers. The callipers gradually let go of the system after 1[s]. An external torque of 0.5[N] accelerate the system. The results of case 2 can be seen as the red lines in Figure 4.15.

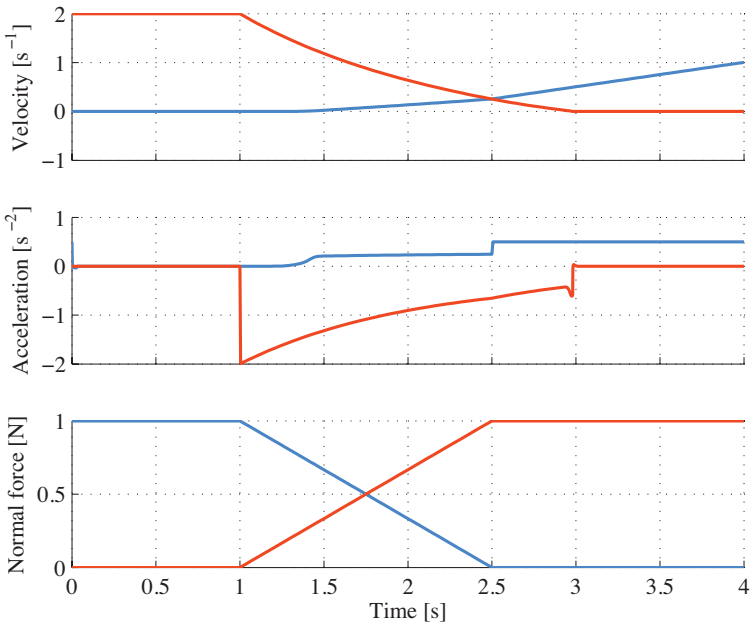

Figure 4.15: Angular velocity, acceleration and normal force, at given time, for scenarios: clamping (red) and releasing (blue).

Figure 4.15 shows how friction affects the system for the two stated scenarios: clamping (red) and releasing (blue). In the case of clamping, the graph makes a large jump towards negative acceleration when normal force is applied. The rapid deceleration is caused by viscous friction, $f(v)$, which is large due to high angular velocity of the unit-inertia. Acceleration decreases until the next jump because of decrease in friction torque and angular velocity. The second jump in acceleration occurs when the unit-inertia stops. Results from the case of releasing also show two large changes in acceleration. The first change comes from overcoming stiction. The second jump happens at time = 2.5[s], when the normal force equals 0[N]. Equation 4.19, the viscous friction is removed, resulting in a jump in acceleration. The system then reaches a steady acceleration equal to the sum of torques on the system divided by the inertia of the system, $\frac{0.5[\text{Nm}]}{1[\text{kgm}^2]} = 0.5[\text{s}^{-2}]$. At the start the acceleration curve makes a jump. This is considered to be caused by the applied initial forces and is neglected.
The new, revised model performs as expected. Normal force is variable and may be adjusted to regulate the amount of friction from each calliper. The set of equations adjusted for rotary motion behave in the same way as for the standard set of equations, designed for translational movement.

Chapter 5

Modelling and simulation

Modelling and simulation include the topics of mathematical modelling of the combined mechanical and hydraulic system, and corresponding control sequences. The intention of modelling and simulating the system is to verify the feasibility of its functions and construction. Modelling has been done using the computer software, SimulationX and Matlab, where the latter has been used mostly for verification and assisting calculations. Modelling has been conducted by continuously building on a simplified model of the system, expanding it to gain accuracy in relation to reality, while maintaining a stable and correct model of the piston driven yaw mechanism. Explanations of the mathematical expressions used to model the system in SimulationX are described in Section 5.1. Discovered inaccuracies and the reason for their exclusion can be found in Section 5.2. [8]

5.1 Mathematical model

The mathematical model is developed from the general information deducted from experiments and the developed design. All calculations are done by a 2D-model, described in this section.

5.1.1 Connection between discs

The connection between the two discs, tower, and nacelle are modelled with the special connection under study in mind. The two discs must be able to connect individually to the tower, nacelle, or both. This is done using hydraulic brake callipers, as described in Section 5.1.4. To better illustrate how the system is to operate, a linear representation of the system can be used, as seen in Figure 5.2. The tower is considered as ground and therefore immobile, while the nacelle is movable. The nacelle and tower are both infinite in length, to assimilate the behaviour in a rotary system. The letters a and b represent the two clamping cases required. Case a holds the inner ring to the tower and the outer ring to the nacelle. Case b holds the outer ring to the tower and the inner ring to the nacelle. The cylinders are represented by a black line and are retractable and extendible. Notice that this linear model does not consider the friction in the bearings connecting the elements. It is only meant as a visual aid of understanding.

$$\Sigma M_o = I_o \alpha_o = M_{oi} + M_{Ao} + M_{Bo} - M_{ot} + T_o \tag{5.1}$$

$$\Sigma M_i = I_i \alpha_i = T_i - M_{Ai} - M_{Bi} - M_{oi} \tag{5.2}$$

$$\Sigma M_n = I_n \alpha_n = -M_{Ai} + M_{Bi} - M_{nt} \tag{5.3}$$

By modelling the calliper contact as shown in Figure 5.2, the clamping connection will be defined by the magnitude of the friction torque. Figure 5.3 show rotary free body diagrams of three movable parts in the system: outer ring, inner ring and nacelle. The mass of the hydraulic cylinders are considered negligible, relative to the inertia of the larger elements. The cylinders are therefore not modelled as separate bodies. The sums of torques acting on the outer ring, inner ring and nacelle are expressed in Equation 5.1, 5.2 and 5.3 respectively.
The definition of the torques are described throughout this section. The formulation of the cylinder torque, T_o and T_i, can be found in Section 5.1.3. The friction torques (M_{oi}, M_{ot} and M_{nt}) in the bearings connecting

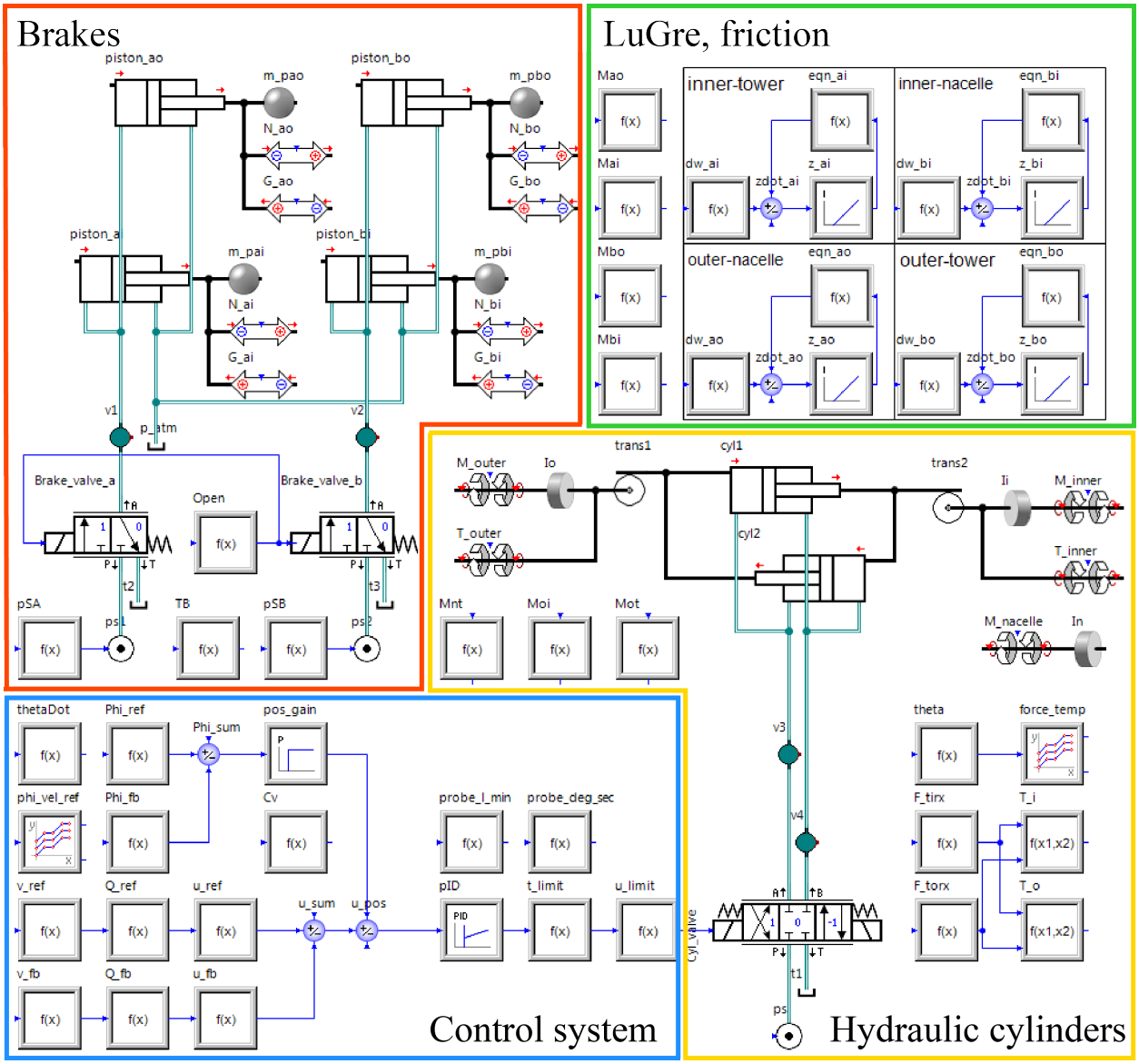

Figure 5.1: SimulationX model overview divided into four major subsystems. Subsystems are categorized into different colours. Green: LuGre friction, see Section 5.1.2. Yellow: hydraulic cylinders, see Section 5.1.3. Red: brakes, see Section 5.1.4. Blue: control system for the 4/3 valve in the yellow sub system, see Section 5.1.5.

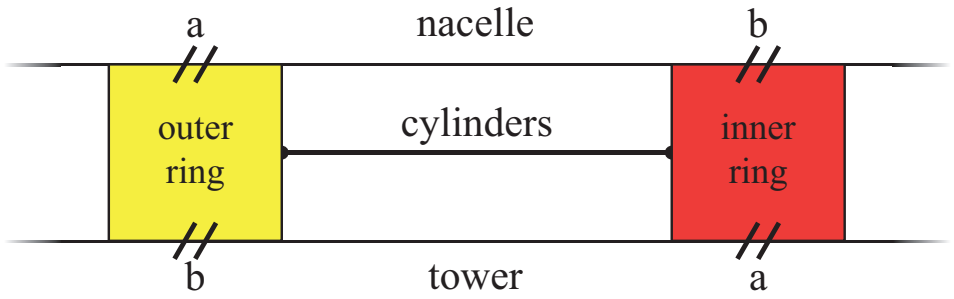

Figure 5.2: A simplified, translational representation of the connections between the discs. This is not a mechanical representation, only a visual aid to understanding the controllable connections between the two discs, nacelle and tower.

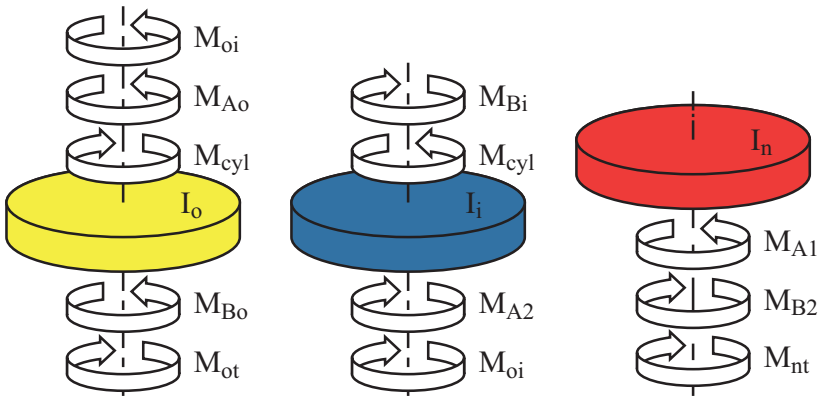

(a) The outer disc. (b) The inner disc. (c) The nacelle.

Figure 5.3: Rotary free body diagrams with applied torques.

the elements is described in Section 5.1.2. Description of the modelled hydraulic brake callipers can be found in Section 5.1.4.

5.1.2 Bearing friction

The bearings used in the connections between the moving elements are ball and slide bearings. Bearings are designed with minimal friction in mind. Because friction will work against motion of the system, it is important to implement it in some form. To reduce the complexity of the model, the LuGre friction model will not be used for the bearings. A basic model for friction is used because friction in bearings is not critical around zero velocity.

$$\mu(\omega) = \mu_b \tanh(k\omega) \tag{5.4}$$

$$\mu(\omega) = \begin{cases} -\mu_b, & -\infty < \omega < -\frac{1}{k} \\ \mu_b k\omega, & -\frac{1}{k} < \omega < \frac{1}{k} \\ \mu_b, & -\frac{1}{k} < \omega < \infty \end{cases} \tag{5.5}$$

No more than a simple static friction model, as discussed in Section 4.2.1, is required to model bearing friction as the dynamics of bearing friction is not critical to the accuracy of the model. A combination of coulomb and viscous friction is desired to include the characteristics of both. Coulomb-viscous friction is described in Equation 5.5. The equation is a piecewise function, which may cause numerical instability in the model. Instability is solved by implementing a tanh-function, as described in Equation 5.4, instead of the piecewise coulomb-viscous function. Hyperbolic tangent functions are great for this, as they emulate the piecewise function well, and are continuous and valid for all values of ω. A general plot of the two functions can be seen in Figure 5.4. The upper limit of the frictional coefficient is determined by the parameter μ_b.

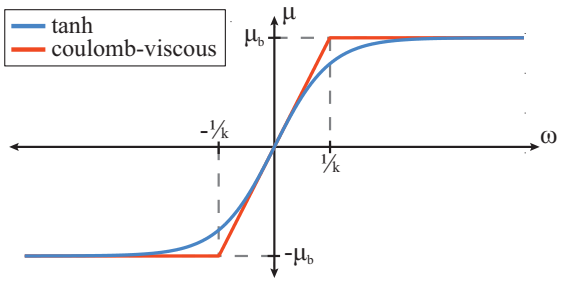

Figure 5.4: The frictional coefficient, μ, as a function of the relative angular velocity between the two frictional surfaces. Calculated using both a tanh-function (Equation 5.4) and a coulomb-viscous-function (Equation 5.5).

The parameter k controls the required velocity to achieve the maximal friction coefficient. The larger k, the lower angular velocity is required. Definition of the frictional coefficient is used to determine the frictional torques in the three slewing bearings. Expressions for the torques can be found in Equation 5.6 through 5.8. Expressions are products of the frictional coefficient as a function of relative angular velocity, the axial force in the bearing, and distance from the centre of rotation to the middle of the contact area in the bearing.

$$M_{ot} = \mu_b g(m_o + m_i) r_{ot} \tanh(\omega_o) \tag{5.6}$$
$$M_{oi} = \mu_b g(m_i) r_{oi} \tanh(\omega_i - \omega_o) \tag{5.7}$$
$$M_{nt} = \mu_b g(m_n) r_{nt} \tanh(\omega_n) \tag{5.8}$$

5.1.3 Hydraulic cylinders

Hydraulic cylinders generate torque which rotates the nacelle. In addition to hydraulic cylinders, the system contains a hydraulic valve and a number of mechanical components, ensuring correct transition from piston force to rotational torque. The modelled hydraulic cylinders are a part of the model in SimulationX, as shown in Figure 5.5. The six cylinders generating the torque are combined into two cylinders in the SimulationX model. For simulation purposes, to combine them will be an accurate approximation, as the cylinders will operate mostly synchronous anyway. The models require a diameter as input for piston- and rod-side area calculation. Therefore the equivalent piston- and rod diameter is calculated from Equation 5.9. The equivalent area will be three times the area of one cylinder when the equivalent diameter equals the diameter of one piston multiplied with $\sqrt{3}$, given the number of cylinders is $n_{cyl} = 6$.

$$\begin{aligned} A_{eqv} &= \frac{n_{cyl}}{2} A \\ \frac{\pi}{4} {d_{eqv}}^2 &= \frac{n_{cyl}}{2} \frac{\pi}{4} d^2 \\ d_{eqv} &= \sqrt{\frac{n_{cyl}}{2}} d \end{aligned} \tag{5.9}$$

Figure 5.5 shows the setup between *cyl1* and *cyl2*, installed in opposite directions. The mechanism requires this setup to act forces in the same direction, with different magnitudes, corresponding to piston-side and rod-side. Functionality can be checked by calculating the sum of position and velocity for *cyl1* and *cyl2*, as these should be opposing and their sums equal zero at all instances. The cylinders are connected mechanically to the inner and outer discs at each end, through a rotation-translation transformer, with a gearing of $1[\frac{\text{m}}{\text{rad}}]$. The lever arm is not included, because it is implemented in the calculation of torque generated from tangential forces in the following section.
The hydraulic pistons are connected to the hydraulic system through a 3/4 proportional direction valve. The detailed coupling can be read from Figure 5.5, where port P goes to hydraulic power unit, and port T goes to tank. The valve is controlled by a normalized guiding signal spanning from -1 to 1, where zero is closes the valve for all flow. What each signal correspond to, can be seen in the Figure 5.5.

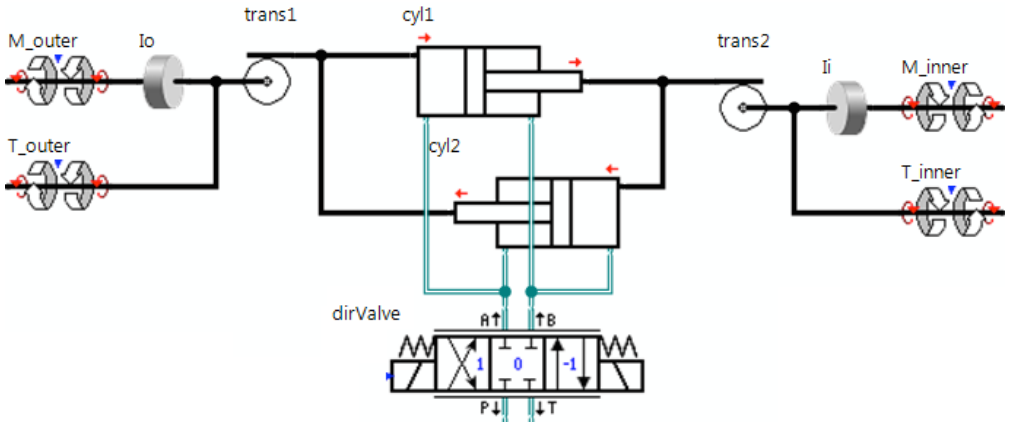

Figure 5.5: The visualization in SimulationX of the mathematical model used to emulate the hydraulic cylinders.

Tangential forces

Diameter of the hydraulic cylinders is identified in Section 3.6.1. Properties of the concept describe how important it is to model the torque contribution correctly. Because the tangential forces are approximately 20% lower than the cylinder forces, the cylinder orientation have to be taken into account. Figure 3.19a illustrates the angular displacement of the cylinders, relative to the tangential line through the interaction-points with the discs. The calculation of tangential forces was implemented to SimulationX as pre-calculated curves, rather than calculating all values directly for each time-step, avoiding severely increased calculation time.

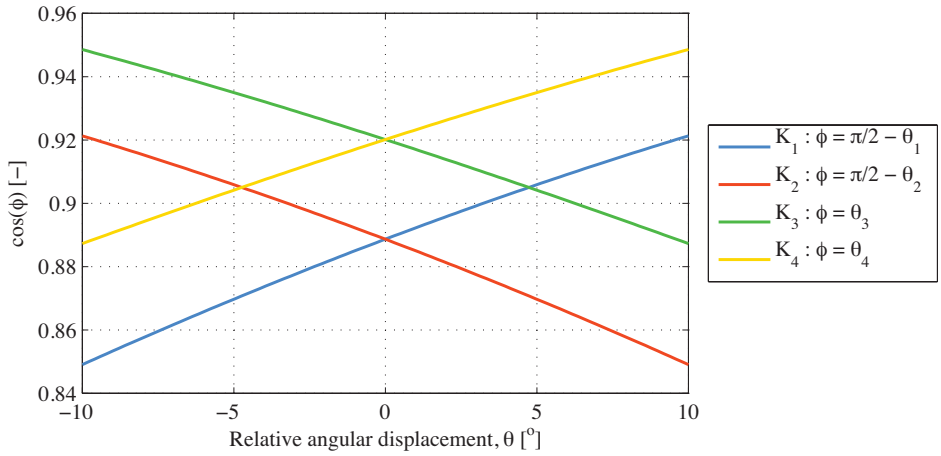

Figure 5.6: Lookup-graph of tangential factors for the two hydraulic cylinders, in one pair, in relation to their interaction points with the discs. The plots are used to return the tangential factor for a given relative angular displacement, θ.

Equation 5.10 to 5.13 was used to generate a lookup-graph for the tangential factor of the entire cylinder force, seen in Figure 5.6. This factor is multiplied with its corresponding cylinder force: K_1 and K_3 with F_1 and K_2, and K_4 with F_2. The plot in Figure 5.6 only yield values as long as the relative angular displacement between the outer and inner disc is within the interval: $-10[°] \leq \theta \leq 10[°]$. As the stroke of the mechanism is 18[°] (± 9[°]), the lookup-graph covers the relevant interval. The relative angular displacement between the outer and inner disc, θ, is expressed in Equation 5.16.

$$K_1 = \cos(\frac{\pi}{2} - \theta_1) \tag{5.10}$$
$$K_2 = \cos(\frac{\pi}{2} - \theta_2) \tag{5.11}$$
$$K_3 = \cos(\theta_3) \tag{5.12}$$
$$K_4 = \cos(\theta_4) \tag{5.13}$$
$$T_{ro} = \frac{1}{2} n_{cyl} r_o (F_1 K_1 + F_2 K_2) \tag{5.14}$$
$$T_{ri} = \frac{1}{2} n_{cyl} r_i (F_1 K_3 + F_2 K_4) \tag{5.15}$$
$$\theta = \theta_o - \theta_i \tag{5.16}$$

The torques affecting outer and inner disc can be expressed as in Equation 5.14 and 5.15, when knowing cylinder forces, $F_{1...2}$, and tangential factors, $K_{1...4}$. Torque is implemented in the model as a summation of calculated torques, T_{ro} and T_{ri}, and the torque output by the rotation-translation transformers. Torque-blocks in Figure 5.5 named *T_outer* and *T_inner* includes the summations. SimulationX does not allow adding gains directly to forces and torques.

5.1.4 Hydraulic brake callipers

Hydraulic brake callipers are used to clamp brake discs and generate frictional torque, locking inner or outer disc to either the nacelle or tower. The function, representing uncommon use of components, requires solid proof of functionality. The mechanism require twenty brake callipers in total, ten on top and ten on bottom. Ten of these (five on top and five on bottom) are connected to the inner disc and the other ten (five on top and five on bottom) are connected to the outer disc. Relations are visualized in Figure 5.8.

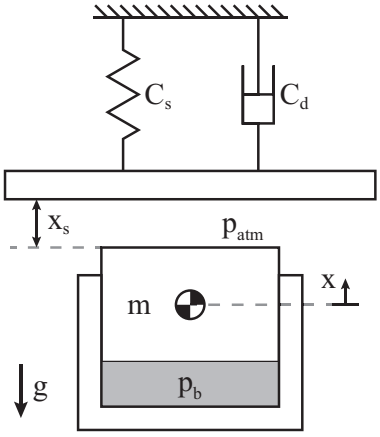

Figure 5.7: Mathematical model of the lower piston of a hydraulic brake calliper.

Hydraulic brake callipers and normal force

The hydraulic callipers are modelled as hydraulic pistons, with atmospheric pressure on one side and hydraulic pressure on the other. Hydraulic pressure is varies with the control signal, described in Section 5.1.5, with a maximum pressure equal to 205[bar]. The normal force is defined by the force generated when this piston has travelled a distance, x_s, which correspond to distance from piston start position to disc surface. The normal force is defined in Equation 5.17, where x is the position of the piston. A visualization of this model can be seen in Figure 5.7. Each calliper contains two pistons. One on top of the brake disc and one on the bottom, together clamping the brake disc. The mass of these pistons will lessen the responsivity of calliper, even though the mass of the pistons is small, relative to the force exerted by them. Because of placement and direction of motion when engaging the brake disc, the two pistons will be affected differently by gravity. Figure 5.7 show a model of the lower piston, where the gravitational force works against the clamping motion.

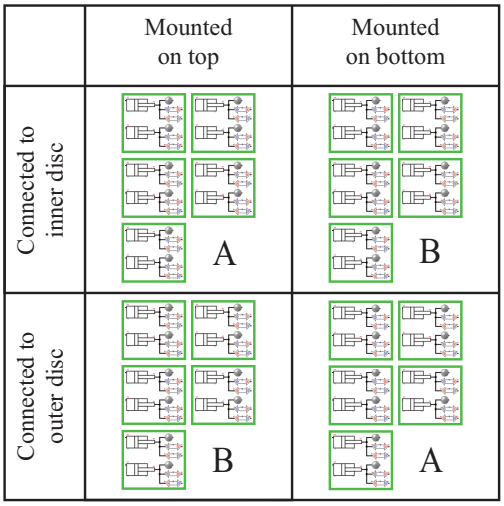

Figure 5.8: Placement and connectivity of twenty hydraulic brake callipers, divided into four equal groups. All green squares resemble one hydraulic brake calliper, containing two pistons, modelled in SimulationX.

$$N = \begin{cases} 0, & x < x_s \\ -C_s(x - x_s) - C_d\dot{x}\sqrt{x}, & x \geq x_s \end{cases} \tag{5.17}$$

Hydraulic brake callipers are severely simplified. Modelling each calliper as two individual pistons would increase the models complexity without gaining any accuracy in results. Figure 5.8 illustrate how five and five brake callipers are connected to the same disc, on the same side of the mechanism and are to operate in the same way. Columns describes which side of the yaw mechanism the calliper is mounted on, rows indicates which disc the calliper is connected to. A or B indicates when the calliper is activated. These four groups of five callipers are modelled as four pistons in Figure 5.9.
The pistons and masses in Figure 5.9 are identical in terms of parameters. The rod diameter is set to $0[mm]$ to make the area of both sides of the piston equal. The piston is in its zero-position when fully retracted. Mass blocks are added to introduce mass of the pistons and the effect of gravity, and are both defined with a mass m_p. Blocs named with a capital G are the gravitational force acting on the pistons, which equals $G = m_p g$. Blocks named with a capital N are the calculated normal forces, defined in Equation 5.17. The block termed *air* is the atmospheric gage pressure of 0[bar]. *valve_a* and *valve_b* are 3/2 proportional direction valves which control the fluid flow to the two groups, a and b, of hydraulic brake callipers. These two valves are both controlled by a signal input, marked as a blue line coming inn from left, marked with lower-case a and b. The hydraulic brake callipers are connected to their respective valve at port A. Port P at each valve goes to the hydraulic power unit, and port T goes to tank.

Frictional connection

LuGre friction model is used in following connections, described in Section 4.6: inner disc and nacelle, outer disc and nacelle, inner disc and tower, outer disc and tower. The LuGre friction model is implemented as seen in Figure 4.5, where the normal force is calculated using Equation 5.17 and the relative angular velocity are retrieved from the model. Each connection contains individual LuGre friction models. Models require individual velocity input, describing contact between different components. The input angular velocities for each of the four connections are given in Equation 5.18 through 5.21.

$$\omega_{Ao} = \omega_n - \omega_o \tag{5.18}$$
$$\omega_{Bo} = -\omega_o \tag{5.19}$$
$$\omega_{Ai} = \omega_i \tag{5.20}$$
$$\omega_{Bi} = \omega_i - \omega_n \tag{5.21}$$

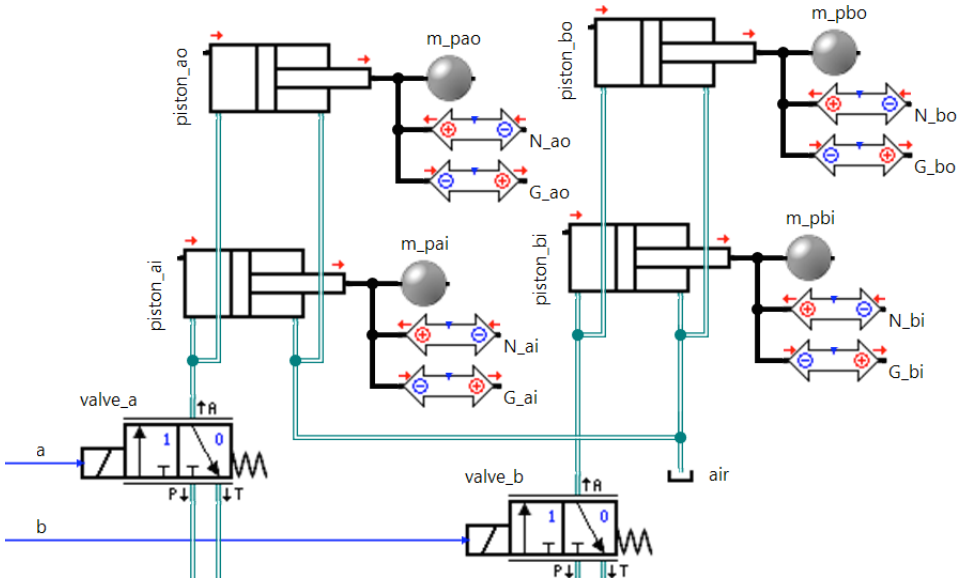

Figure 5.9: Twenty brake callipers modelled in groups of four, after functionality. See Figure 5.8.

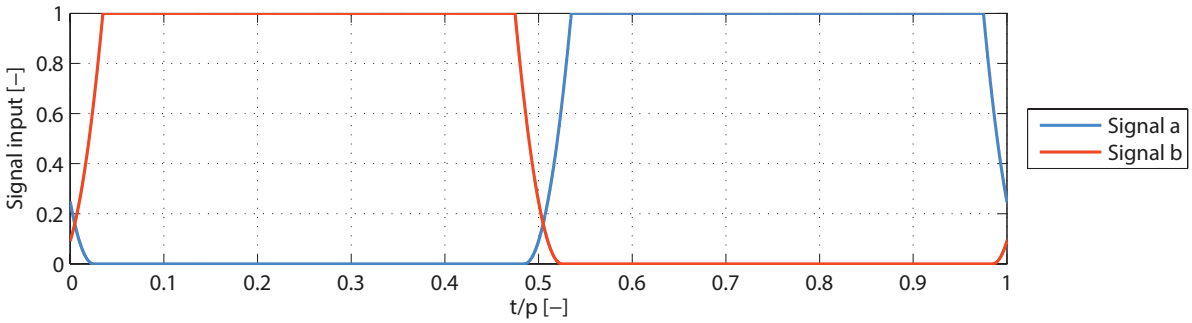

Figure 5.10: Signal input of pressure source within the hydraulic brake systems during one operating cycle, t/p. Ramps are parabolas with equal durations.

Modelled hydraulic brake callipers in combination with the LuGre friction model, for rotary systems with variable normal force, provides four torques: M_{Ao}, M_{Bo}, M_{Ai} and M_{Bi}. Frictional torques describes the controllable contact between discs, tower and nacelle. They are used in Equation 5.1 through 5.3 in Section 5.1.1.

5.1.5 Control signal

Control signals are implemented to manipulate actuator displacement and velocity in the mathematical model. The actuators work together to achieve a steady angular rotation of the nacelle. Investigation of the sequence involving release and grip between brakes is essential. Sequences are explained in Figure 3.6

Control of hydraulic brakes

Normal force from hydraulic brakes is altered through a variable pressure sources and 3/2 proportional directional control valves. Pressure source is altered to provide the best scenario regarding callipers griping and releasing the two discs. The 3/2 control valve is kept open at all time providing a minor peak flow of $15[\frac{\text{l}}{\text{min}}]$ during activating/deactivating of brakes, shown in Figure 5.10. Volume of brakes equals $0.2035[\text{dm}^3]$ for each calliper at 3[mm] stroke. The valve is not removed to represent a more complete system, in terms of pressure drop and future improvements. Signal input in Figure 5.10 describes how the pressure sources vary in the grip and release sequence. Ramps are parabola shaped, with equal duration, but acts and halts at various times. Parabola parameters are set by trial and error that represents a good exchange of momentum

between inner and outer discs. The signal, s_b, affects the output pressure, p_b, by multiplying it with pressure constant, p_s.

$$p_b = s_b \cdot p_s \tag{5.22}$$

Control of hydraulic cylinders

Velocity and stroke of cylinders are controlled by a 4/3 proportional directional control valve. The control valve receives signal based on inner and outer discs angular displacement and velocity. Discs contain empty space that can be utilized, installing sensors to provide needed feedback. Position sensors inside the hydraulic cylinders is possible, but requires a larger dead volume in the cylinder.

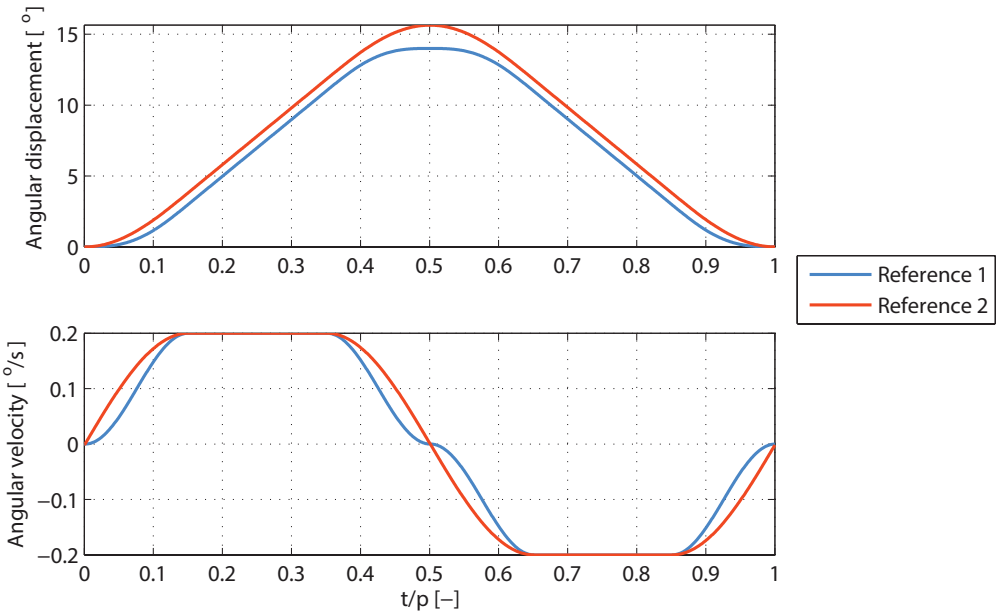

Figure 5.11: Angular displacement and velocity are deviation between inner and outer disc,defined as $\theta_o - \theta_i$ and $\omega_o - \omega_i$. Profiles are references used to control the valve opening in Figure 5.12, shown as ω_{ref} and θ_{ref}.

Two candidates for reference signal are graphed for one period, p, in Figure 5.11. Maximum angular velocity for the reference signals equals $0.2[\frac{^\circ}{s}]$. References in Figure 5.11 are deviations between inner and outer disc, $\theta_o - \theta_i$ and $\omega_o - \omega_i$. Blue indicates smooth exchanges at releasing and gripping between brakes shown in Figure 3.6. The blue signal uses two sequenced cosine half periods to ramp down and up, see $t/p = 0.5$ in Figure 5.11. Red line acts with one cosine half period during the exchange between brakes. Red obtains quicker exchanges between brakes and cylinder momentum. Determined reference is used as θ_{ref} and ω_{ref} in Figure 5.12. The lever arm differs with the sign of angular velocity. The rotating component in the mechanism is either the inner or outer disc, dependant on direction of rotation.

$$\omega r_i \quad , \quad \omega < 0 \tag{5.23}$$
$$\omega r_o \quad , \quad \omega > 0 \tag{5.24}$$
$$Q \quad = \quad vA_r + vA_p \tag{5.25}$$
$$\tag{5.26}$$

Velocity multiplied with cylinder areas, piston- (A_p) and rod-side (A_r), results in required flow at given velocity, seen in Equation 5.25. Required flow, Q, pressure drop, Δp, and flow coefficient, C_v, results in signal u. Signal affects the area shown in orifice Equation 5.27.

$$uA_v = \frac{Q}{C_v \Delta p} \tag{5.27}$$
$$C_v = \frac{Q}{\Delta p} \tag{5.28}$$

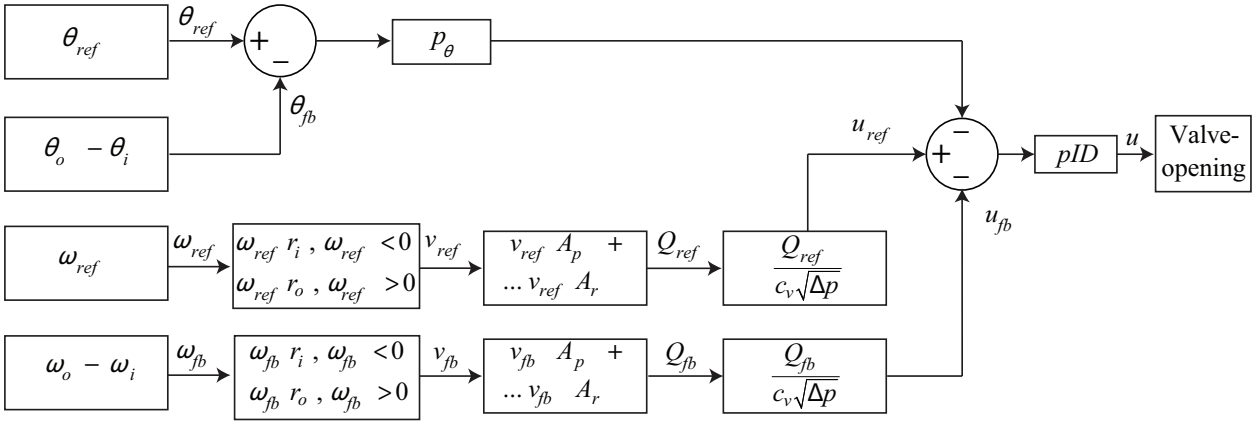

Figure 5.12: Control loop for the 4/3 proportional directional control valve, controlling hydraulic cylinders.

The flow coefficient, C_v, is a design parameter representing flow capacities of valves from manufacturers at different sizes and types. The parameter is given in valve product specifications, determined experimentally. It express flow capacity at a given pressure drop. Values used in the flow coefficient are nominal flow at $150[\frac{\text{l}}{\text{min}}]$ and pressure drop at 35[bar]. Values used in gain, p_θ, and pID are shown in Table 5.1.

Table 5.1: Parameters used in the control loop for hydraulic cylinders, Figure 5.12.

Control parameter	p_θ	p_{pid}	I_{pid}	D_{pid}
Value	-0.1	1	0.1	1

5.2 Assumptions and misrepresentations

Some assumptions and simplifications are made to ensure a stable model. Simplifications make misrepresentations in relation to how the system would operate and respond in reality. Adjustments are not to be mistaken for errors in the model, they are mere differences between the system modelled and the how the system would be in reality.

5.2.1 Hydraulic cylinders

The hydraulic cylinders generate the major torque component in the mechanism, which rotate the nacelle. Representing this correctly is vital to validate the feasibility of the mechanism as an entirety. Due to the way the model was created from the start, parts of the mechanics are hard to implement without increasing the complexity and calculation time severely. Implementation of the hydraulic cylinders into the mathematical model can be seen in Section 5.1.3.
Using SimulationX and its library of components, the hydraulic cylinders are modelled as described in Section 5.1.3 and shown in Figure 5.5. As the cylinders are modelled here, SimulationX defines them as rigidly connected to each other in both ends; barrel to rod. This means that both cylinders will have equal, but opposite, stroke and velocity. In reality the cylinders orientation relative to the direction it pushes is not as modelled, as well as it changes throughout the stroke. Orientation can be seen in Figure 5.13 as the cylinder forces and velocities have to be decomposed to find the radial and tangential components. Similar effect is present for velocities. Section 5.1.3 involves the description of tangential forces generated from cylinders and how they change throughout the cycle.

$$v_{t1ro} = v_{t2ro} \qquad v_{t1ri} = v_{t2ri} \tag{5.29}$$

The tangential velocities in both end points of the two cylinders are defined in Equation 5.29, which correspond with Figure 5.13b. The correction of velocity requires some larger changes to the model. By utilizing the 3D-library in SimulationX, the software would calculate the correct velocities and forces for each cylinder

and disc, variable shift in orientation taken into account. But as the major concern does not include the velocity of either the discs or cylinders, this is not critical for the functionality. This change is therefore left as a recommended future improvement to the model.

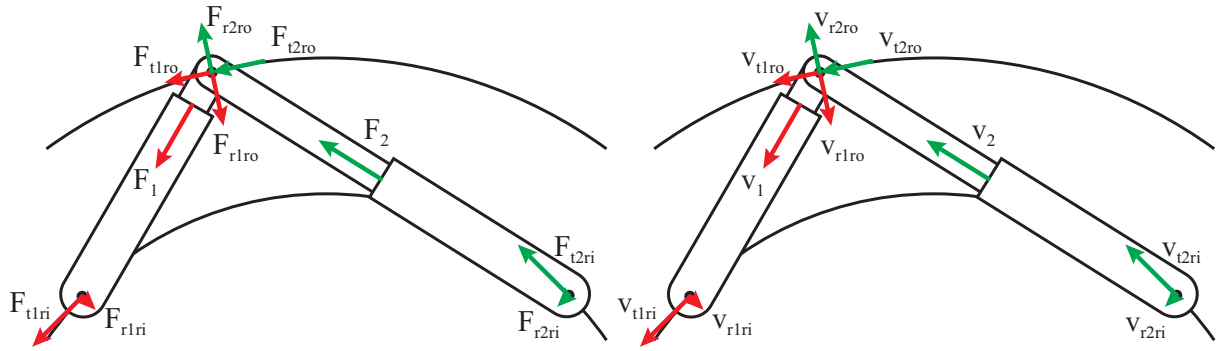

(a) Radial and tangential forces.

(b) Radial and tangential velocities.

Figure 5.13: Cylinder forces and velocities decomposed as radial and tangential components.

5.2.2 External forces

During the development of the model, the external forces were discussed. The effect of these are periodical and would make the control sequence work harder to obtain a stable movement. No concrete information has been found about the loads acting on the yaw mechanism, except the static loads stated in the product description. Dynamic load information would be ideal for simulation purposes, but is hard to retrieve. These loads could be calculated from wind measurements, using a specific wind turbine as reference. Existing, publicly available wind measurements are not frequent enough to catch the minor changes which are interesting for the simulation of a yaw mechanism. Investigations within these topics would be interesting to obtain a more detailed insight into influence of wind speed and direction.

Chapter 6

Results

Simulation results, spanning over a longer simulation time, ensures stability of the model, presenting angular displacement, velocity and acceleration for the rotating components. Friction is investigated through altering parameters. Reference control signal is compared with the feedback determining system accuracy. Hydraulic cylinders and brakes are investigated by evaluating the dynamic response of the components, resulting from the applied control signals. Results from described tests are presented and discussed in this chapter.

6.1 Simulation results

Results from simulations with the two reference signals, presented in Section 5.1.5, are described in the following section. Reference signals, predetermined paths, differs between a system with smooth velocity changes and a more rapid and continuous signal. A completely linear graph of nacelle displacement is not expected, as the reference signals focus on low acceleration.

6.1.1 Reference 1

The first reference signal contains smooth transitions between brake sequences, grip and release, and change of cylinder velocity. The system aims to minimize rapid changes in acceleration. Figure 6.1 provides shows angular displacement, θ, of the nacelle, inner and outer disc at given time.

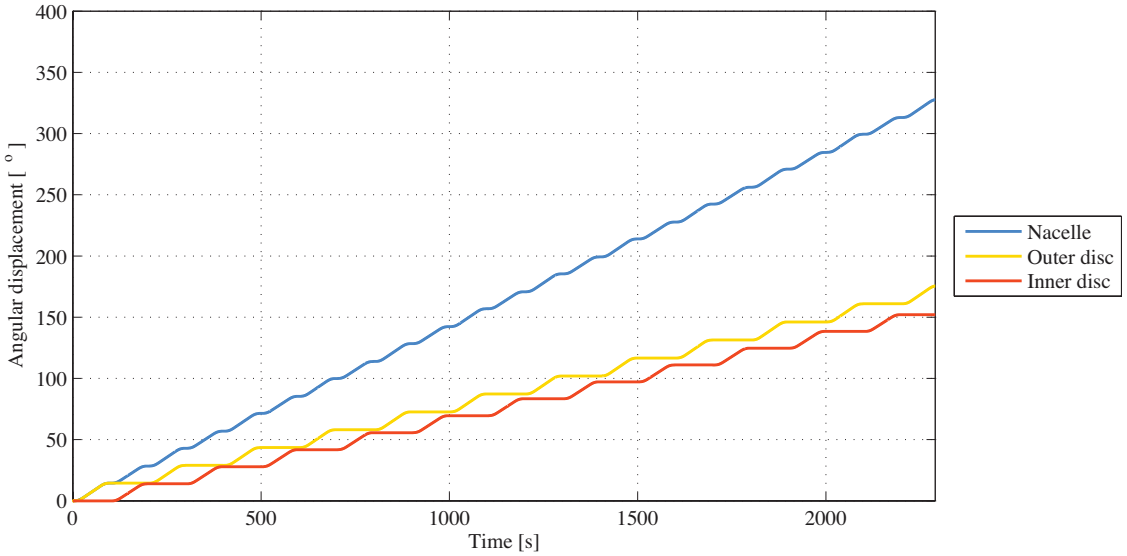

Figure 6.1: Angular displacement from nacelle, inner and outer disc at given time. The system uses the first reference from Figure 5.11.

At time equals 2300[s], the nacelle reaches an angular displacement of approximately 330[°]. Inner and outer discs roams away from each other as the radius used to calculate the angles are unequal. Slow acceleration is

shown in the Figure 6.1 as the nacelle creates a stair shaped graph. Figure 6.2 displays the angular velocity, ω, from nacelle, inner and outer disc at given time.

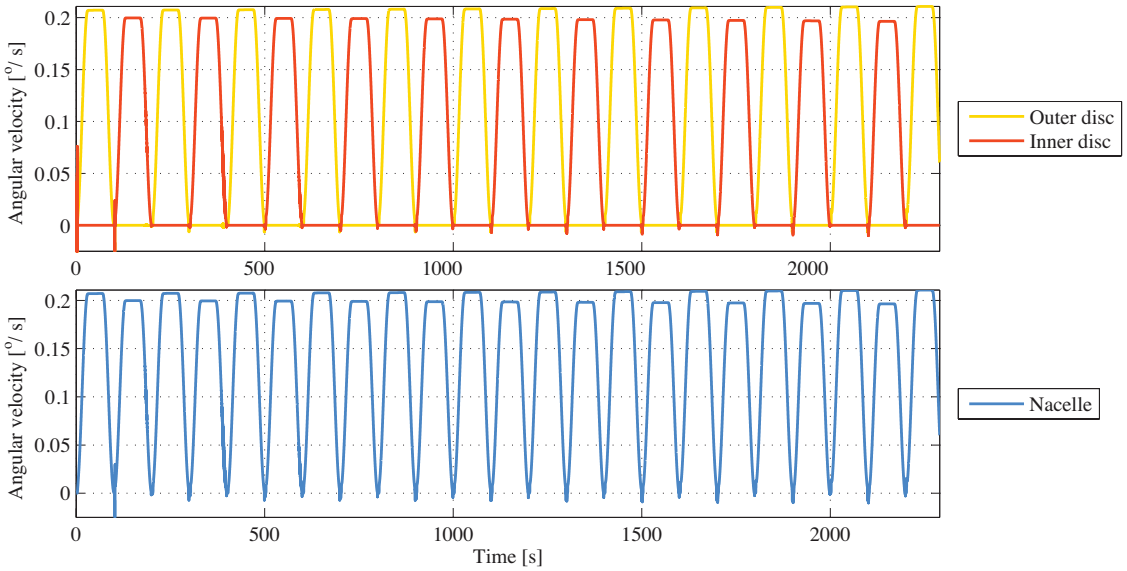

Figure 6.2: Angular velocity of inner and outer disc (upper graph) and nacelle (lower graph) at given time.

The inner disc reaches highest angular velocity at close to $0.2[\frac{\circ}{\text{s}}]$, while the outer disc peaks at approximately $0.207[\frac{\circ}{\text{s}}]$. The difference can be explained by the change of inner and outer radius to the discs. The nacelle shares the change in maximum angular velocity as it is generally locked to either inner or outer disc. Angular velocities of nacelle, inner and outer disc are presented in Figure 6.2.

$$\frac{v_{\text{max, i}}}{v_{\text{max, o}}} = \frac{0.2}{0.207} \approx 0.966 \quad , \quad \frac{r_i}{r_o} = \frac{1.13}{1.17} \approx 0.966$$

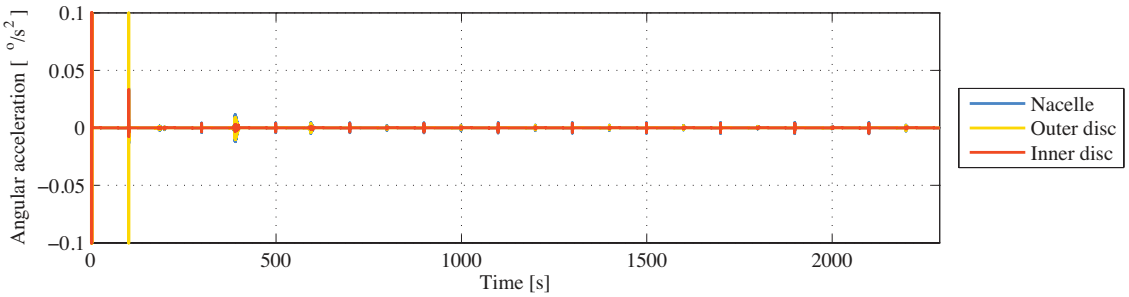

Figure 6.3: Angular acceleration from nacelle, inner and outer disc at given time. The acceleration contains smoother transitions compared to the second reference signal (5.11), shown in Figure 6.6.

The acceleration, in Figure 6.3, is kept at a low value throughout the simulation. Peaks at the beginning are to be expected, as the system builds up pressure and flow.

6.1.2 Reference 2

The second reference signal represents a more rapid and continuous path. Aim of the predetermined path is for the nacelle to spend minimum time at lower velocities.
At time 2300[s], the nacelle reaches an angular displacement of approximately 360[°], Figure 6.4. Compared to the slow and more stable system, an approximate angular displacement of 30[°] differentiates the two references at the end the simulation.

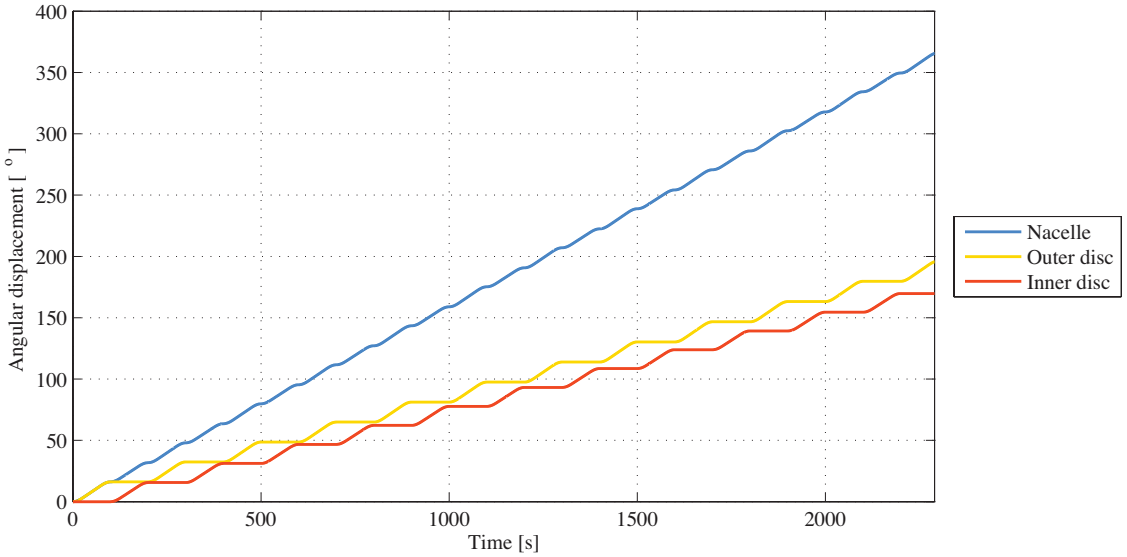

Figure 6.4: Angular displacement of nacelle, inner and outer disc at given time. The system uses the second reference signal from Figure 5.11.

Figure 6.5 represents angular velocities of nacelle, inner and outer disc at given time. Simulation includes higher average nacelle velocity compared to results using first reference signal, seen in Figure 6.2. The two predetermined paths share the same maximum velocity and difference in angular displacement of inner and outer disc.
Larger angular acceleration spikes in transitions between positive and negative velocity, as seen in Figure 6.6. Higher values at $\pm 0.8[\frac{^\circ}{s^2}]$ are expected, as the acceleration is largest when the velocity equals zero.

6.2 Test of friction model ruggedness

The brake callipers require verification in form of the LuGre friction model used to generate the braking force. This model has to respond as expected. As there exist no experimental results with such brake callipers to compare the response with, the model parameters can only be estimated. Investigation of the models area of stability is vital, if experimental results should turn up at a later stage. A defined interval of stable values for each parameter would in such case be helpful to easily approximate the models level of stability with given parameters. The test is performed on the full model, as defined in Chapter 5, and simulated for 450[s].

Table 6.1: Interval of stable values for the parameters in the LuGre friction model, where the result is categorized by **S**table, **U**nstable and Jump in **V**elocity.

Par:	50%	60%	70%	80%	90%	Init.	110%	120%	130%	140%	150%
μ_s	U, V	S, V	S, V	S	S	0.8	S	S	S	S	S
μ_c	S	S	S	S	S	0.4	S	S	S	S	S
K_v	S	S	S	S	S	0.4	S	S	S	S	S
v_s	S	S	S	S	S	0.1	S	S	S	S	S
v_d	S	S	S	S	S	0.01	S	S	S	S	S
σ_0	S	S	S	S	S	10^5	S	S	S	S	S
σ_1	S	S	S	S	S	$2 \cdot \sqrt{10^5}$	S	S	S	S	S

The interval is defined from a predefined stable point, using parameters from Table 4.1. Parameters are increased to 150% and decreased to 50% of its initial value. The stability is checked for every 10% increase/decrease of each parameter. Only one parameter is changed at the time. Results from the stability check can be seen in Table 6.1. The categorization of results is done by some abbreviations defined as follows:

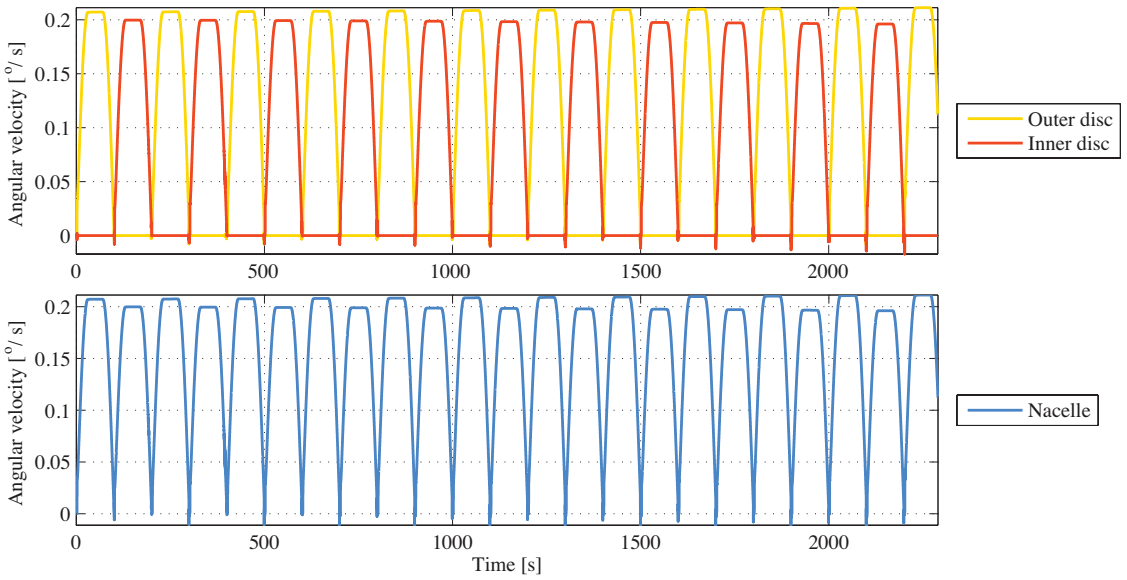

Figure 6.5: Angular velocity of inner and outer disc (upper graph) and nacelle (lower graph) at given time.

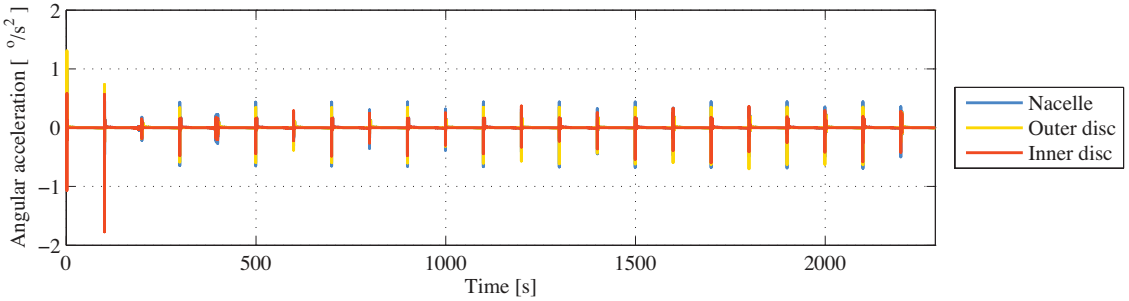

Figure 6.6: Angular acceleration from nacelle, inner and outer disc at given time.

- **Stable (S)**, means the system operates as usual without large deviations from the results found with the initial values.
- **Unstable (U)**, means the system operates unusual. Either one of the discs or nacelle spins off, or the system oscillates.
- **Jump in velocity (V)**, means the system experience unusually large jumps in velocity.

Parameters with greater effect on the basic functionality of the system is the frictional coefficients for stiction, μ_s, and coulomb friction, μ_c. Changing these within the given interval does not show any significant deviations, except when μ_s is lowered below 70% of its initial value. Velocity decreases rapidly causing an error in position when the two groups of callipers switch, i.e. every 100 second. If μ_s is lowered to or below 50% of its initial value, the system loses its functionality as the callipers cannot hold the system from rotating. This reaction is categorized as unstable. Changes in coulomb friction do not affect the motion of the nacelle, or other parts of the system. This is because the nacelle is motionless when the discs switch between clamping and releasing.
Changes in parameters covering viscous friction, K_v, result in no instability. Very low angular velocities in the system, means the frictional contribution due to viscosity is minor.
Stribeck velocity, v_s, defines the transition from stiction to coulomb friction. Judging the insignificance of the coulomb friction coefficient, μ_c, the results from changes to v_s is as expected. No significant effect on the result is seen.
Previous investigations of the parameters in the LuGre friction model are seen in Section 4.5. These show how variables considering damping (σ_1 and v_d) and stiffness (σ_0) have to be changed with a larger factor in order to see any change. By doubling σ_1, the system starts oscillating heavily at certain points of the

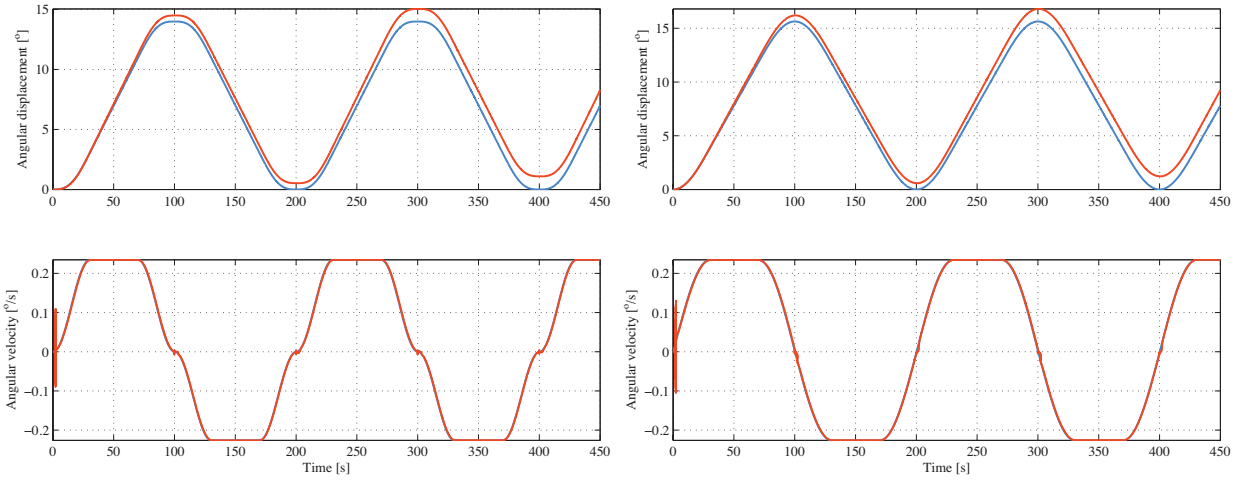

(a) Results using the first reference.

(b) Results using the second reference.

Figure 6.7: Reference (blue) and feedback (red) of the relative angular displacement and velocity between the outer and inner disc, for the two different velocity profiles and their corresponding displacement profile.

periodic cycle. Reducing σ_0 beyond a quarter of its initial value gives the same result. This correspond with the relation to a spring-damper system, where σ_0 and σ_1 correspond to spring and damper coefficients, respectively. Setting $v_d = 0.0001$, does not make the system oscillate, but gives very large accelerations.

6.3 Sequence control

The system is controlled by valves which are manually controlled by synchronized curves. This control loop is described in Section 5.1.5. Results are plotted in Figure 6.7 for the two reference velocity profiles investigated. These plots show how the feedback velocity (red) covers the reference velocity (blue) and are approximately equal. A jump in feedback velocity can be seen, for both scenarios, when the velocity passes through zero. This is the effect of clamping and releasing brakes, involving stiction becoming active when velocity equals zero. An increasing shift in displacement can be seen in both scenarios. This is not dependant on the profile itself, but the inaccuracy in modelling of the hydraulic cylinders, as described in Section 5.2.1. This could be solved by correcting the models deviation from reality. The system is guided through the periodical sequence as expected, following the angular velocity reference curve.

6.4 Hydraulic brake callipers

The hydraulic brake callipers are modelled as single-acting cylinders, with atmospheric pressure applied on rod-side, see Section 5.1.4. The flow curve shown in Figure 6.8a makes a jump for each hundred second, because the system switches between activating group A or B of brake callipers. Flow surges inn to build pressure, when a group of callipers is activated. The flow goes to zero, when the required pressure is achieved. Deactivation of a group of callipers results in a minor surge of flow to tank. The higher peaks at $t = 0$[s] and $t = 100$[s] occurs because the system have to build up pressure. The results from $t = 200$[s] and onwards are similar and considered as normal behaviour.
The description of the flow curve correspond with the clamping force curve in Figure 6.8b. The two groups of hydraulic brake callipers, A and B, switch between clamping every hundred second. The clamping force of 3.47[MN] is generated by five brake callipers, which means each brake calliper generate 694[kN] of clamping force, which equals the expected force.

6.5 Hydraulic cylinders

The hydraulic cylinders are modelled as two double-acting pistons, as described in Section 5.1.3. Figure 6.9a shows flow through the 4/3 directional control valve at each port. The flows periodic motion correspond

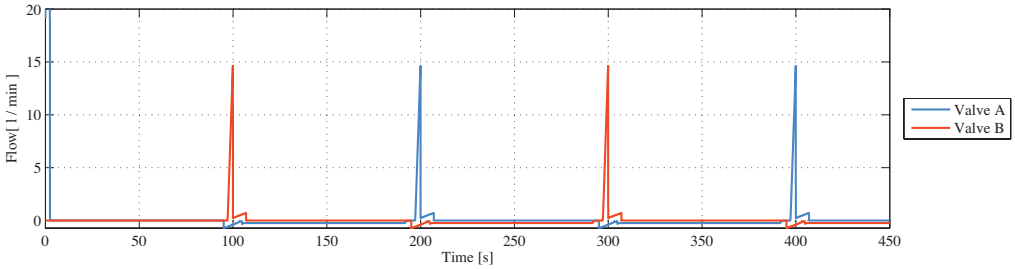

(a) Flow curve for the two hydraulic valves, A and B. Flow correspond to ten brake callipers.

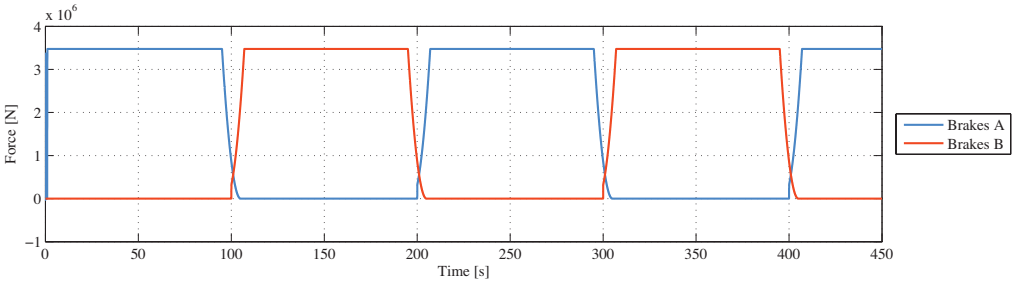

(b) Clamping force generated from the two hydraulic systems, A and B. Force correspond to five brake callipers.

Figure 6.8: Flow and clamping force curves for the hydraulic calliper system, which is divided into two groups, A and B, as described in Section 5.1.4.

with the valve signal described in Section 5.1.5, as the forces generated by the hydraulic cylinders should switch direction each hundred second.
The hydraulic cylinders are modelled in opposite directions, as represented in Figure 6.9b, where the pressure drops have opposite signs. It is expected to have the cylinder forces fluctuate each hundred second between positive and negative values. This is not represented in Figure 6.9b. The reason for this is the way the hydraulic cylinders are modelled. They are modelled in opposite directions, but they are connected rigidly to each other in the same one-dimensional plane. In reality this is not how they are modelled. They are mounted in the same two-dimensional plane, but are angled differently in relation to the object in which they respectively push and pull. The detailed reasoning and solutions for why the forces do not represent the expected results can be found in Section 5.2.1.
Note that the flow curve in Figure 6.9a will have some of the same shape, but the values will be different when the system is modelled correctly according to how the real mechanism would operate.

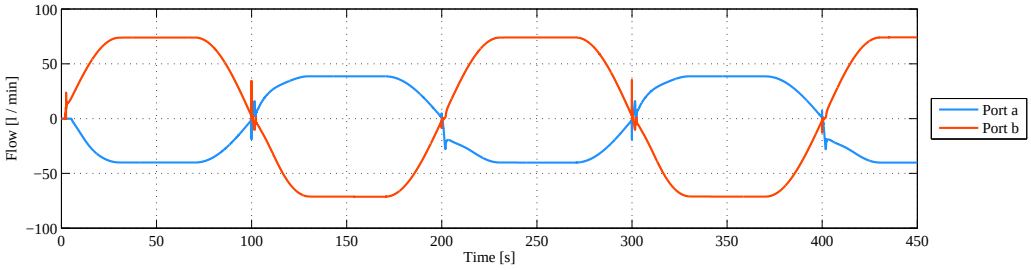

(a) Flow curve through the two ports, a and b, of the 4/3 directional control valve.

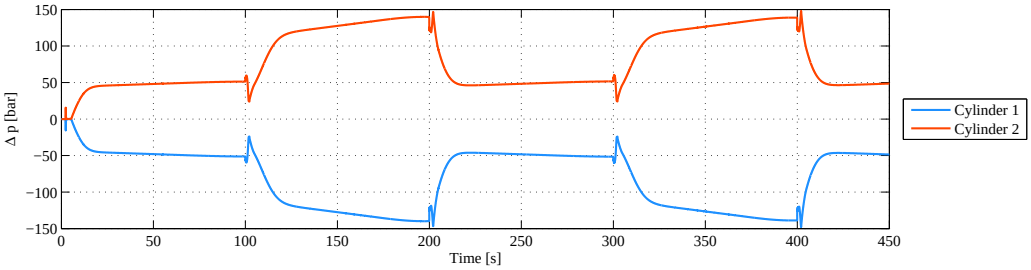

(b) Pressure drop over hydraulic cylinder 1 and 2, as marked in Figure 5.5.

Figure 6.9: Flow and pressure drop curves for the hydraulic cylinders, modelled as described in Section 5.1.3.

Chapter 7

Conclusion

The goal of the project was to develop a piston driven yaw mechanism for wind turbines. It was desirable that this yaw mechanism could be assembled and disassembled inside the wind turbine without requiring the use of costly equipment. It was also desirable that the proposed yaw mechanism should be more reliable than current yaw mechanisms. Three candidate solutions for yaw mechanisms were investigated. The candidate "grip and rotate" was found to best met the project requirements. Product development is done to such lengths required to create a representative visual design. Suitable components were selected and a 3D CAD model was developed. Based on the selected components and the 3D model a mathematical model of the yaw system was developed. This model uses LuGre to emulate the friction in the yaw system. The functionality of the yaw system was investigated by running simulations on the developed model. Visualizations of how the yaw system works was developed. The findings and results of the project were documented in this thesis. The design is based on present well proven, technology in a combination never used for yaw mechanisms. Advantages with its unique design are found in the ability to be disassembled, serviced and repaired. Results from simulations approve functionality of the piston driven yaw mechanism, disregarding minor limitations in its ability to emulate reality. Simulations show how the model is stable, even for longer simulations. It seems reasonable to assume that the reduction in point loads along with the use of the well proven technology of hydraulic cylinders and brake callipers will result in increased reliability compared to current solutions. The idea stated, developed and modelled in this thesis is a solid candidate for a piston driven yaw mechanism.

Bibliography

[1] REN Alliance. Ren alliance press release: How to follow the ipcc mitigation scenario. Web-article, 11 2013. Read: March 17th, 2014. URL: http://www.ren-alliance.invotech.se/index.php?q=node/17.

[2] Brian Armstrong-Hélouvry, Pierre Doupont, and Carlos Canudas de Wit. Survey of models, analysis tools and compensation methods for the control of machines with friction. *Automatica*, 30(7):1083–1138, 1994.

[3] Svendborg Brakes. Svendborg brakes range catalogue. Published through homepage. Downloaded; February 5th, 2014.

[4] European commission. Communication from the commision to the european parlament, the council, the european economic and social committee and the commitee of the regions, a policy framework for climate and energy in the period from 2020 to 2030. 1 2014. COM(2014) 15 final.

[5] P.R. Dahl. A solid friction model. Technical report, The Aerospace Corporation, El Segrundo, CA, 7 1968. Tehnical Report TOR-0158(3107-18)-1.

[6] Jan Dodd. Enercon looks at new e-126 7.5mw prototype. Web-article, 8 2013. Read: January 20th, 2014. URL: http://www.windpowermonthly.com/article/1194352/enercon-looks-new-e-126-75mw-prototype.

[7] E. C. Fitch and I. T. Hong. *Hydraulic Component Design and Selection*. BarDyne, Inc., 5111 N. Perkins Road, Stillwater, Oklahoma 74075, USA, 2004.

[8] Andrzej Garbacik, Kazimierz Szewczyk, and Jacek S. Stecki. *Hydraulic control systems: System design and analysis*. Monash University, Monash, Australia, 1997.

[9] ENERCON GmbH. *ENERCON Product overview*. ENERCON GmbH, Dreekamp 5 · 26605 Aurich, Germany, 7 2013. Read: January 20th, 2014. URL: http://www.enercon.de/p/downloads/ENERCON_Produkt_en_web_072013.pdf.

[10] David A. Haessig and Bernard Friedland. On the modelling and simulation of friction. *J. Dyn. Sys. Meas. Control*, 133(3):354–362, 9 1991.

[11] A. Harnoy and B. Friedland. Dynamic friction model of lubricated surfaces for precise motion control. *Tribology Transactions*, 37(3):608–614, 3 1994.

[12] D.P. Hess and A. Soom. Friction at a lubricated line contact operating at oscillating sliding velocities. *Journal of Tribology*, 112(1):147–152, 1 1990.

[13] igus Inc. iglide prt slewing rings. Published on web, 11 2012. Downloaded; March 21th, 2014.

[14] TyssenKrupp Rothe Erde India. Rothe erde slewing bearings. Published through homepage, 2014. Downloaded; March 18th, 2014.

[15] Dean Karnopp. Computer simulation of slip-stick friction in mechanical dynamic systems. *Journal of Dynamic Systems, Measurement, and Control*, 107(1):100–103, 1985.

[16] Mervento Ltd. Mervento 3.6-118 catalogue. Published through homepage, 2012. Downloaded: January 9th, 2014.

[17] J. F. Manwell, J. G. McGowan, and A. L. Rogers. *Wind Energy Explained: Theory, Design and Application*. John Wiley & Sons Ltd., Chichester, West Sussex, United Kingdom, 2 edition, 2 2010.

[18] Mark Walter Elza Michiels. Combined radial-axial slide bearing, united states patent 6761483, 7 2004. Read: March 21$^{\text{th}}$, 2014.

[19] Arthur Morin. New friction experiments carried out at metz in 1831-1833. *Proceedings of the French Royal Academy of Sciences*, 4:1–128, 1833.

[20] H. Olsson, K.J. Åström, C. Canudas de Wit, M. Gäfvert, and P. Lischinsky. Friction models and friction compensation. *European Journal of Control*, (4):176–195, 1998.

[21] Henrik Olsson. *Control Systems with Friction*. PhD thesis, Lund Institute of Technology, Box 118, S-221 00 LUND, Sweden, 1996.

[22] Industrial Press. *Machinery's handbook*. Industrial Press, Inc., 989 Avenue of the Americas, New York, New York 10018, USA, 29 edition, 2012.

[23] Ernest Rabinowicz. The nature of the static and kinetic coefficients of friction. *Journal of Applied Physics*, 22(11):1373–1379, 11 1951.

[24] Osborne Reynolds. On the theory of lubrication and its application to mr. beauchamp tower's experiments, including an experimental determination of the viscosity of olive oil. *Philosophical Transactions of the Royal Society of London*, 177:157–234, 1986.

[25] Thomas F. Stocker, Dahe Qin, Gian-Kasper Plattner, Melinda M.B. Tignor, Simon K. Allen, Judith Boschung, Alexander Nauels, Yu Xia, Vincent Bex, and Pauline M. Midgley. *Climate Change 2013: The Physical Science Basis. Contribution of Working Group I to the Fifth Assessment Report of the Intergovernmental Panel on Climate Change*. Cambridge, university press, 32 Avenue of the Americas, New York, NY 10013-2473, USA, 2013.

[26] R. M. Sørensen, M. R. Hansen, O. Ø. Mouritsen, and P. E. Fenger. Hydraulic yaw system for wind turbines with new compact hydraulic motor principle. *EWEA 2011 Scientific Proceedings*, pages 111–114, 2011.

[27] Det Norske veritas and Forskningscenter Risø. *Guidelines for Design of Wind Turbines*. Det Norske Veritas, Copenhagen, Denmark, 2 edition, 2002.

[28] John F. Walker and Nicholas Jenkins. *Wind energy technology*, volume 4 of *10*. John Wiley & Sons, Chichester, West Sussex, United Kingdom, 1997.

[29] World Wind Energy Association (WWEA). 2013 half-year report. Technical report, Charles-de-Gaulle-Str. 5, 53113 Bonn, Germany, 10 2013. Read: January 13$^{\text{th}}$, 2014. URL: `http://www.wwindea.org/home/index.php?option=com_content&task=view&id=402&Itemid=43`.

Appendix A

Problem description

12.Development of Hydraulic Piston Drive for Yaw Control of Wind Turbine

Key words: Product Development, Mechanical Design, Hydraulic Systems, Modelling and simulation, Finite Element Analysis, Hydraulic Piston Drive, Renewable Energy, Wind Turbines, Wind Turbine Research.

Introduction

In recent years an increasing number of wind turbines has entered into the market. In general wind turbines seems to increase in size and capacity. As the Wind Turbines becomes larger, one major mechanical design challenge arises, the mechanism which controls the orientation of the rotor. This is referred to as the mechanism for yaw control. Control around the yaw axis is of great importance to assure en efficient energy production. It is also important to be able to "park" the rotor in any orientation around the yaw axis. The mechanisms most currently used today consist of several hydraulic or electrical motors with gearboxes and breaking mechanisms which are situated around the circumference of a large gear. This mechanism is associated with certain challenges:

1. They are costly to produce
2. Requires considerable maintenance
3. Troubled by malfunctions such as damage to main gear (yaw control) or overloading of hydraulic/electric motors
4. Large expenses along with considerable down time if damage to the main gear (yaw control) occurs

It has become apparent that a new approach to yaw control is could be of great importance to the Wind Turbine manufactures.

Incepti AS is a newly established company in Arendal which specialises in product development. Our goal is to optimise the innovation process from idea to product. We achieve this by close cooperation between inventors, producers and experts. For the year 2013/2014 Incepti AS would like to propose a master thesis as part of our latest research towards developing a Hydraulic Piston Drive for yaw control of Wind Turbines. It is our hope that this thesis will allow two students to gain valuable insight in the product development process as it is carried out in the industry as well as delivering valuable information to the research project conducted by Incepti AS.

It is desirable that the project will result in a test rig which may be used to demonstrate the suitability of the proposed Hydraulic Piston Drive and allow research and optimisation to be carried out. We believe that a supervisor from the University of Agder together with an external supervisor from Incepti AS would be optimal to assure an efficient development process for this project. We hope that the project will attract two highly motivated students with good skills within the field of Simulation and Modelling of Hydraulic Systems as well as Control System Design. Incepti AS is positive to publishing results from this project and may together with the university, assist in writing such research papers. The students working with this project will receive considerable support from Insepti AS during the progress of the project.

Project description

The goals described below are tentative and may be altered later in the project
Develop a concept for an Hydraulic Piston Drive capable of controlling the orientation of a Wind Turbine Rotor around its yaw axis as well as "parking" the Rotor in any orientation around the yaw axis.

1. Develop and evaluate concepts to meet the projects goals
2. Develop mathematical models to simulate and optimise the selected concept
3. Select components for the concept
4. Develop Solid Works model and production drawings for a test rig for the concept

5. Conduct Finite Element analysis of critical components of the test rig
6. Produce a test rig for the concept
7. Conduct limited test on the test rig to verify mathematical model and suitability of concept
8. Write project report
9. Publish results if desirable

Responsibilities
The responsibilities listed below are tentative and may be altered later in the project

- The University of Agder together with Incepti AS will be responsible for task 1
- The University of Agder will be responsible for task 2. Incepti AS will assist in supplying critical data
- Incepti AS will be responsible for task 3
- Incepti AS will be responsible for task 4
- The University of Agder will be responsible for task 5.
- Incepti AS will be responsible for task 6
- The University of Agder together with Incepti AS will be responsible for task 7 and 9
- The University of Agder will be responsible for task 9.

Outcome

The project work will be documented in the form of a project report describing the developed product. The project will result in a test rig capable of demonstrating the suitability of the developed product. One or two scientific papers may be published as a result of the project.

Contact persons:

Incepti AS: Johan Johnsen
UiA: Michael R. Hansen

Appendix B

Material data sheets

AISI 1030 Steel, as rolled

Categories: Metal; Ferrous Metal; Carbon Steel; AISI 1000 Series Steel; Medium Carbon Steel

Material Notes: Moderate strength and hardness in the as-rolled condition. Fair machinability and weldability. Precautions must be taken when welding to avoid cracking during cooling.

Key Words: SAE J414, ASTM A108; ASTM A29;ASTM A510; ASTM A512; ASTM A519; ASTM A544; ASTM A545; ASTM A546; ASTM A576; ASTM A682, DIN 1.1172; FED QQ-S-635 (C1030); FED QQ-S-700 (C1030); MIL SPEC MIL-S-11310 (CS1030); SAE J403; SAE J412

Vendors: No vendors are listed for this material. Please click here if you are a supplier and would like information on how to add your listing to this material.

Physical Properties	Metric	English	Comments
Density	7.85 g/cc	0.284 lb/in³	

Mechanical Properties	Metric	English	Comments
Hardness, Brinell	179	179	
Hardness, Knoop	200	200	Converted from Brinell hardness.
Hardness, Rockwell B	88	88	Converted from Brinell hardness.
Hardness, Vickers	188	188	Converted from Brinell hardness.
Tensile Strength, Ultimate	550 MPa	79800 psi	
Tensile Strength, Yield	345 MPa	50000 psi	
Elongation at Break	32 %	32 %	In 50 mm
Reduction of Area	57 %	57 %	
Modulus of Elasticity	205 GPa	29700 ksi	Typical for steel
Bulk Modulus	140 GPa	20300 ksi	Typical for steel
Poissons Ratio	0.29	0.29	Typical For Steel
Shear Modulus	80.0 GPa	11600 ksi	Typical for steel
Izod Impact	75.0 J	55.3 ft-lb	

Electrical Properties	Metric	English	Comments
Electrical Resistivity	0.0000166 ohm-cm @Temperature 20.0 °C	0.0000166 ohm-cm @Temperature 68.0 °F	annealed specimen

Thermal Properties	Metric	English	Comments
CTE, linear	11.7 µm/m-°C @Temperature 20.0 °C	6.50 µin/in-°F @Temperature 68.0 °F	
Specific Heat Capacity	0.486 J/g-°C @Temperature >=100 °C	0.116 BTU/lb-°F @Temperature >=212 °F	annealed
Thermal Conductivity	51.9 W/m-K	360 BTU-in/hr-ft²-°F	

Component Elements Properties	Metric	English	Comments
Carbon, C	0.27 - 0.34 %	0.27 - 0.34 %	
Iron, Fe	98.67 - 99.13 %	98.67 - 99.13 %	As remainder
Manganese, Mn	0.60 - 0.90 %	0.60 - 0.90 %	
Phosphorous, P	<= 0.040 %	<= 0.040 %	
Sulfur, S	<= 0.050 %	<= 0.050 %	

References for this datasheet.

Appendix C

Svendborg brakes: DEB-0120-004-DA-MAR

SVENDBORG BRAKES

GLOBAL LEADING EXPERTS

DISC BRAKE: BSAC 120 DUAL-ACTION

Name: DEB-0120-004-DA-MAR
Date: 03.07.2012
Revision: -

TECHNICAL DATA AND CALCULATION FUNDAMENTALS

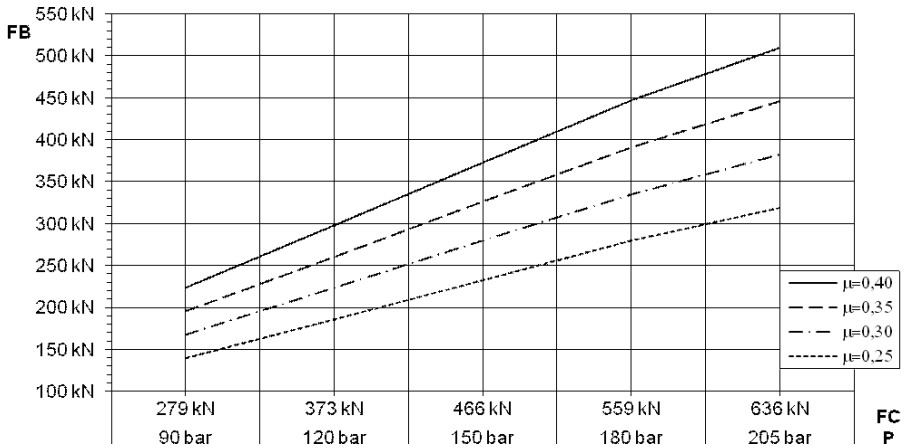

SVENDBORG BRAKES

GLOBAL LEADING EXPERTS

SPECIFICATION: DISC BRAKE BSAC 120 DUAL-ACTION

BRAKING TORQUE

The braking torque M_B is calculated from following formula where:
a is the number of brakes acting on the disc
$\mathbf{F_B}$ is the braking force according to table above [N] or calculated from formula
$\mathbf{D_O}$ is the brake disc outer diameter [m]
$\mathbf{F_C}$ is the clamping force [N]
A [cm^2], **P** [bar] and μ see values below
The actual braking torque may vary depending on adjustment of brake and friction coefficient.

$$M_B = a \cdot F_B \cdot \frac{(D_O - 0{,}136)}{2} \text{ [Nm]}$$

$$F_B = F_c \cdot 2 \cdot \mu \text{ [N]}$$

$$F_C = A \cdot P \cdot 10 \text{ [N]}$$

CALCULATION FUNDAMENTALS

	DUAL-ACTION
Weight of calliper half (without brake pad):	Approx. 99 kg
Weight of caliper:	Approx. 198 kg
Overall dimensions:	572 x 318 x 278 mm
Pad width:	138 mm
Pad area:(organic)	58,500 mm^2 (*)
Max. wear of pad:(organic)	7 mm (*)
Nominal coefficient of friction:	μ= 0.4
Total piston area - each caliper half:	A=339,3 cm^2
Total piston area - each caliper:	678,6 cm^2
Volume for each caliper at 1 mm stroke:	67,8 cm^3
Volume for each caliper at 3 mm stroke:	203,5 cm^3
Actuating time (guide value for calculation):	0.8 sec
Pressure connection/port:	1/4" BSP
Drain connection port R:	1/4" BSP
Max. operating pressure Pmax	205 MPa
Min. operating pressure Pmin	90 MPa
Recommended pipe size:	10 mm
Operating temperature range	
General usage:	-20°C to +70°C
For brake applications in wind turbines:	-40°C to +60°C

(For temperatures outside this range contact Svendborg Brakes)

(*) On each brake pad.

Appendix D

ThyssenKrupp Rothe Erde, slew bearing

Technical drawing of single row slew bearing with raceway and sealing details.

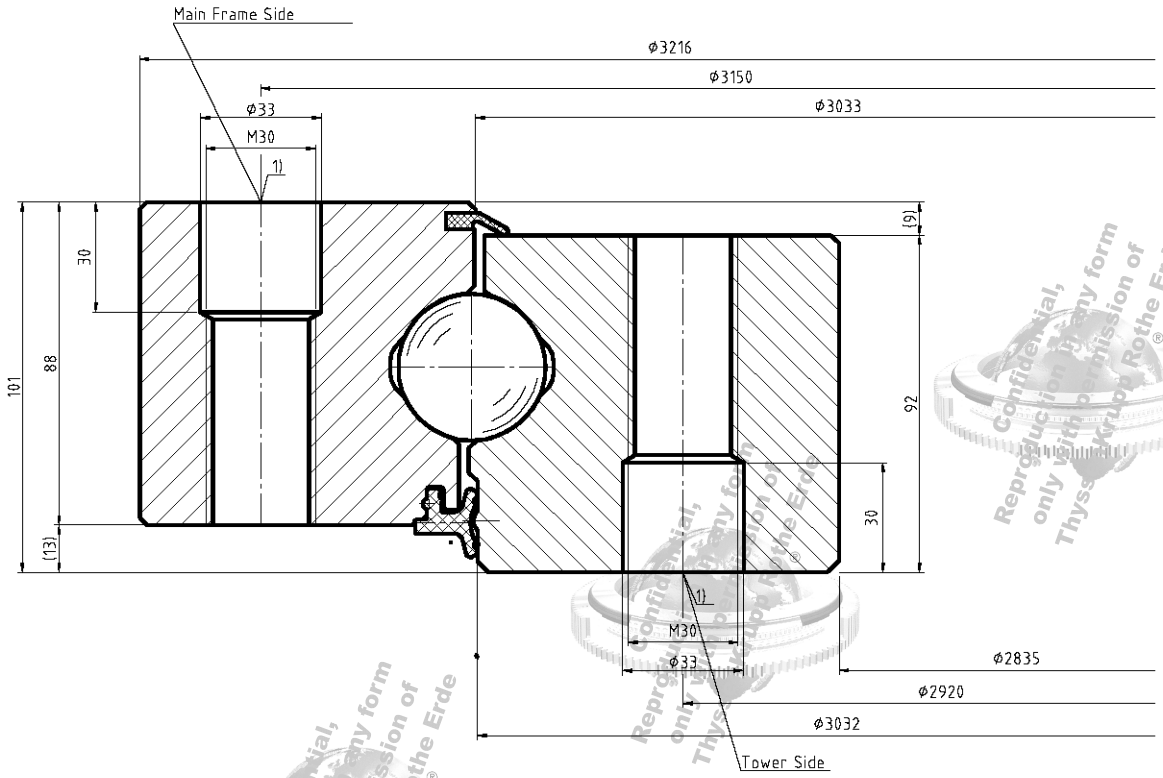

1) ⌖ Ø 0.70 MOUNTING SURFACE SIDE

OUTERRING 100 HOLES, EQUALLY SPACED FOR BOLTS M30
INNERRING 100 HOLES, EQUALLY SPACED FOR BOLTS M30

Untolerierte Durchmesser-Maße (spanend bearbeitet) Dia. dim. without tolerance (machined)						
≤315	≤1000	≤2000	≤4000	≤6300	≤10000	
±1.6	±2.5	±3.5	±5.0	±7.0	±10.0	

Schutzvermerk ISO 16016 beachten
Copyright reserved

	Datum/Date	Name
Bearb. Drawn by	16.05.2014	Mülle
Gepr. Check by	20.05.2014	Bus

Rothe Erde

Werkstoff/Material:
Rings
42CrMo4 V

Maßstab Scale 1:1 | Gewicht Weight 1126 kg/kgs

Ident-Nr. Ident-No. **83161510**

Benennung / Title
BALL BEARING
SLEWING RING

Zeichnungs-Nr. / Drawing No. **060.40.3035/00.160514.2** Blatt Page A2

Entwurf/Arisen from: 062.60.3035/01.241103.2"A"